SESSION J

Data Acquisition and Processing

Chairman, JOHN T. MENGEL

Data Acquisition from Spacecraft

JOHN T. MENGEL *is Assistant Director, Tracking and Data Systems at the NASA Goddard Space Flight Center. In this capacity, he administers the functions of tracking, data acquisition and reduction, communications, and related computing operations which provide orbital and flight data on satellites and space vehicles for Goddard and NASA as a whole. Mr. Mengel transferred to NASA from the Naval Research Laboratory in 1959. At NRL he provided telemetry systems for V–2 upper atmosphere research programs at White Sands, and for the Viking Project. He was responsible for the development and production of the Project Vanguard Minitrack system for radio tracking of satellites and space vehicles in the upper atmosphere. Mr. Mengel, a member of the Institute of Radio Engineers and the American Geophysical Union, appears in the Who's Who in America. He was graduated from Union College in 1939 with a B.S. degree in Physics.*

Introduction

By John T. Mengel

This morning's session is concerned with four typical areas of the field that is receiving the major impact of many of the sessions you attended yesterday. The acquisition of data from spacecraft, and the processing of this data into a form suitable for the spacecraft experimenter to make adequate and detailed analyses and deductions. The four areas to be covered are orbital data processing, scientific flight data acquisition and processing, meteorological satellite data processing (as typical of all applications satellites) and data acquisition from planetary spacecraft.

All of these areas have one problem in common: As spacecraft and experimental capabilities increase, data acquisition and data processing problems increase at a terrifying rate. As oversimplified examples of this increase, let me mention the following facts: In the initial satellite period, 1958 and 1959, we had 11 scientific satellites, whose bandwidths were 10 to 30 kc, and which required only manual reduction to provide analog strip charts to the experimenter.

In the 1960 and 1961 period, there were 13 satellites, with bandwidths now to 100 kc, for a total of about 26×10^9 data points. These are currently being reduced automatically. In the next two years, 1962 to 1963, there are 37 satellites—launched or planned—with telemetry data bandwidths to 300 kc and some TV type channels to 3.5 Mc, for a total of about 18×10^{11} data points.

Another example—from the daily operational status reports provided each morning on our network status. A typical report of last June 2, 1962, indicated six satellites being tracked, 3 of which were giving 1320 minutes total of telemetry data per day.

A similar report for October 31, 1962, shows 13 satellites being tracked, nine of which are giving a total of 4672 minutes of telemetry coverage per day.

With that background, I present your first speaker, Dr. Joseph W. Siry.

N63-11106

23. Data Processing for Orbit Determination

By Joseph W. Siry

DR. JOSEPH W. SIRY *is Chief of the Theory and Analysis Staff, Tracking and Data Systems Directorate of the NASA Goddard Space Flight Center. He began his career in space research with the Naval Research Laboratory, where he headed the Theory and Analysis Section of the Rocket-Sonde Research Branch, and later that same branch of the Vanguard program. Dr. Siry has served as Executive Secretary of the Upper Atmosphere Rocket Research Panel's Committee for the IGY and as the U.S. representative to international geophysical meetings in Russia and Finland. He received his B.S. degree in Physics from Rutgers University and his M.A. and Ph. D. degrees in Mathematics from the University of Maryland. He is a member of the International Association of Geomagnetism, American Rocket Society, Sigma Xi, American Mathematical Society, American Astronomical Society. He received the Arthur S. Fleming Award in 1960.*

INTRODUCTION

Orbit determination for artificial satellites and spacecraft has developed upon the foundations laid by university research workers over the centuries. Elaborate theories have been developed to cope with the problem of determining the orbits of the planets and of their natural satellites. Modifications of these theories have been developed in order to make them applicable to some of the special problems associated with the orbits of artificial satellites.

The fundamental problem of orbit determination is that of comparing theories such as these with observational data obtained from satellite tracking stations. Various aspects of this problem are indicated in Figure 23–1. Preparations for orbit determination for the satellites to be launched during the International Geophysical Year were based upon the assumption that the principal perturbations would be due to the earth's oblateness and its atmosphere.

Satellites are slowed down and lose energy due to the aerodynamic drag force which is encountered primarily in the neighborhood of perigee. When a satellite loses energy, its orbital period decreases. Thus, the observed decrease in the period of a satellite orbit can be interpreted in terms of atmospheric density in the neighborhood of perigee. It was thought prior to the IGY that the atmospheric density varied with height, but not significantly with latitude, longitude or time. Measures of air density were available from the sounding rocket programs pursued prior to the IGY. The IGY orbits were to have perigee altitudes of about 200 miles and apogee altitudes of about 1400 miles. This perigee height was selected since it would permit the study of atmospheric density in the region near 200 miles altitude, which was above the level for which the sounding rocket data were available.

The satellites were designed to be spherical. The effective cross-sectional area presented to the aerodynamic flow would thus be constant and predictable, even though the satellite's attitude or orientation would not necessarily be known.

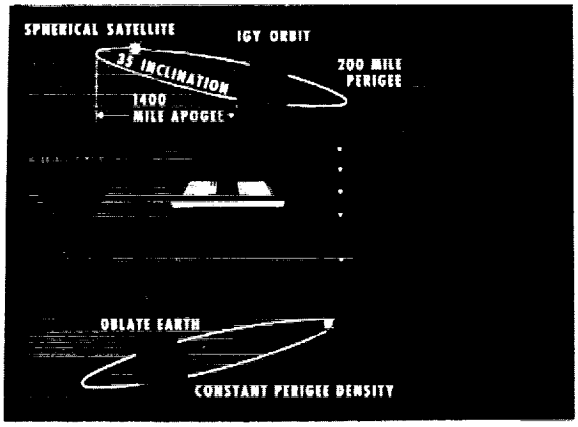

FIGURE 23–1.—Orbit determination.

The inclination of 35° was the maximum which could be achieved safely with the launching rocket vehicle systems then contemplated.

Orbit determination systems have been called upon to do many things since the space age began. There is always interest initially in the early estimates of the principal orbital parameters such as the period, the perigee and apogee heights, and the inclination. In addition, it is necessary to provide accurate predictions for the tracking and data acquisition stations in order to insure that additional tracking and telemetry information will continue to flow into the data gathering and processing systems. General viewing predictions also provided for satellites which can be seen visually by observers around the world. It was also necessary to furnish detailed ephemerides for the experimenters whose instruments operated in the IGY scientific satellites. Information consisting of the longitude, the latitude and the altitude of the satellite at each minute of its active radio lifetime is normally furnished to each scientist conducting an experiment with satellite-borne instrumentation.

It was anticipated that analysis of satellite orbital tracking data would yield new information concerning air densities and the shape of the earth. In particular, it was hoped that it would be possible to obtain more accurate measures of the oblateness of the earth.

Orbit determination includes the analysis of the tracking system which is used to furnish the data upon which the ephemerides and analyses are based. Accordingly, it was anticipated that important information about the tracking system would be derived from the orbit determination program.

These, then, were and still are the principal aspects of the science of orbit determination. As the space programs have become more sophisticated and complex, a number of facets of orbit determination have developed correspondingly.

A number of surprises were in store for those analyzing orbital data as they sought to glean geophysical information. For example the very first satellite showed that the atmospheric density was greater than previously supposed by a factor of the order of five. The oblateness of the earth was found to be significantly different from the estimates obtained on the basis of geodetic information. A number of additional geophysical discoveries were made. Some of these are indicated in figure 23–2. For example, it was learned from orbital information that the earth is actually pear shaped. Quantitative information has now been obtained about a number of the zonal harmonics of the earth's gravitational field. Further studies have also begun to shed more light on the ellipticity of the earth's equator. A number of new and important discoveries were made concerning the earth's atmosphere, using orbital data. It was found that the atmosphere actually bulges on the side of the earth which faces toward the sun. The bulge effect is greatest in longitudes that correspond to the early after-

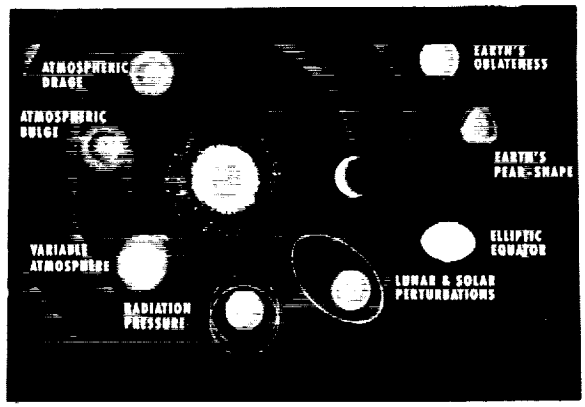

FIGURE 23–2.—Environment factors affecting orbit determination.

noon hours. This was discovered by observing that the satellite orbital period decrements, and hence the corresponding atmospheric densities, increased as the perigees of elliptical satellite orbits moved from the dark side of the earth around toward the bulge. In addition, it was observed that the atmospheric density actually increased rather sharply shortly after certain types of solar flares were observed to occur on the sun. This is indicated in figure 23–3. In addition to specific changes in atmospheric density in response to individual solar events, a general correlation was found to exist between solar activity and atmospheric density at high altitudes. The active regions on the sun are not homogeneously distributed with respect to longitude. They occur more frequently in some solar longitudes than in others, for example. These clusters of active regions rotate with the sun, whose rotational period is 27 days. It has been found that the atmospheric density at high altitudes varies with a period of 27 days, and that the correlation with solar activity is marked. This correlation is more pronounced in the neighborhood of the atmospheric bulge. The pressure of radiation upon a satellite is small and is often considered to be negligible. Acting over a long period, however, it does produce a detectable effect, even upon the orbit of an ordinary satellite. Radiation pressure can result in a significant perturbation of the orbit in the case of a low-density satellite such as Echo. Lunar and solar perturbations can also be observed, even on the orbits of close earth satellites.

Thus, there has been an unfolding panorama of changes in the natural environment as it affects satellite orbit determination.

As the space programs have evolved, numerous decisions were made concerning the design of the satellite and the orbit. A number of these had important effects upon the problem of

FIGURE 23–3.—Variable atmospheric drag effects on satellite orbits.

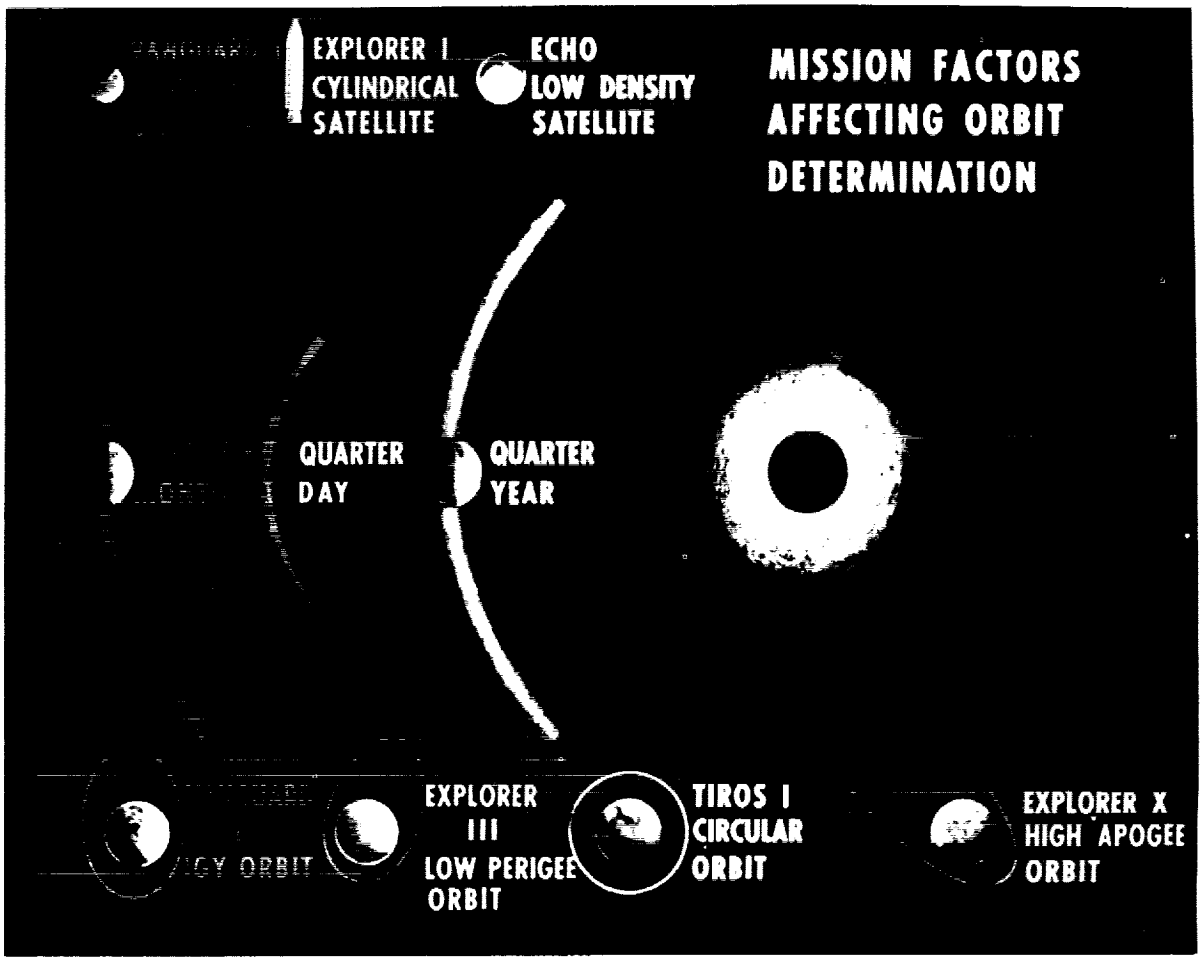

FIGURE 23–4.—Mission factors affecting orbit determination.

orbit determination. Some of them are indicated in Figure 23–4. For example, the original designs called for spherical satellites. Shortly after the space age began, however, long, slender cylindrical satellites were put into orbit. These were tumbling satellites whose orientation was not known. Accordingly, the effective cross-sectional area which they presented to the aerodynamic flow was not known or predictable. This complicated the problem of predicting the satellite's future position. It also rendered more difficult the interpretation of satellite deceleration data in terms of atmospheric density. The Echo satellite had a much lower areal density than any of its predecessors. As a result, even though it was launched into a nearly circular orbit at a height of about 1000 miles, it was significantly affected by atmospheric drag. In addition it was affected in a striking way by radiation pressure. The radiation pressure effect, barely discernable for ordinary satellites, produced a depression of Echo's perigee of literally several hundreds of miles. The variation of the perigee and apogee heights of Echo due to this effect can be seen in Figure 23–5.

Many of the orbits themselves varied significantly from the type initially planned for the IGY. For example, the orbit of Explorer III had an unusually low perigee height of about 117 miles. The low perigee of Explorer III resulted in an extremely large drag effect. The period deceleration was of the order of a thousand times greater than that which was encountered in the case of other IGY satellites. The first Tiros satellite, designed to obtain new information about cloud cover and weather, brought new problems from the orbit determi-

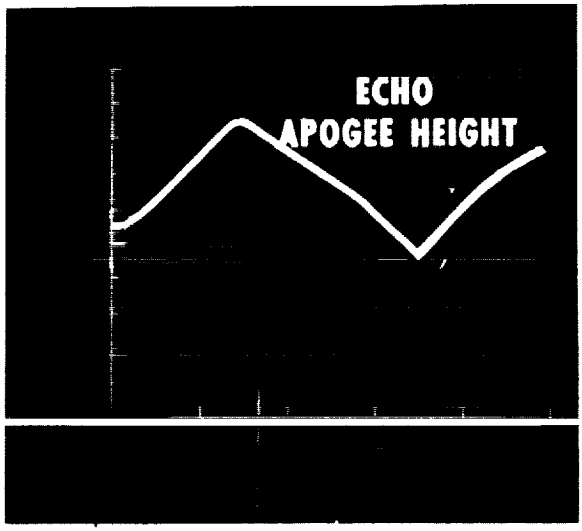

FIGURE 23-5.—Radiation pressure effect on ECHO orbit determined.

nation standpoint. The orbit of this satellite was very nearly circular. This meant that certain orbit determination theories, which had been developed originally for the elliptic satellite orbit case, had to be modified appropriately to handle this type of orbit.

Following the initial scientific satellite studies, interest grew in the regions well beyond the immediate neighborhood of the earth. Accordingly, high apogee satellite orbits were planned. Explorer VI, for example, was launched into an orbit having an apogee height of about 24,000 miles. This was followed by Explorer X, whose apogee was at 180,000 miles from the earth, or three-quarters of the way to the moon's orbit. In this satellite, the experimental equipment operated until the satellite reached the neighborhood of apogee on the first orbit, or for a period of approximately two and a half days. Explorer XII was launched into an orbit having an apogee of about 48,000 miles. Its experimental equipment operated for over three months. The orbit of each of these satellites was significantly affected by the lunar and solar perturbations. Accordingly, it was necessary to include the effects of these gravitational forces in determining the orbits of these new high-apogee satellites.

The original IGY plans called for a satellite with an active life of about a fortnight. As the useful lifetimes of satellites increased, and the periods over which their orbits were determined increased correspondingly, it became customary to determine orbits on a weekly basis. This meant that differential corrections were performed each week, using the data covering a one week interval. The orbit determination theories were adequate to handle this type of orbital time span. These separate arcs were discontinuous. The minimum distances between them in the regions where they overlapped were of the same order as the uncertainities in position in the individual arcs, however. Thus, a piece-wise continuous representation of the orbit could be obtained by means of a sequence of week long orbital arcs. For certain purposes, however, the precision obtained in this way was not sufficient. For example, in carrying out certain types of magnetic experiments in satellites it was found to be desirable to obtain a truly continuous representation of the orbital path over the entire active lifetime of the satellite. This was done in the case of the satellite Vanguard III, for example. In this case the orbital arc considered had a duration of approximately a quarter of a year. New theoretical methods had to be developed to handle this type of case. Some indication of the severity of the problems associated with orbital arcs of this length can be had by recalling that classical astronomy deals with observations of the planets extending back about two centuries. A close earth satellite completes as many orbits in a fortnight as a terrestrial planet does in two centuries. On this basis a quarter of a year for the close earth satellite corresponds to more than a millenium for a terrestrial planet. The difficulties were further increased due to the fact that atmospheric drag force is an important one for artificial satellites, whereas forces of this type are not nearly so significant for the planets and their natural satellites. These new, long orbital arcs required new theoretical developments.

At the other end of the scale, considerable interest has been focused on orbits lasting only a quarter of a day, such as those encountered in Project Mercury, for example. The original Project Mercury mission involved the completion of three orbits of the earth by the astronaut. Some of the theoretical problems associated with

long arcs were not present in this case. On the other hand, however, a number of additional problems had to be considered, in view of the fact that the astronaut's safety was at stake. Special measures had to be taken to insure that adequate information concerning the orbit and the trajectory was available at all times from the moment the launching rocket left the pad until the capsule returned to the surface of the earth in the recovery area. In order to insure that adequate supplies of tracking data were available to meet this objective, extensive use has been made of radar tracking systems. A network was established consisting of some ten radars which were capable of tracking the Mercury capsule during its first orbit. The first of these radars tracked the Atlas rocket as it left the launching pad and traversed the satellite launching trajectory. As the satellite capsule was projected into orbit, it could actually be tracked by two such radars. These radars were capable of obtaining ten complete sets of measures of range, azimuth and elevation each second. These radar measures were of high precision. Thus, within less than a minute after the Mercury satellite entered its orbit, sufficient information was available to determine whether, in fact, the satellite actually was in orbit and, further, whether the orbit was satisfactory from the standpoint of the mission objectives. This information had to be available on this time scale in order to permit the making of the vital decision as to whether the mission should be continued, or whether the manned capsule should be brought safely back to earth in an emergency recovery area in the Atlantic Ocean. Once in orbit the Mercury satellite was tracked again and again by means of precision radars, each of which was capable of obtaining, by itself, enough information to permit the determination of an accurate orbit. In all, ten such radars tracked the Mercury capsule during its first orbit, as is indicated in Figure 23–6. The handling of this tracking information and the

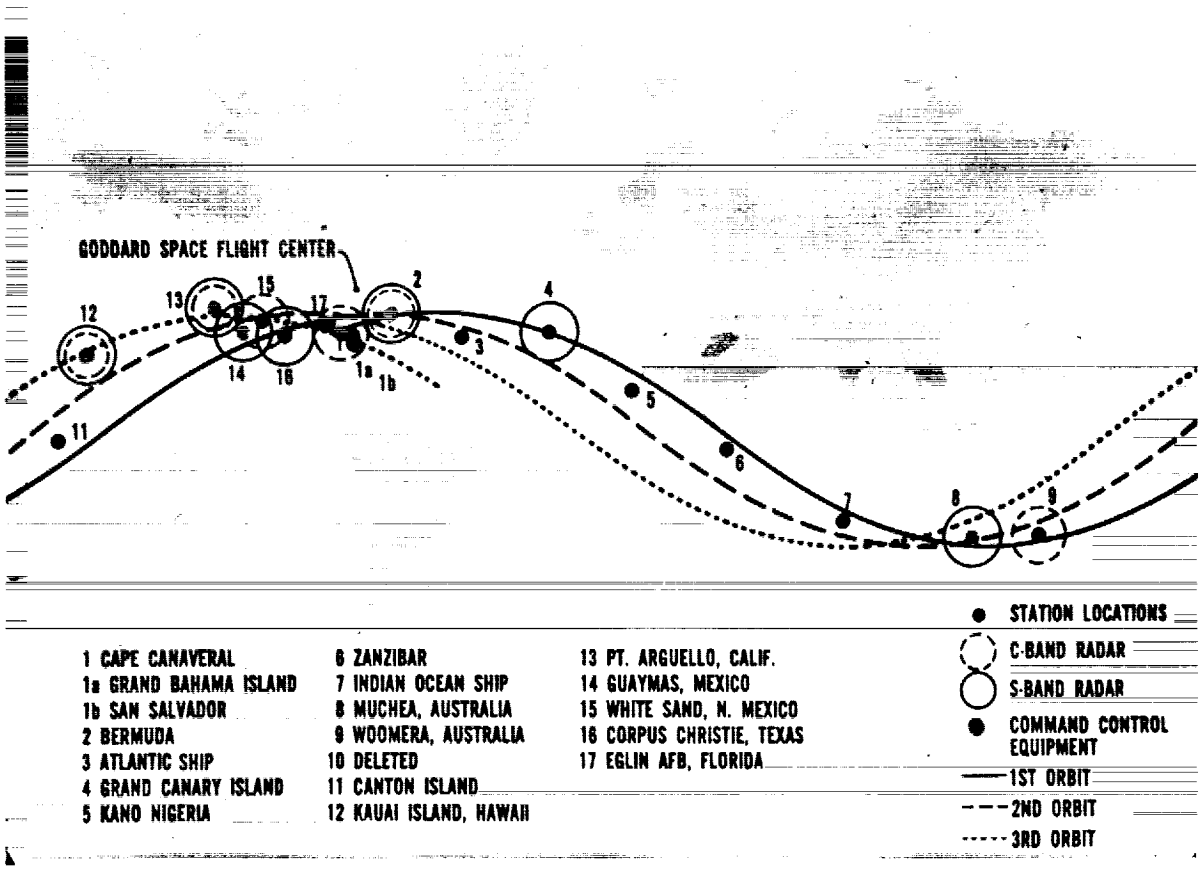

FIGURE 23–6.—Project Mercury.

making of the critical recommendations concerning go and no-go decisions on a real time basis requires the development of extensive computer program systems. These must be capable of rapid, precise orbit determination. This includes the assessment of the accuracy of the incoming tracking data, the determination of the orbital elements, the prediction of the satellite's position in order to permit acquisition by radars, and the making of critical recommendations involving the go, no-go decisions, the time at which the retro rockets should be fired to cause re-entry into the desired recovery region, etc. These programs must all be properly connected in the master, overall Mercury programming system so that they will operate automatically in the real-time situation.

This type of orbit determination operation is in marked contrast to the type conducted for scientific satellites. Scientific satellites are normally tracked by means of the Minitrack system, which operates using the principles of radio interferometry. As a scientific satellite passes over a Minitrack station, measures are obtained giving the direction from the Minitrack station to the satellite. No range information is obtained during such a tracking pass. The Minitrack system utilizes fixed-beam antenna installations. These have several advantages. They do not require special acquisition aids, as do radars of the Mercury type. They will track automatically whenever the satellites enters the antenna beam. The Minitrack system can operate using an extremely light transmitter in the satellite itself. Scientific satellites are generally much smaller than their manned counterparts. The original IGY satellites, for example, weighed about 20 pounds, whereas the Mercury capsules weigh more than a ton, or over a hundred times the weight of the original scientific satellites. In fact, in the Mercury Capsule, the weight of the tracking equipment alone is greater than the entire weight of America's first scientific satellite. Even though the weights involved are different by approximately two orders of magnitude, the Minitrack system for tracking scientific satellites is capable of great precision. In general, however, weight is traded for the rate at which tracking information becomes available to the central computing system. Ordinarily, a scientific satellite is observed roughly once per orbit. Hence, it is necessary to observe the satellite over a time interval corresponding to three or four orbits before reasonably good orbital information can be obtained. This is in marked contrast to the Mercury tracking system which is capable of providing accurate orbital information on the basis of a single radar pass. These two types of orbit determination operations require quite different approaches from the analytical, mathematical, and computing standpoints.

Still a different array of techniques is used to track high-apogee satellites. Satellite orbits extending out to distances of ten earth radii or so have dynamical properties which are significantly different from those of close-earth satellite orbits. For example, once a satellite is more than a few earth radii from the earth, its rate of angular motion is slow. Accordingly, angular tracking systems are less appropriate here than they are for close-earth satellites. The range and the range rate of a high-apogee satellite are, however, changing appreciably over most of the orbit. Accordingly, it is desirable to measure these quantities. It is for this reason that doppler and ranging systems have been developed for tracking spacecraft travelling out toward the moon and deep into space. The Goddard orbit determination system has utilized data of this type in determining orbits of satellites and spacecraft. A new range and range rate tracking system is presently being developed by Goddard especially for use in tracking high-apogee scientific and applications satellites in the forthcoming OGO and Syncom programs.

The present Goddard orbit determination system now in operation includes the basic elements of the type described earlier. In each of the principal areas, however, there has been a significant increase in the complexity of problems to. be considered and a corresponding increase in the complexity of the theories and the computer programs developed for orbit determination. This is indicated in Figure 23–7. For example, the original system was designed to use Minitrack data primarily. At the present time the system is capable of using many different types of data including not only

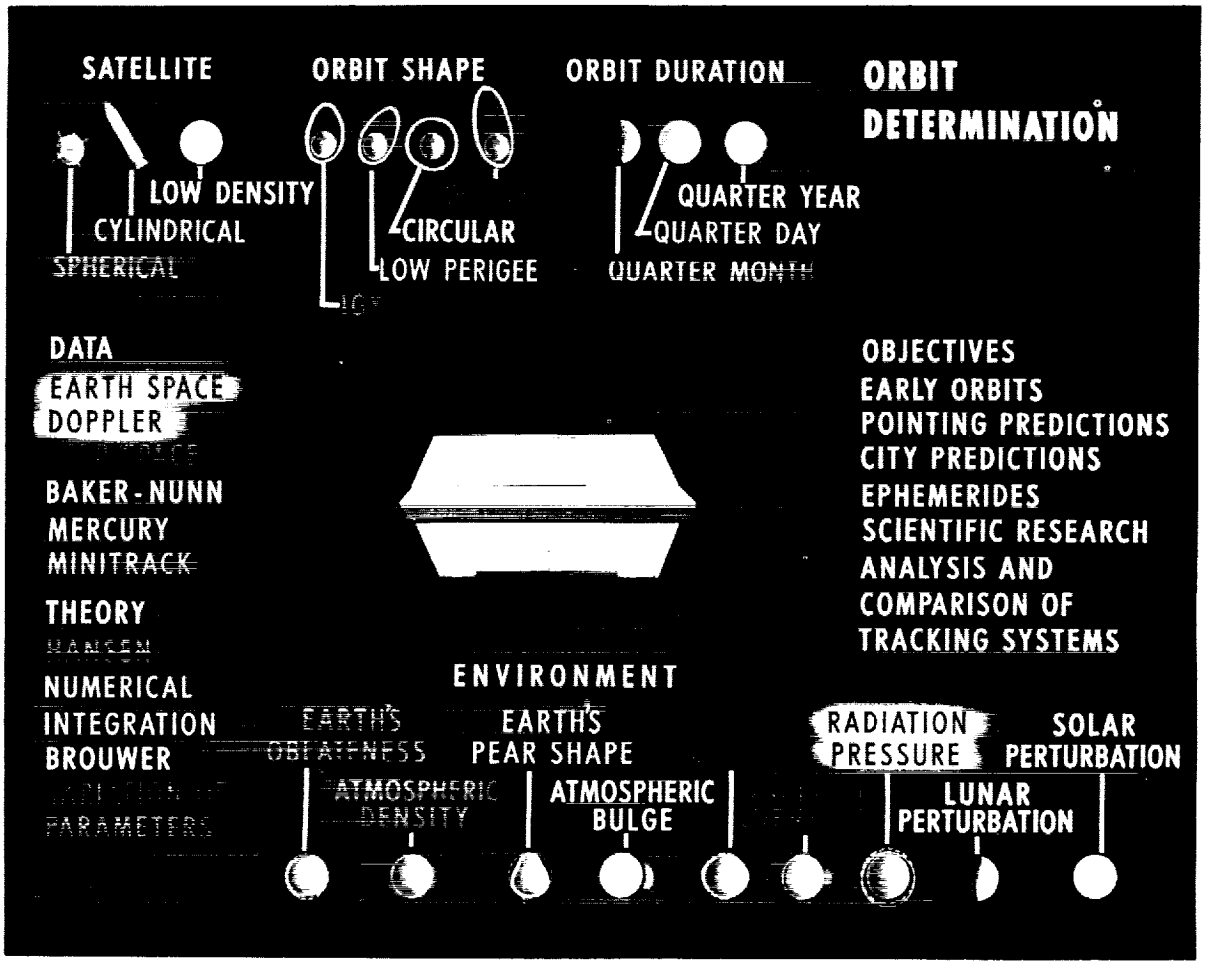

FIGURE 23–7.—Orbit determination.

Minitrack data but also the Mercury radar tracking data referred to earlier, Baker-Nunn precision optical tracking data, data from a number of doppler, range and range rate systems, and data from the Deep Space Information Facility developed by the Jet Propulsion Laboratory of the California Institute of Technology.

In the theoretical area, the original modification of Hansen's theory developed to apply to the close-earth satellite case is now but one of a number of different theoretical methods available for use in the Goddard general orbit determination system. Some of these are indicated in Figure 23–8. A numerical integration method is also available. Some refinements have been added to this method in order to permit control of the buildup of round-off error. A new method developed by Prof. Brouwer of Yale University is also in extensive use. The method of variation of parameters is also used to handle special problems arising in connection with high-apogee satellites, satellites perturbed significantly by radiation pressure, etc.

The environment now is clearly recognized to be far more complex than had been suspected at the time the space age began. The Goddard orbit determination system now takes into account the many new types of perturbations referred to above. Modifications have also been incorporated to deal with the many types of satellites, the different types of orbits and the various orbit intervals discussed above.

Orbit determination objectives have become more numerous in response to the increasing

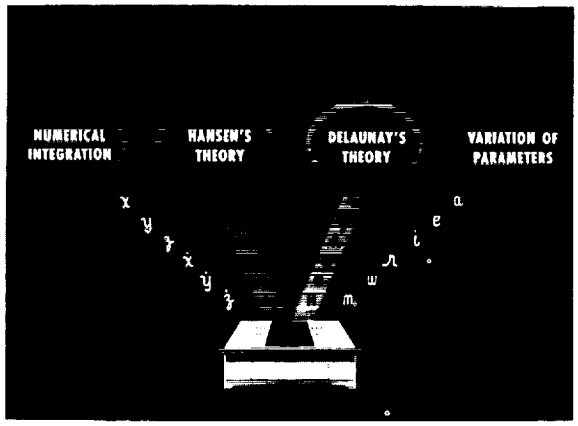

FIGURE 23–8.—Orbit determination theories.

needs of the space programs. The problem of determining initial orbits has grown more complex as the launching trajectories and the orbits themselves have become more varied and complex. Antenna pointing predictions must now be furnished for a wide variety of antenna systems including not only those which are based on direction cosines, azimuth and elevation, and right ascension and declination, but also those which are based on hour angle and declination, prime vertical angle and meridian axis angle, and meridian angle and prime vertical axis angle. Some of these antenna systems are indicated in Figure 23–9.

It is also necessary to furnish predictions with a much greater degree of precision than was necessary heretofore. For example, in the case of Project Echo, the satellite was tracked by means of large 84-foot dishes operating at frequencies in the neighborhood of 2300 megacycles. The beam width of such an antenna system is extremely narrow. The problem was further compounded by the fact that one of the operations involved the simultaneous pointing of two such dishes at the satellite. This mode of operation further decreased the

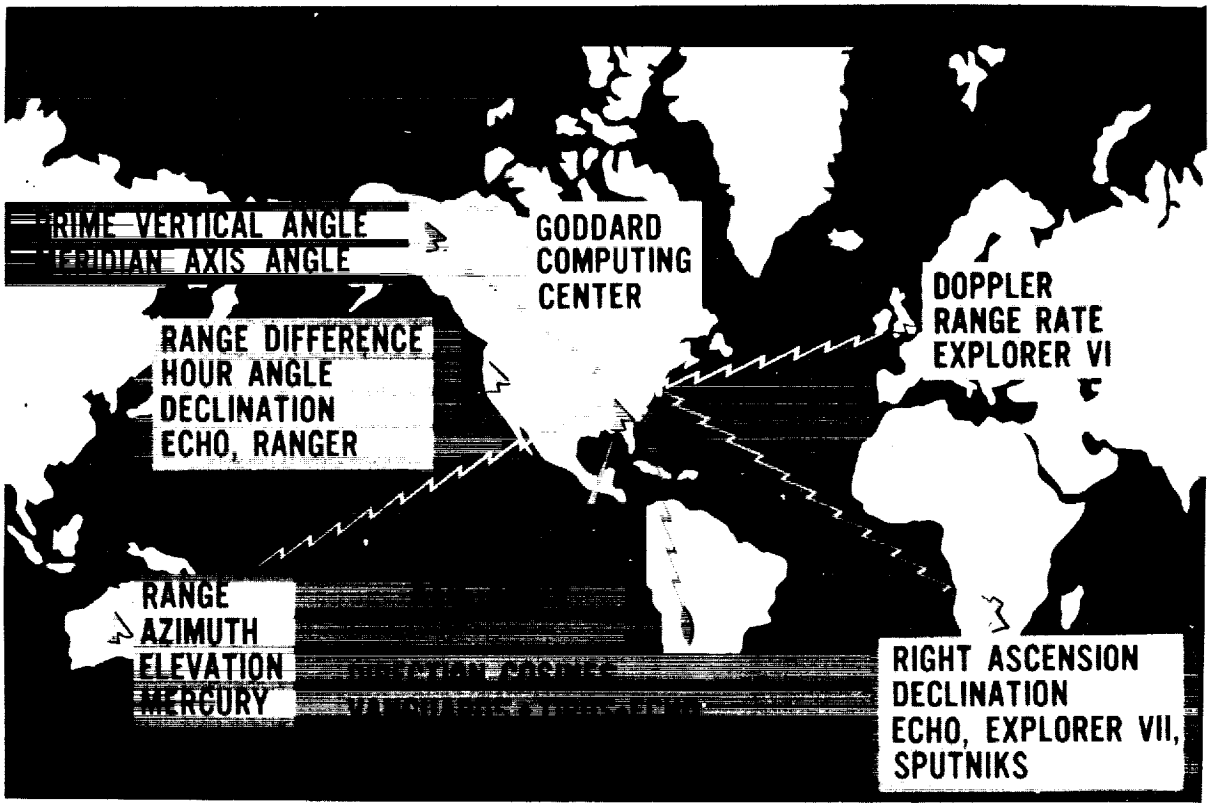

FIGURE 23–9.—Various types of tracking data.

effective beam width of the combined two-antenna system. The beam width of this combined system was approximately 0.15 degrees. Accordingly, it was necessary to furnish pointing predictions with this accuracy. The antenna systems used in Project Echo were not all capable of automatically tracking the satellite. It was necessary actually to point them at the satellite by means of drive tapes generated by the Goddard orbit determination system. These drive tapes were used to point the large antenna systems at the satellite from opposite coasts of the United States. This method was used to transmit messages from President Eisenhower and Senator, now Vice-President, Lyndon B. Johnson across the continent via the Echo satellite. This is indicated in Figure 23–10. Because of the large and unpredictable effect of atmospheric drag upon the orbit and position of Echo, it was decided to redetermine the orbit each day on the basis of the latest tracking information during critical operations. It was found that it was possible, using this approach, to predict the position of the Echo satellite with an accuracy of 0.15 degrees for periods up to a day in advance. On the same basis it was found possible to predict the position of more dense satellites such as Tiros with an accuracy of 0.1 degrees. Greater accuracy was possible in the case of these latter satellites due to the fact they are perturbed to a much smaller degree by the variable and unpredictable atmospheric drag forces. Since Echo was easily visible to the naked eye, great interest was shown in observing this satellite by people all over the world. It thus was necessary to predict the times at which Echo would be visible from cities around the world. Some of the cities for which Echo

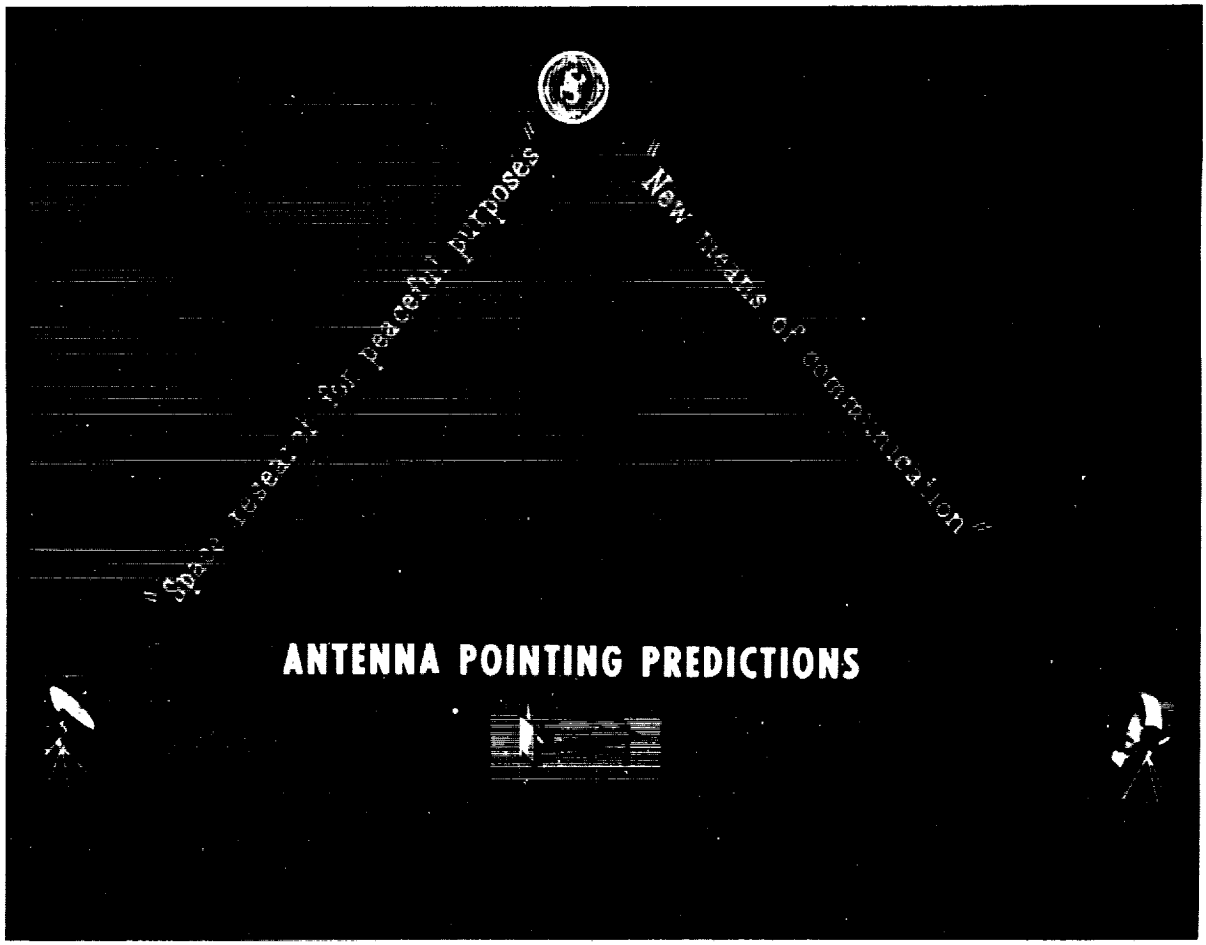

FIGURE 23–10.—Antenna pointing predictions.

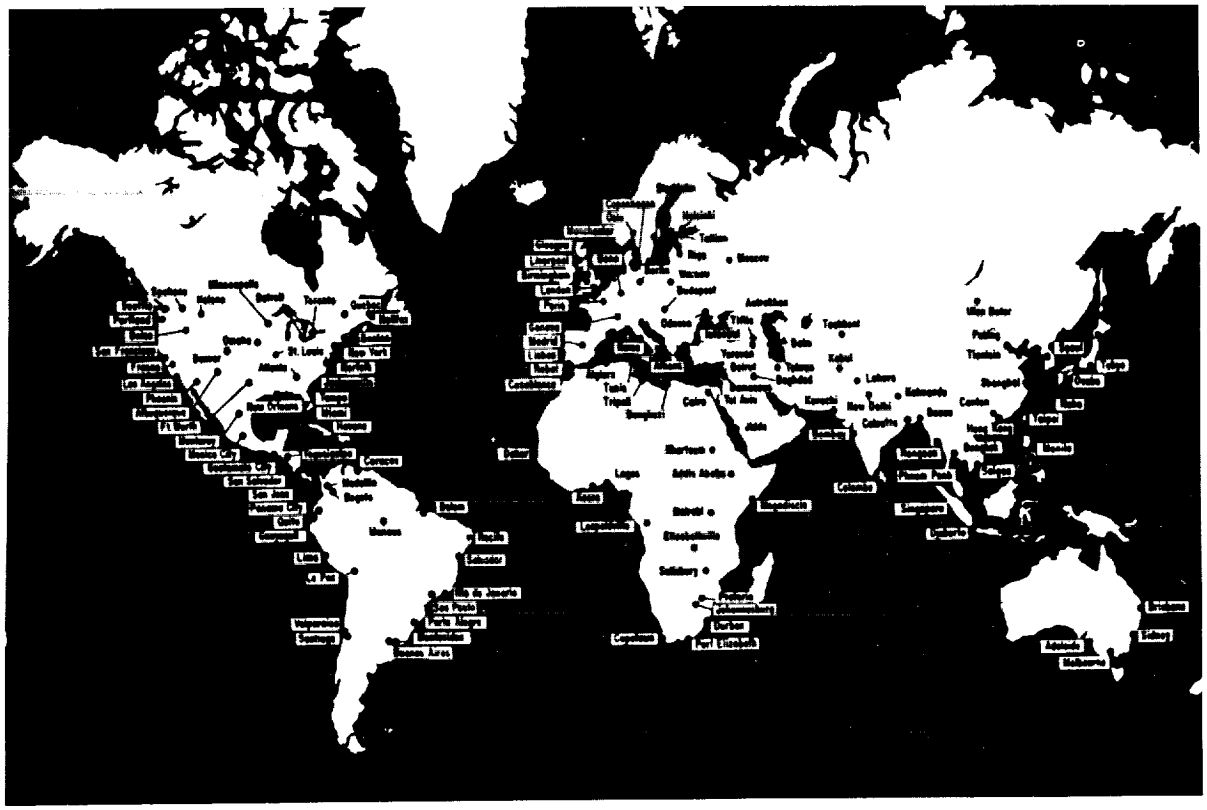

FIGURE 23–11.—Cities for which Echo predictions were computed.

predictions have been made are shown in Figure 23–11. Many of you may have seen and actually used such predictions which frequently appear in our local newspapers. Predictions of this type are furnished continuously for literally hundreds of cities around the world by the Goddard Computing Center.

Many scientific experimenters are now interested not only in the positions of their satellites in geographic space but also in the magnetic parameters of the satellite environment. In such cases it is customary to give the Greenwich time, the satellite position in terms of geographic latitude, longitude, and height, as well as the magnitude of the magnetic field vector and three components of this vector. In addition, certain other geomagnetic quantities of interest to particular experimenters are determined and furnished along with the other ephemeris information. For example, the coordinates of the satellite in B–L space are provided for experimenters studying the radiation belts, both natural and artificial.

The attitudes of satellites such as Tiros are determined on the basis of data obtained from special horizon sensing equipment mounted in the satellite. Detailed information concerning the attitude history of such satellites is also furnished in addition to the basic ephemeris information for use by certain experimenters.

Scientific research results of a number of different types have been obtained from detailed and definitive analyses of orbital tracking data. The contributions of Vanguard I in this connection, indicated in Figure 23–12, are especially notable, since this satellite contained no experimental apparatus, per se. All of the Vanguard I research results have been achieved through orbit analyses. New measures of the earth's oblateness were obtained using the Vanguard I orbital data. The earth was discovered to be pear shaped on the basis of Vanguard I orbital information. The atmospheric bulge and the correlation of atmospheric density with solar activity were discovered by means of Vanguard I tracking data. Solar radiation pressure ef-

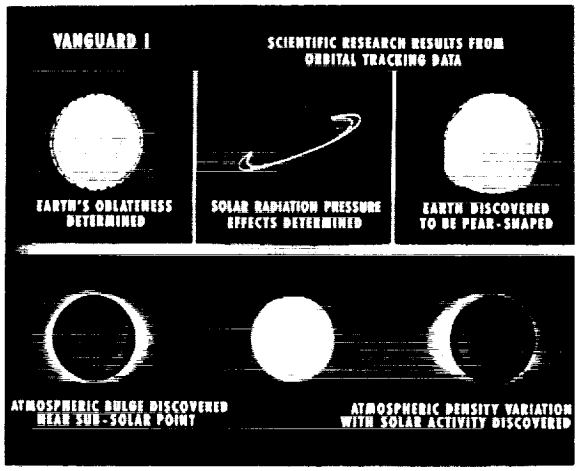

FIGURE 23-12.—Vanguard I scientific research results from orbital tracking data.

fects were first calculated in a definitive way for the Vanguard I satellite. A new measure of the scale of the solar system itself was obtained through analysis of the doppler observations obtained from Pioneer V. This spacecraft was launched into an orbit around the sun which carried it toward the orbit of Venus as is indicated in Figure 23–13. It was tracked to the unprecedented distance of more than 20,000,000 miles from the earth. Careful analysis of the doppler tracking data from this satellite yielded a new measure for the value of the astronomical unit, which corresponds to the mean distance of the earth from the sun.

The accuracy with which orbits are determined has steadily increased through the years. At the present time the uncertainty in a satellite's position as determined on the basis of Minitrack observations is of the order of 100 seconds of arc. The moon is approximately 1800 seconds of arc in diameter. Accordingly, the uncertainty of a satellite position in terms of directional or angular information corresponds to about 1/18th of the diameter of the moon. The corresponding uncertainty in satellite position for satellites at a mean distance of the order of a thousand kilometers is of the order of half a kilometer. This is comparable to the accuracies with which the positions of sounding rockets were known during the period before the IGY. The present precision of orbital information represents an increase of approximately an order of magnitude in accuracy over that which was achieved in the early days of the IGY. Analyses and inter-comparisons of different types of tracking systems have been conducted as new systems came into operation. It has been found, for example, that the Minitrack and Baker-Nunn tracking systems give consistent results.

A number of new, interesting orbit determination problems have arisen in connection with some of the newer NASA programs. In the future, it is planned not only to determine the orbits of satellites and spacecraft but also actually to control and to change them. Project Gemini planners, for example, contemplate the bringing together of two satellites in rendezvous operations. In general the orbits of the two satellites will differ initially. It will be necessary to determine the orbit of each of these satellites precisely. It will then be necessary to determine what changes should be made to the orbits of one or the other or both of the satellites in order to bring the two satellites together. Once the two satellites have been brought reasonably close to each other, the astronauts will take over and guide the satellites during the terminal phases of the rendezvous.

A number of new theoretical problems arise in connection with orbit determination systems now under development. The unsolved problems of principal interest currently are associated with the perturbative forces indicated in Figures 23–2 and 23–14. General perturbation theories have been developed which represent the zonal gravitational harmonics. It is desirable to extend these theoretical developments to treat the other types of perturbations indi-

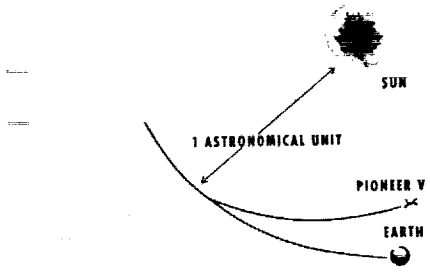

FIGURE 23–13.—Scientific research results from orbital tracking data—size of solar system determined.

cated in Figure 23–14. There is also interest in further development of special perturbation orbit determination systems as they apply to lunar orbits and trajectories. These problems being of a theoretical nature, lend themselves especially well to cooperative efforts involving both NASA centers and universities. NASA is already working closely with university groups in tackling them. NASA and Goddard are looking forward to continued and extended cooperative efforts involving Goddard and university research institutions.

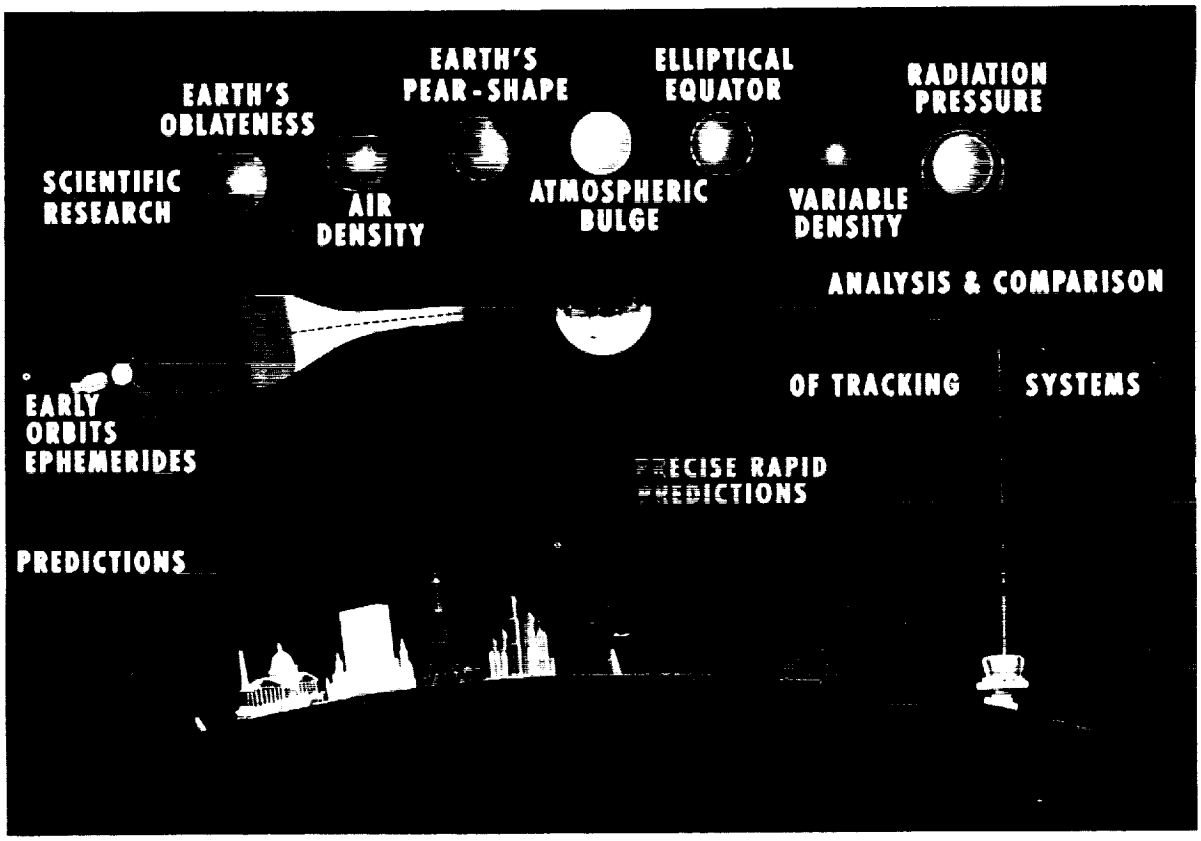

FIGURE 23–14.—Orbit determination.

N63-11107

24. Data Acquisition and Processing from Scientific Satellites

By Albert G. Ferris

ALBERT G. FERRIS *is the Chief of the Space Data Control Branch of the NASA Goddard Space Flight Center. He received his B.S. degree in Electrical Engineering from the University of Detroit in 1951, and is a member Eta Kappa Nu and Tau Beta Pi. Mr. Ferris is also the Ground Systems Manager for the Orbiting Astronomical Observatory and was responsible for much of the ground systems concept. As one of the senior design engineers in the Data Handling and Processing area at Goddard, he was responsible for the design of the Satellite Telemetry Automatic Reduction System and the number of special purpose data equipments and systems. Prior to this he worked at the Naval Research Laboratory on the design and development of data systems.*

INTRODUCTION

The world is becoming increasingly familiar with satellites of many types. Reference is made in the title of this paper to "scientific satellites" and it might well be asked "At this point aren't all satellites scientific?" This is true. Each in its own way, within its capability, contributes to the body or wealth of scientific knowledge. The distinction is, primarily, one of intent and emphasis. A scientific satellite is one whose intended mission is the extension of man's scientific investigation into space. It normally will carry modified or follow on experimental apparatus to that which he has been using on Earth. However, new instrumentation is not excluded.

The conditions of this investigation in space are somewhat different from the Earth-bound situation. The first difference lies in the fact that the satellite when placed in orbit follows a path through space (as opposed to sounding by rockets as controlled cruising in space) and control of the environment for any experimental measurement from a standpoint of either location or the elimination of unwanted disturbances is not possible. The second is that operation of the experimental apparatus must be accomplished over great distances. Because of these two facts experimental investigation in space is carried on in something less than ideal circumstances from the viewpoint of the experimenter. Our job is to make conditions more ideal. As on Earth, the satellite environment requires the orderly and careful collection of data. The result is that somewhat greater amounts of data are obtained in order to insure samplings at the desired position, and the experimental apparatus is exposed to a somewhat greater range of conditions.

The successful execution of the mission for a scientific satellite includes the acquisition and processing of the data collected. In order to deal with the difficulties mentioned above, to reconstruct as nearly as possible the environment of a particular measurement and to place in the experimenters hands intelligible, readable, legible, timely data taken where, when and in form desired, it is necessary to provide the following functions: (1) the satellite must be tracked so that its position can be accurately determined and predicted; (2) both the satellite and the experimental apparatus must be commanded to execute control; (3) the data must be telemetered to the ground; (4) the data must be processed in order to remove the in-

fluence of the transmission medium and the telemetry system (calibration and linearization) and; (5) the data must be analyzed for its information content. Each of these functions is greatly dependent upon the others. No single function can be ignored or performed inadequately without jeopardizing the entire mission.

DATA ACQUISITION

The tracking, command and telemetry functions are the essential parts of data acquisition. A geographically distributed network of stations for this purpose has been established. Dr. Siry in his paper has provided information on the tracking problem, especially in the area of satellite predictions which are very germane to the data acquisition problem. In figure 24–1 is shown a block diagram of the essential functional elements of a data acquisition station. A typical sequence of operation might be as follows. After contact is established with the satellite on the basis of the tracking predictions, the telemetry data would be received, conditioned, synchronized and displayed in order to determine satellite status. Immediately following this, commands would be initiated to establish the desired conditions in the satellite data handling system and to initiate playback of the scientific data either in real-time or from a storage media. If the satellite makes use of a stored command sequence for out-of-contact operation it would be inserted and verified at this time. For the remainder of the contact a variety of data operations would be undertaken to obtain further data or to exercise the experimental apparatus for calibration or diagnostic purposes. The role of time is shown by the block marked "time standard." Correlation of the time of occurrence of any specific measurement with its position as measured by the tracking data is accomplished on a time base, this base is provided by the block labelled "time standard." As shown, all of the data is recorded on magnetic tape so that it may be sent to the Central processing facility.

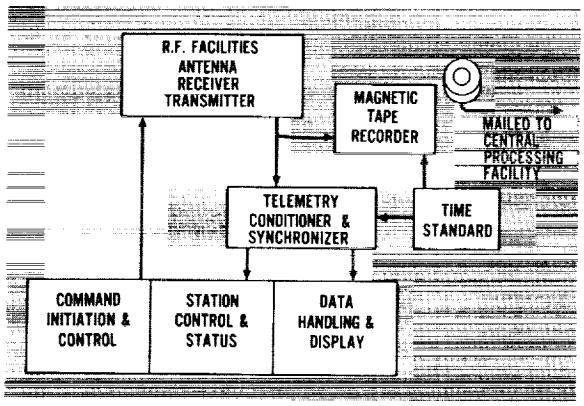

FIGURE 24–1.—Data acquisition station.

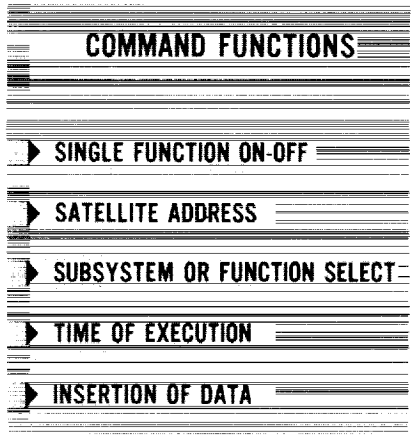

FIGURE 24–2.—Command scope.

The requirement in the command area is dependent upon the complexity and sophistication of the satellite and the experimental apparatus which it carries. It is through the command system that explicit and detailed manipulation of the spacecraft and its scientific payload is possible. Reliable unambiguous control is essential. In figure 24–2 is shown the scope of command requirements from simple satellite on-off to full insertion of operational data. Each element provides for greater flexibility and capability. Early satellites used a simple on-off command, if any, in order to conserve power, etc. As satellites become more complex and it became possible to program their operation both in real-time and in noncontact time due to the use of tape recorders or other storage media, additional detail and refinement of command capability was required. At the present time systems over the full range of command capability are being designed.

The primary means of communication from the satellite to the ground station is through the telemetry system. This link carries all of the scientific data as well as information con-

cerning the status and operation of the orbiting equipment. Primarily, two types of telemetry are handled by the network. The first and oldest of these is the Goddard pulse frequency modulation (PFM) system which originated with the Vanguard program and has been very useful where compact size, low weight and low power consumption were essential.

The second is the pulse code modulation (PCM) system which will be used very extensively beginning in the next year. Standards for both of these systems as applied to scientific satellites have been prepared by the Goddard Space Flight Center. The specific design of the telemetry system is a function of the satellite requirements. A diversified capability in the ground system is a necessity. In figure 24–3 is shown a summary of the characteristics of a typical telemetry station in the network. In most cases, nominal or approximate figures are shown. Considerable variation in each area and in combining of parameters is possible depending upon the particular station used, and the type of transmission, data rate, etc. required by the satellite. The use of 1700 megacycles for video transmission shown in the figure is not a general network capability as yet; it will generally be used for TV and similar applications.

The quality of data transmission is very dependent upon satellite systems design and ground system parameters. As shown in figure 24–3, large, high gain antennas are used where possible. Figure 24–4 is a view of an 85′ antenna. Three such antennas are installed or planned at the present time for Alaska, North

ANTE TYPE	ANTE GAIN (APPROX.)	FREQ. (NOMINAL)	BAND-WITH	MOD.	TYPE TRANS.	NOMINAL DATA RATE
YAGI ARRAY	15db.–25db.	136 mc	1 MC	AM/FM/PM	PFM/PCM	PCM-200 KPS
		400 mc	1 MC	AM/FM/PM	PFM/PCM VIDEO	PFM-50 SAMPLES SECOND
PARA-BOLIC DISH	35db–45db.	1700 mc	– – –	AM/FM/PM	VIDEO	VIDEO-SYSTEM PARA.

FIGURE 24–3.—Telemetry systems characteristics.

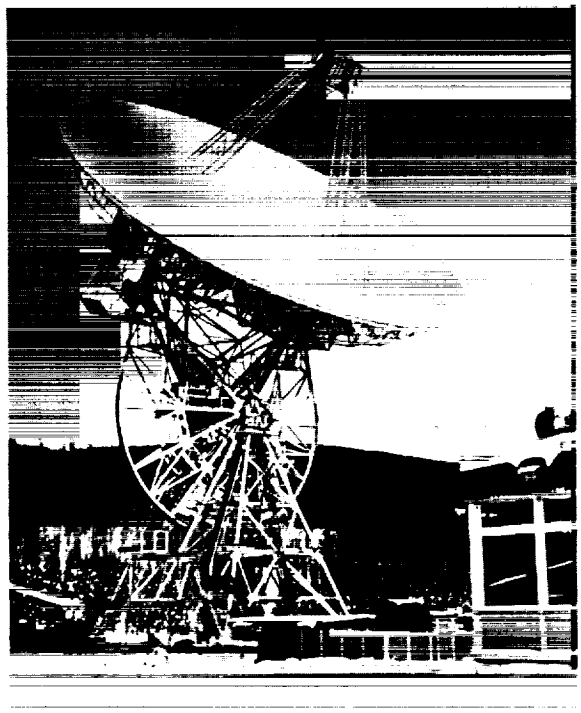

FIGURE 24–4.—85 foot antenna at Alaska.

Carolina and the Western Pacific. Smaller dish antennas of approximately 40 feet dia. will be installed at South Africa, Chile and Australia. The use of these antennas combined with signal conditioning techniques help to overcome the difficulty of varying and/or poor signal-to-noise ratios.

The function of signal conditioning is shown in figure 24–1 as the telemetry conditioning and synchronizing block. Although the scientific data is recorded prior to passing through this unit, it is essential that sufficient data be processed and displayed at the station so that performance of the overall system including the satellite equipment can be monitored. This information together with instructions and ground rules provided by the experimenter are used to determine and formulate the command program. A very complex spacecraft such as the Orbiting Geophysical Observatory or the Orbiting Astronomical Observatory requires complex and extensive instrumentation including ground computers, in order to accomplish these functions. For less sophisticated satellites many of these functions are provided by the on-site operator. In figure 24–5 is an interior view of one of the network stations show-

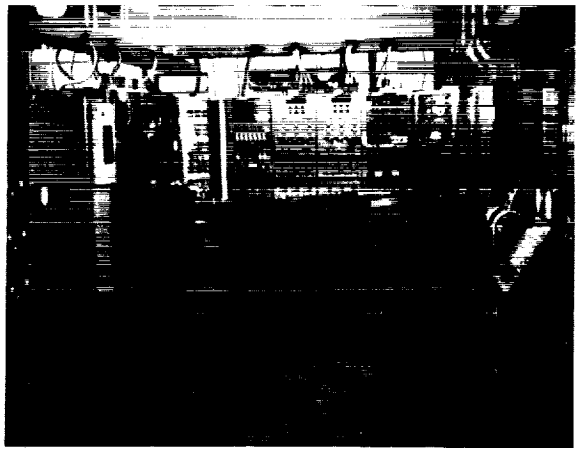

FIGURE 24–5.—Inside view of telemetry station.

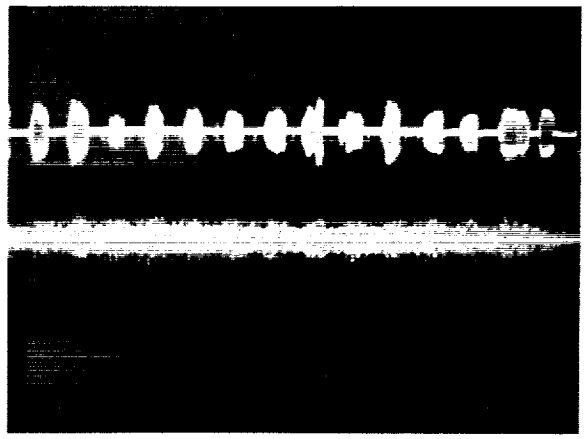

FIGURE 24–6.—Noisy data (PFM)—Explorer XII.

ing equipments used to fulfill the functions discussed. This instrumentation is typical of that used for the smaller scientific satellites.

DATA PROCESSING

The volume of data obtained from scientific satellites can be, and quite often is, very large. The variety in this data is limited in scope only by the ingenuity and inventiveness of the experimenters. Since the objective is the extraction of quality data, and not the test of system capability near its threshold, signals of "good or better" signal-to-noise ratio are demanded. This may be achieved by a general overall improvement of the communication system and/or the use of signal conditioning and enhancement such as indicated above. It is still necessary for the processing system to deal with signals of marginal SNR. This, of course, greatly complicates the overall processing picture in that uncertainty as to data results and difficulty in processing causes multiple reprocessings of the same data. An example of low SNR signal input to the data processing system is shown in figure 24–6. This shows the improvement possible in SNR by the use of signal conditioning equipment. This is an example of the PFM signal received from Explorer 12.

As early as possible, the processing system should provide a compact, unaltered, rapid-access library of all the data. It should also provide a versatile and flexible means of data manipulation. As stated previously, an essential consideration in the processing of satellite telemetry data is correlation of telemetry data with satellite position. In general, the tracking solution is obtained independently as a function of time. Therefore, the ground processing system is required to insert ground time in the telemetry data. A digital form of the data as early as possible answers all of these requirements. The problem is not technically different from what has been done in this field thus far. However, the scope is quite a bit wider than that encountered previously. The approach taken provides flexibility making it possible to utilize a general-purpose computer for data shuffling and/or "bit fiddling".

The functional requirements of the Central data processing facility are shown in figure 24–7. The data is received on one-half inch tape as recorded directly out of the receivers

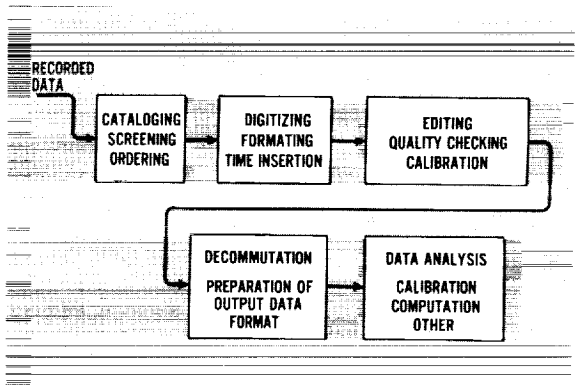

FIGURE 24–7.—Data processing functions.

with ground time recorded in parallel. The first requirement is to catalog, screen and order the data according to the manner in which it was taken. The importance of this operation is apparent when it is realized that data is received in a disordered fashion due to the fact that it takes varying times for the recordings to reach the Central facility from the field station. It is at this point that both functional or operational efforts are located.

The next step in the process is the conversion of the data, if required, to a computer format. It is at this point that ground time is inserted uniquely with the data as required. A system for preparing the data for computer entry has been developed at the Goddard Space Flight Center. This equipment is shown in figure 24–8. A more detailed description of this equipment is available in a paper by Creveling, Ferris and Stout (ref. 1).

The remaining operations make strong use of general-purpose computers. The objective of these operations is to produce for the given experimenter data in a suitable form. Significant effort is made to assure that the data is consistent in time because of the importance of this parameter in the overall operation. In addition, calibration of the data in order to remove the influence of the telemetering medium is applied. The analysis of the data is generally considered to be the responsibility of the experimenter. Where possible and desirable, some analysis of the data is performed under his direction. A number of data output forms from the complete process are available. These are shown in figure 24–9. The most generally available and useful form is digital magnetic tape in computer format. On this magnetic tape, in addition to the scientific data, there are entered various housekeeping data and other pertinent information such as attitude data as computed. The other types of data output are print-out of the data types as shown, and plotted data. An example of printed summary data is shown in figure 24–10.

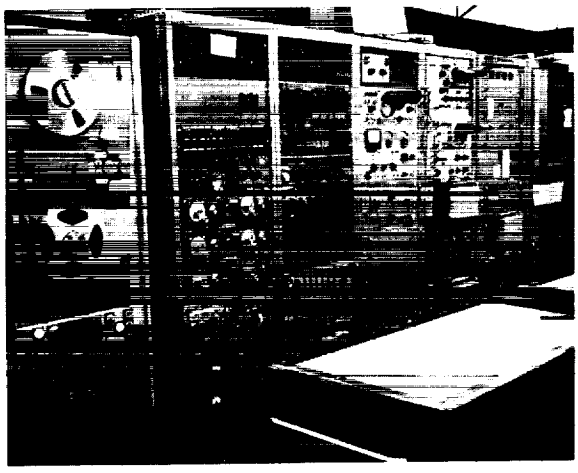

FIGURE 24–8.—Data processing equipment.

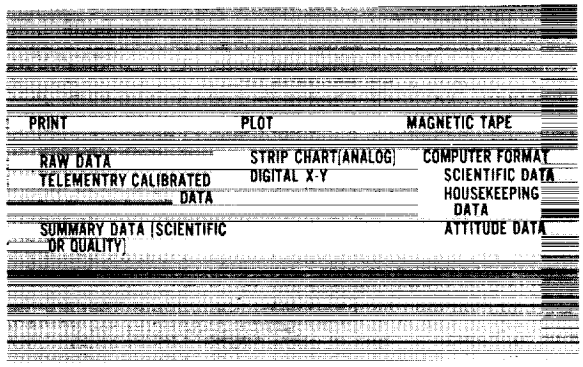

FIGURE 24–9.—Data processing output forms.

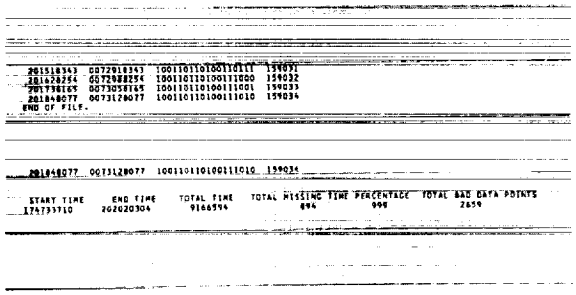

FIGURE 24–10.—Typical data page.

CONCLUSION

The development of a system to perform the functions indicated presents many technological difficulties. These are associated with the difficulty in achieving adequate signal-to-noise ratio signals, the volume of data required to be taken in order that the "kernel" of data is obtained, and the wide variation in processing requirements. In each area specific technical

problems are being attacked with some success. In addition to these specific technical areas there are areas where development of equipment and techniques would increase the efficiency of the processing operation. These are shown in figure 24–11.

The inclusion of much extraneous data makes it highly desirable to be able to screen the complete data telemetered in order to select the usable portion. If this is accomplished early in the process, a better utilization of the greater portion of the processing capability can be achieved. Because the volume of data involved is significant a rapid data screen is desirable. Careful consideration of this possibility in both ground systems design and satellite data systems design is important.

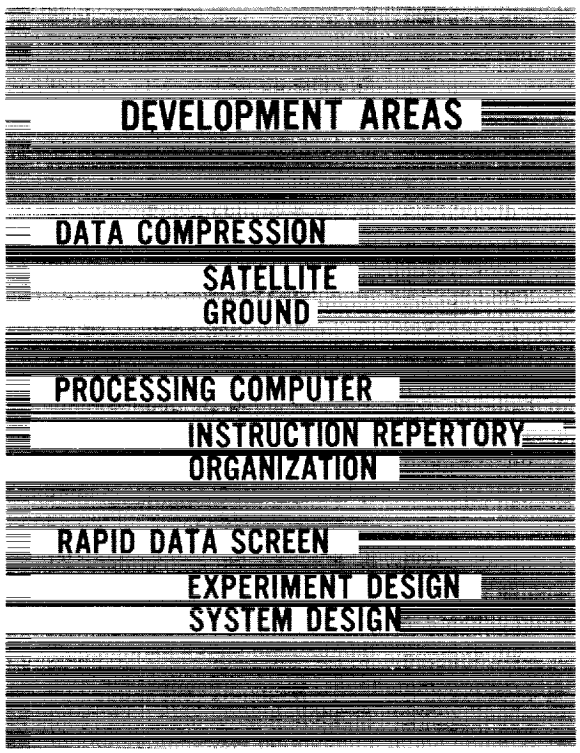

FIGURE 24–11.—Summary of problem and work areas.

A related area of concern is data compression. This might be called an extension of the rapid data screen to the satellite itself. Criteria for data compression are a function of the experiment and its environment. Work in this area is vitally concerned with the basic information content of the data, and a determination of the means for practically measuring and conveying that information in an adaptive manner. An early testing of any development in this area might be accomplished by applying the techniques to the screening of data at the data acquisition site in order that the limited communications capability available could transfer to the user a greater knowledge of the experimental results in any given time.

The utilization of a general-purpose computer throughout a significant portion of the data processing operation has provided a great deal of capability and flexibility. As more experience is gained with the specific and unique requirements of processing data from scientific satellites, it becomes clear that a machine of somewhat special capability might be required. This effort will concern itself with the basic organization of the machine from the standpoint of volume-data input and output, and the fundamental instruction repertory required to facilitate many of the data processing operations. You are invited to participate with us in our overall program of development.

REFERENCE

1. CREVELING, C. J., FERRIS, A. G., and STOUT, C. M.: Automatic Data Processing. IRE Trans., Professional Group on Space Electronics and Telemetry, vol. SET–8, no. 2, June 1962.

25. Data Processing from Meteorological Satellites

By William R. Bandeen

WILLIAM R. BANDEEN *is engaged in the reduction, analysis, and interpretation of data from the Tiros meteorological satellites and in the planning for future generation meteorological satellites. He was graduated from the U.S. Military Academy in 1948 with a B.S. degree in Engineering. In 1955 he earned an M.S. degree in Meteorology from New York University and during the next three years was assigned to an IGY upper air rocket research program at the Army's Signal Research and Development Laboratory. Since joining the NASA Goddard Space Flight Center in 1959, he has been associated with the meteorological satellite program. He is a member of the American Meteorological Society, American Geophysical Union, and American Rocket Society.*

SUMMARY

The capability of the Tiros meteorological satellite to observe vast oceanic areas and uninhabited land masses, where much of our weather originates, and the increased capability of the second generation Nimbus meteorological satellite to observe virtually the entire world twice daily have opened new vistas for man in his constant probing to unlock the secrets of the atmosphere around us. With these new sources of information, however, have come major problems of reducing, analyzing, disseminating, storing, and retrieving the increasingly vast quantities of data gathered on a continuing basis by meteorological satellites. This paper discusses the Tiros satellite and the flow of data through its different sensory subsystems and concludes with a brief look at plans for the future Nimbus satellite system.

INTRODUCTION

The successful orbiting and operation of six consecutive Tiros meteorological satellites by the National Aeronautics and Space Administration have opened broad new sources of information to man in his constant striving to observe, describe, understand, forecast, and—perhaps even in some measure—control the physical processes that take place in the atmosphere. However, with the capability of Tiros to observe vast oceanic areas and uninhabited land masses where much of our weather originates, and with the increased capability of the second generation Nimbus meteorological satellites to observe virtually the entire world twice daily have come major problems of reducing, analyzing, disseminating, storing, and retrieving the increasingly vast quantities of data gathered on a continuing basis by meteorological satellites. In this paper we shall discuss the Tiros satellite and the flow of data through its different sensory subsystems, and we shall conclude with a look into the future when the Nimbus satellite system becomes a reality.

THE TIROS METEOROLOGICAL SATELLITE

The Spacecraft

The Tiros (Television and Infra-Red Observation Satellite) spacecraft (ref. 1) is shaped like a pillbox, 42 inches in diameter and 19 inches high, and weighs about 285 pounds (fig. 25–1). The top and sides are covered with solar cells. All Tiros satellites have carried two television cameras, but only Tiros II, III, and IV to date have also carried scanning and

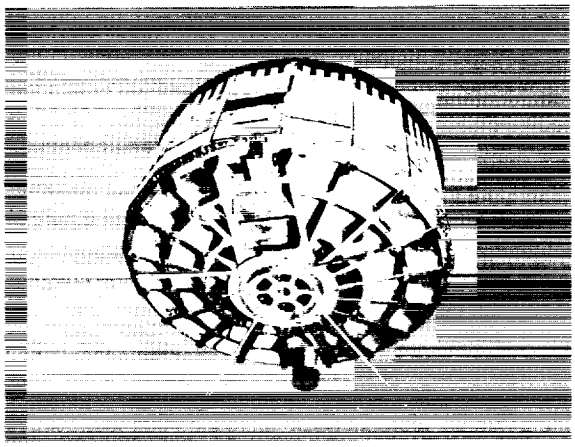

FIGURE 25–1.—Tiros II meteorological satellite. The lens of the wide field-of-view camera protrudes beneath the baseplate. The medium resolution scanning radiometer looks through rectangular apertures in the side (foreground) and baseplate. The narrow field-of-view camera and low resolution radiometer view through small apertures in the baseplate.

nonscanning radiometers to sense infrared and reflected solar radiation from the earth and its atmosphere (table 25–I).

TABLE 25–I.—*Meteorological Instrumentation Carried on Tiros Satellites*

	I	II	III	IV	V	VI
Narrow field-of-view (12.7°) ½″ vidicon camera	X	X				
Medium field-of-view (76.6°), low distortion, ½″ vidicon camera				X	X	X
Wide field-of-view (104°) ½″ vidicon camera	X	X	XX	X	X	X
*Five channel, medium resolution, scanning radiometer		X	X	X		
Two cone, low resolution, nonscanning radiometer		X	X	X		
Isolated hemisphere heat balance radiometer			X	X		

*The 8–30 micron channel was omitted on Tiros IV

Tiros is stabilized by spinning in the range 9–12 rpm. When the spin decays in the earth's magnetic field to about 9 rpm, a pair of small peripheral rockets can be fired on command from the ground, spinning the satellite up to 12 rpm again (cf. fig. 25–3).

Orbital Characteristics

The Tiros orbit is nominally circular, 475 statute miles above the earth with a period of about 100 minutes. Its motion is "direct" (in the same sense as the earth's rotation), and its inclination to the equatorial plane for the first four Tiros satellites was about 48°. To increase latitudinal coverage, the inclination was increased to 58° for Tiros V and VI (fig. 25–2).

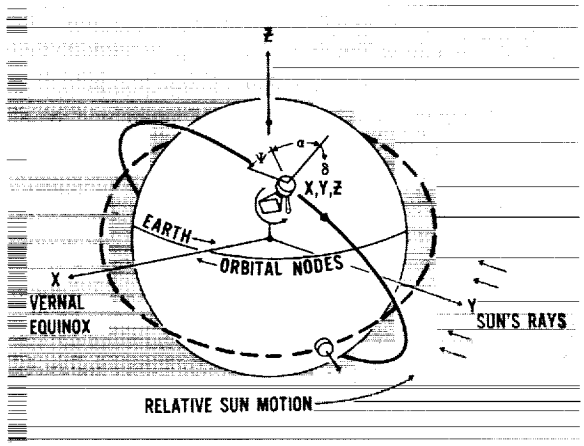

FIGURE 25–2.—Motions of earth, sun, orbit, and satellite. The sun's motion relative to an inertial coordinate system centered in the earth is to the east as is the earth's rotation. The regression of the orbital nodes is to the west. The position coordinates (X, Y, Z) and angular coordinates ($\alpha\delta\psi$) of the satellite must be known to locate data on the earth.

Many motions of satellite, orbit, earth, and sun combine to create major problems in data reduction and occasional frustrations in programming the satellite. Because of the earth's equatorial bulge, the orbital nodes regress to the west at the rate of about 5.5°/day (for the 48° inclination orbits) relative to the earth-sun line. When the great Atlantic Coast tides were wreaking destruction along the Eastern United States during 5–8 March 1962, Tiros IV was blind to them because its orbit was in the position of the dashed curve of figure 25–2, and its cameras could see the earth only in the southern hemisphere.

Magnetic and Gravitational Torques

Shortly after the launch of Tiros I, the satellite pictures gave evidence that, instead of remaining essentially spin stabilized in space, the

spin vector was moving southward by as much as 3° to 5° per day (fig. 25–3). Subsequent investigation showed that this angular motion could be explained very well by the effect of two torques, viz., a primary torque caused by the interaction of a magnetic dipole along the spin axis with the earth's magnetic field, and a secondary torque caused by differential gravity in the earth's gravitational field (ref. 2). As a result, a closed current loop of wire has been placed around the baseplate of all Tiros satellites since the first, with several levels of current in both directions capable of being commanded from the ground. Thus, it is possible in some measure to steer the spin axis in space in order to effect the most favorable geometry for picture taking and to prevent the direct rays of the sun from shining on the scanning radiometer sensors except for occasional short periods of time.

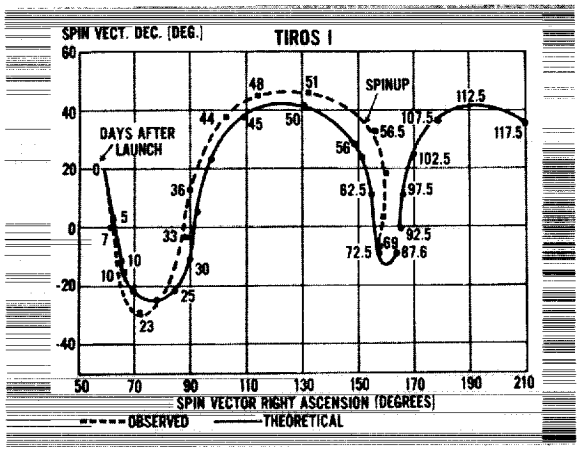

FIGURE 25–3.—Observed motion of the Tiros I spin vector based on an analysis of photographs (dashed line) compared with the theoretical motion based on the effects of a magnetic dipole moment along the spin axis and differential gravity (solid line). Declination is + north and − south of the celestial equator. Right Ascension is + east of the vernal equinox along the celestial equator. On the 56th day the satellite's spin was increased from 9.4 rpm to 12.9 rpm upon command from the ground.

Command and Data Acquisition

There are two Command and Data Acquisition (CDA) stations in the Tiros system. There are presently located at NASA's Wallops Station, Virginia, and at the Pacific Missile Range (PMR), California. Control of the system is centered in the Tiros Technical Control Center at the Goddard Space Flight Center (GSFC), Greenbelt, Maryland. Tiros passes within interrogation range of one of the CDA stations during about 8 of its 14.4 daily orbits of the earth. During each interrogation pass, provided there are favorable conditions of satellite attitude and solar illumination, "direct" pictures may be read out without intermediate storage from the television cameras upon command from the ground. Also, a "remote" sequence of 32 pictures for each camera may be programmed to be taken in the future, and any remote pictures previously taken and recorded on magnetic tape may be read out during an

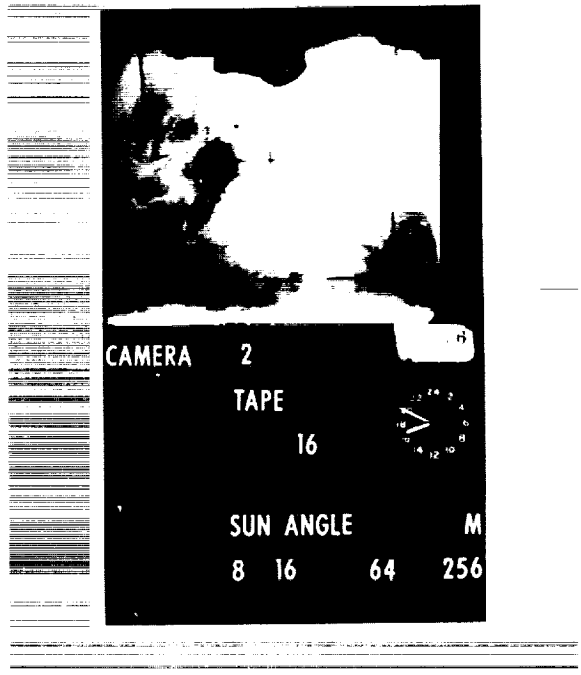

FIGURE 25–4.—Photograph taken by Tiros III during orbit 43 at 1054 GMT on 15 July 1961. The coast of Libya and the Mediterranean Sea are clearly visible. The data on the display panel indicate that: The picture was taken by camera number 2 (an error—actually the picture was taken by camera 1) and recorded on magnetic tape; the readout of the picture occurred during orbit 46; this was frame number 16 of the sequence read out at Wallops Station (indicated by "M" in the lower right); and the "sun angle" (angle measured in the plane of the baseplate between a zero radial reference and the normal projection of the sun's rays) was 8+16+64+256=344 degrees. The clock gives the time when the film was produced and has no relation to the picture-taking time.

interrogation pass. In addition, stored data from any radiation experiments on board may be read out during the pass.

Picture Presentation at the CDA Station

Television pictures read out are presented on a cathode ray tube at the CDA station, where the image is photographed on 35 mm film for operational use and for future research and archival purposes. Figure 25–4 shows a Tiros frame complete with all display panel information photographed simultaneously with the television picture. The distinctive African coastline along the Mediterranean Sea clearly places this picture over the Sahara Desert in Libya with north at the top of the picture. However, many pictures do not show identifiable landmarks, and are of little use without first geographically locating the information.

Attitude Determination and Geographic Location of Picture Data

Several geographic location methods have been employed throughout the Tiros program, some graphical in nature utilizing libraries of special grid bases and map projections, and

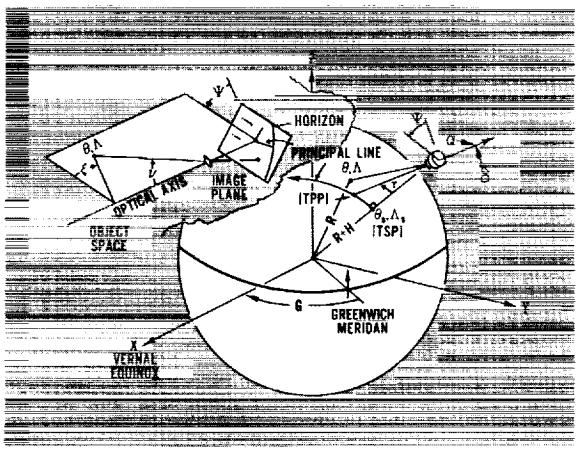

FIGURE 25–5.—Schematic illustrating the parameters of equation (1) in the problem of geographically locating picture information. Also illustrated are the radial (ρ) and tangential (ξ) angles in object space to the picture element; the tilt angle (τ) between the local vertical and the camera optical axis and the points of their respective intersections with the earth's surface, i.e., the terrestial subsatellite (TSP) and principal (TPP) points; and the great circle on earth passing through these points, the "Principal Line."

others employing digital computers and plotters (refs. 3 and 4). The problem of geographically locating picture information is depicted in figure 25–5. The normalized image coordinates i, j of a picture element identified by latitude θ and longitude Λ are shown as a function of eight parameters, all of which except R, the radius of the earth, are themselves functions of time t. This relationship is express mathematically by

$$[i,j]_{\theta\Lambda}=f[\theta_s(t), \Lambda_s(t), H(t), G(t), R, \alpha(t), \delta(t), \psi(t)] \quad (1)$$

The shutter time of a picture is determined from interrogation data at the CDA station (although the satellite clock system is subject to spurious effects that occasionally cause deviations in the actual times of remote pictures). The subsatellite latitude $\theta_s(t)$ and longitude $\Lambda_s(t)$ and the geometric height above the earth $H(t)$ are predicted by the NASA orbital calculations. The Greenwich Hour Angle $G(t)$ is known (sidereal time), and the radius of an assumed spherical earth is known. The remaining parameters that must be determined are the astronomical right ascension $\alpha(t)$ and declination $\delta(t)$ of the satellite spin vector and the Euler spin angle $\psi(t)$ of the satellite in fixed space. (Here it is also assumed that the optical axis is parallel to the spin axis, although there is usually a small deviation between the two.)

Several sources of data for the determination of spin vector attitude (i.e., α and δ) are available, including a horizon sensor, the thermal channels of the scanning radiometer when one is carried, and the photographs themselves. In addition, theoretical calculations based upon the magnetic and gravitational characteristics of the satellite are available for smoothing observed data and for prognosticating future attitude values. The attitude required for real-time operational use at the CDA stations is determined by on-site teams employing a small digital computer in conjunction with graphical techniques. A definitive after-the-fact determination of attitude history is made on an IBM–7090 computer by NASA. These attitude data are used by GSFC in the reduction of the

radiation data and by the National Weather Satellite Center (NWSC) of the U.S. Weather Bureau for the production of latitude-longitude grids for research and archival use with the television pictures.

The spin angle ψ must be determined for each individual frame. The "sun angle," which is computed automatically in the ground station and photographed with each frame, together with a knowledge of the attitude and the solar ephemeris, is sufficient for determining ψ. However, it has been found that the computed sun angle is not always reliable and cannot be used generally without other supporting data. The most straightforward way of determining ψ is from the earth's horizon if it is present in the picture. The principal line, which on earth is that great circle passing through the subsatellite and principal points, is uniquely determined in the image plane by the straight line that passes through the image principal point and intersects the apparent horizon at right angles (in the absence of distortion). From geometry, the spin angle of the image principal line readily follows. For this reason the magnetic attitude coil of Tiros is intentionally programmed to yield strings of pictures including horizons. However, when frames do not have horizons, the spin angle may be determined from comparative techniques involving several frames in a picture sequence.

After all parameters are determined, it is possible to calculate the radial (ν) and tangential (ξ) angles in object space to each picture element on earth. The functions i (ν, ξ) and j (ν, ξ) are calibrated for each camera before launch, reflecting its optical distortion characteristics and including the particular electronic distortion occurring in the calibration itself. Fiducial marks etched on the vidicon face allow corrections to be applied for the individual electronic deviations from the calibration that are present in each frame. Generally, in computer work, individual electronic distortion is disregarded; but in very precise manual work it is incorporated.

In spite of many improvements in attitude determination and picture gridding, the accurate location of picture data on the earth's surface remains a problem in the utilization of the Tiros television data.

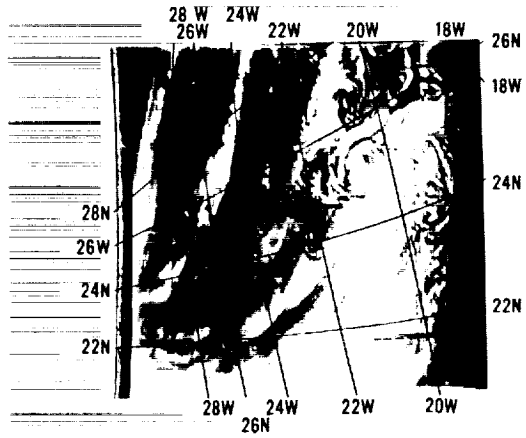

FIGURE 25–6.—Photograph of pronounced eddies taken by Tiros V during orbit 187 at 1401 GMT on 2 July 1962.

Figure 25–6 shows a picture taken by the low distortion camera of Tiros V during orbit 187 at 1401 GMT on 2 July 1962, overlaid with a latitude-longitude grid. From the grid and separate wind data, it is seen that the striking eddy patterns occur some 500 km downwind from the Canary Islands, suggesting a role played by the Islands in their formation. Hubert and Krueger, of NWSC's Meteorological Satellite Laboratory (MSL), have recently analyzed this situation and will publish their findings in the November 1962 issue of the Monthly Weather Review in a paper entitled "Satellite Pictures of Mesoscale Eddies" (ref. 5). We feel that such pronounced circulation patterns as those of figure 25–6 hold a wealth of information for research into problems of atmospheric dynamics, and we should particularly like to stimulate interest in the universities in attacking such problems with the aid of the large library of available Tiros photographic data.

Operational Use of Television Data

The primary method for rectifying and displaying Tiros picture information for operational use is the nephanalysis chart showing graphical representations of areas of similar cloud amount and type. The nephanalyses are prepared manually by a team of meteorologists at each CDA station utilizing perspective latitude-longitude grids produced in advance by an on-site digital computer-plotter system, over-

laid on opaque prints prepared within minutes following a satellite interrogation. The nephanalyses are transmitted via facsimile from the CDA stations to NWSC, adjacent to the National Meteorological Center (NMC) in Suitland, Maryland, where professional weathermen maintain a quality control over the products before further distribution is made.

Figure 25–7 shows a nephanalysis chart that was drawn from pictures taken on 11 September 1961 during orbit 880 of Tiros III. Above the chart is a special mosaic of the string of pictures taken in the remote picture sequence which shows clearly Hurricanes Debbie and Esther. Twenty-four hours earlier Tiros first viewed the vortex near 11° N, 30° W that developed into Esther, the first hurricane to be discovered by a satellite.

The nephanalysis charts are routinely transmitted over weather facsimile circuits within the United States; and, in addition, key photographs are transmitted over photo-facsimile circuits to selected forecast centers. The nephanalyses are also transmitted in numerical code via international teletype circuits; and recently the routine broadcast of the nephanalysis charts to Europe, Australia, and the Far East was begun over newly established radio facsimile circuits.

Also, directed messages are sent immediately to the weather services concerned whenever evidence of a severe storm situation is first detected by Tiros. These special advisor messages have been especially valuable in warning of typhoons in the Pacific.

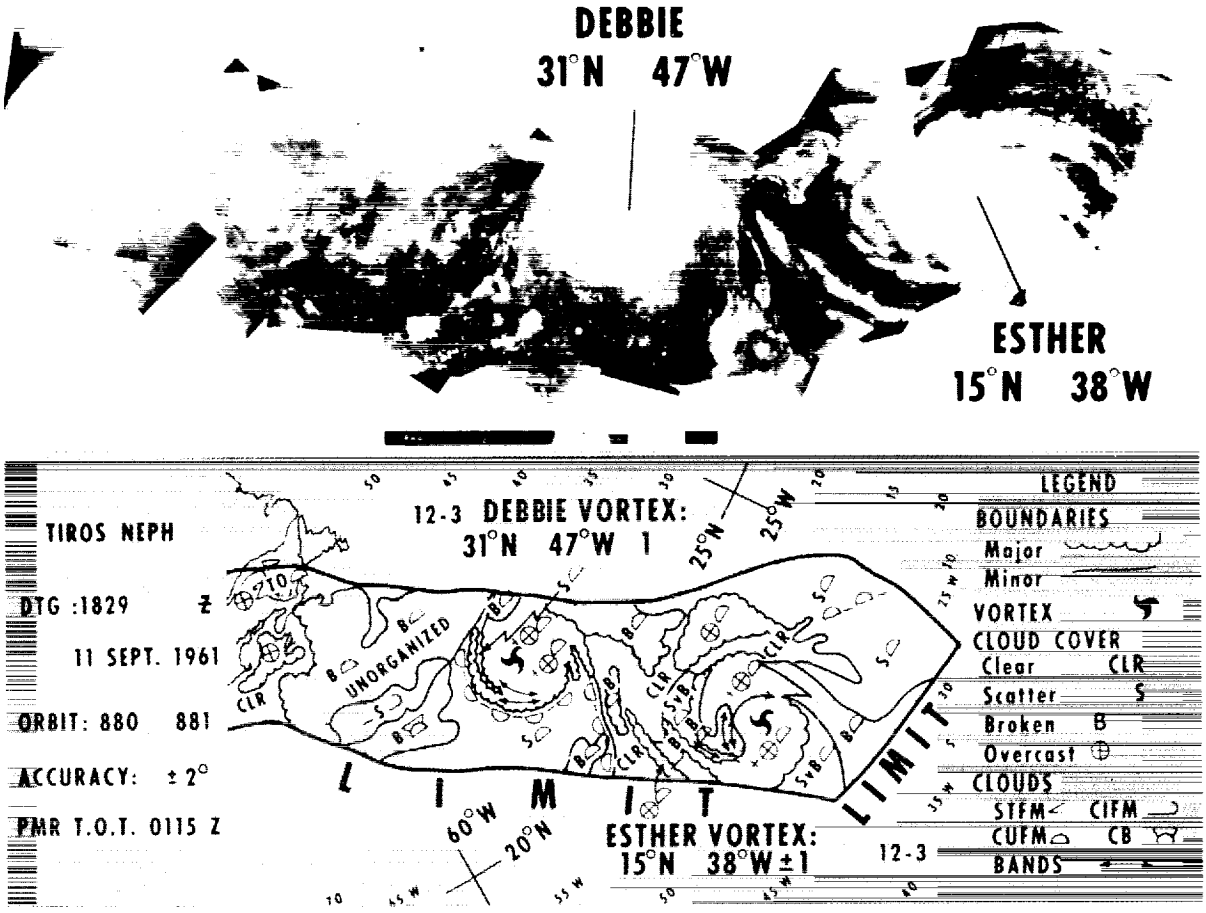

FIGURE 25–7.—Mosaic of photographs showing Hurricanes Debbie and Esther taken by Tiros III during orbit 880 on 11 September 1961 and the resultant nephanalysis chart drawn for operational use.

Research Use of Television Data

In addition to their operational use, pictures are widely used in research. Figure 25–6 shows an outstanding example of the research use of pictures. Figure 25–8, which has become a classic, shows a mosaic of photographs taken during orbit 704 of Tiros I on 20 May 1960 and the striking correlation of cloud pictures and the surface analysis. Incidentally, the first application of Tiros data in the National Meteorological Center was to use these pictures to position a 500 mb low near 45° N, 179° E.

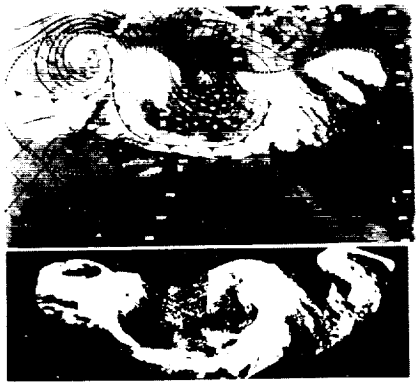

FIGURE 25–8.—Mosaic of photographs taken by Tiros I on 20 May 1960 (bottom), and experimental cloud depiction chart prepared by superimposing the pictures on the National Weather Analysis Center's 0000 GMT map analysis of the same date (top).

A document entitled "Catalogue of Meteorological Satellite Data—Tiros Television Cloud Photography" is published for each Tiros satellite as part of the "Key to Meteorological Records Documentation Series." The catalogues are for sale by the Superintendent of Documents, U.S. Government Printing Office, Washington 25, D.C. Each catalogue contains information regarding the obtaining of copies of the photographs, the latitude-longitude grids, and detailed listings of times for all frames from the National Weather Records Center, Asheville, N.C. Each catalogue also lists pertinent reports published by the Meteorological Satellite Laboratory of NWSC that should be of interest to the serious worker with Tiros photographs.

Description of the Radiometer Experiments

In addition to the television cameras, Tiros II, III and IV carried experiments to sense infrared and reflected solar radiation (refs. 6 and 7). The most complex of these experiments is the medium resolution, scanning radiometer, sensing the earth and atmosphere in five spectral regions (figs. 25–9 and 25–10). The nominal bandwidths of the five channels are:

Channel 1_____ 6.0–6.5 microns
–water vapor absorption

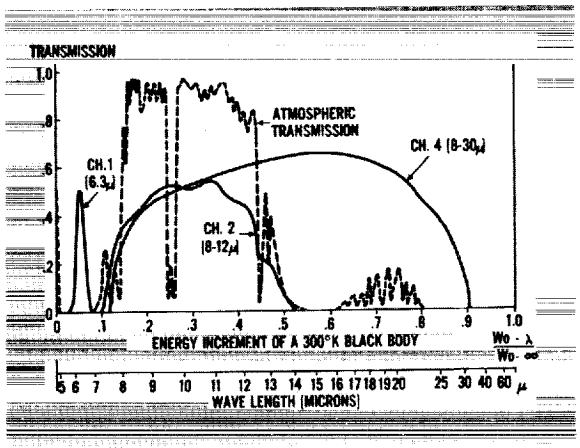

FIGURE 25–9.—Typical response curves of the three infrared channels of the Tiros medium resolution radiometer. The dashed curve indicates the approximate transmission characteristic of one atmosphere.

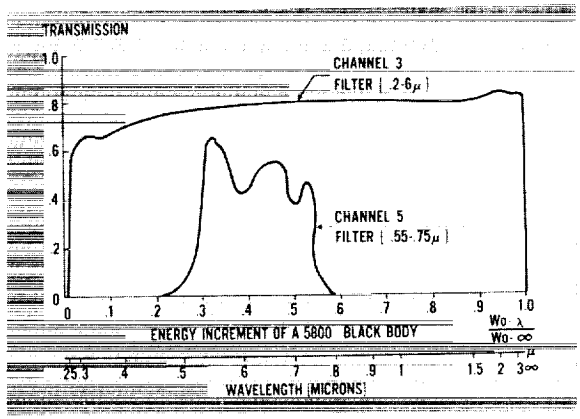

FIGURE 25–10.—Typical response curves of the two channels of the Tiros medium resolution radiometer sensitive to reflected solar radiation. Channel 3 includes more than 99% of the energy in the solar spectrum, whereas channel 5 includes the narrower region wherein the television cameras and the human eye are sensitive.

Channel 2_____ 8–12 microns
–atmospheric window
Channel 3_____ 0.2–6 microns
–reflected solar radiation
Channel 4_____ 8–30 microns
–terrestrial radiation
Channel 5_____ 0.55–0.75 microns
–response of TV system

The physical significance of the experiment has been reported previously and will not be repeated here (refs. 8 and 9).

The scanning radiometer employs a chopper that causes each sensor to view alternately, and at a rapid rate, in two directions 180 degrees apart (fig. 25–11). The response from each channel is proportional to the difference in the irradiation of the sensor bolometer from the two directions. The bidirectional axes of the channels are parallel to one another and inclined to the spin axis by 45°. The scanning radiometer is shown in figure 25–12.

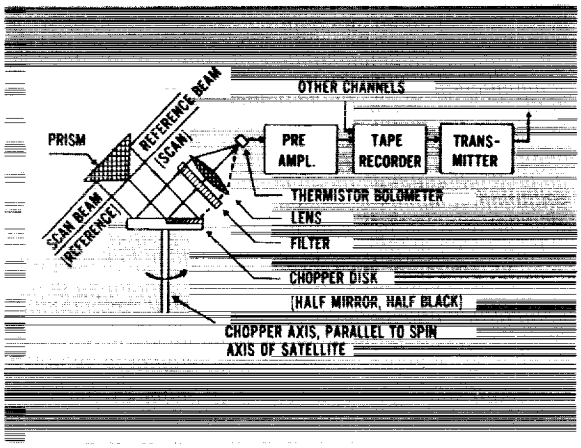

FIGURE 25–11.—Block diagram of one channel of the bidirectional Tiros medioum resolution radiometer.

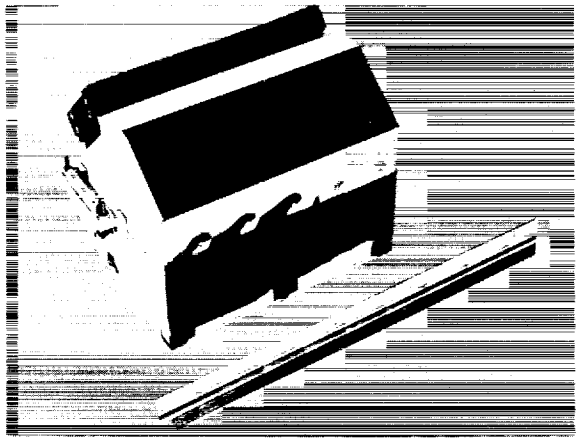

FIGURE 25–12.—Exterior view of the Tiros medium resolution radiometer showing the viewing apertures in one direction of the five channels.

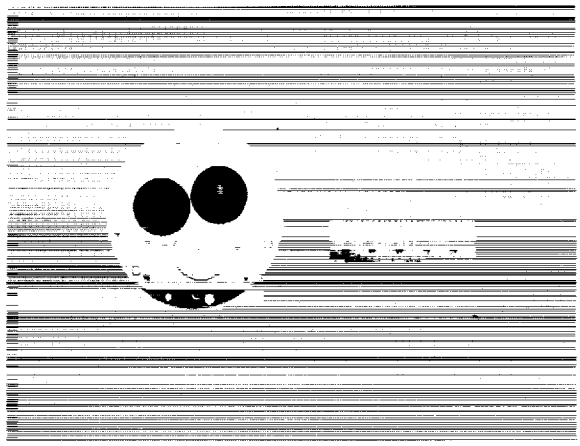

FIGURE 25–13.—Exterior view of the Tiros low resolution radiometer showing the black detector (left) and the white detector (right).

The calibration of the infrared channels is in terms of equivalent temperatures of a blackbody target filling the 5° field-of-view, whereas the calibration of the solar channels is in terms of that portion of radiant emittance from a target filling the field-of-view to which the channel responds through its filters and other optical elements.

The two low resolution radiometer channels consist of a black and white detector, each mounted in the apex of highly reflective cone (fig. 25–13). The optical axes of the cones are parallel to the satellite spin axis. The black detector is equally sensitive to reflected sunlight and long-wave radiation, whereas the white detector is coated to be reflective in the visible and near infrared. Knowing the radiometer housing temperature, which is telemetered, the equilibrium temperature of each detector is a function of two unknowns: the apparent blackbody temperature of the earth, and the amount of reflected sunlight within the 50° field-of-view, both of which can be determined by solving the two equations simultaneously. The University of Wisconsin experiment, consisting

essentially of a black and white hemisphere isolated in space, works on the same principle as the two-cone radiometer. Being an omnidirectional experiment, the isolated hemispheres can collect data throughout the entire orbit, but they are of lower resolution than data from the cones.

Scan Geometry of the Medium and Low Resolution Radiometers

The scan geometry of the two radiometers is shown in figure 25–14. The spin of the satellite causes the 5° field-of-view of the five channel radiometer to scan over earth and space in several distinctive modes. The motion of the satellite in orbit causes the advancement of the individual scan lines. The response of the low resolution cones (whose axes are parallel to the spin axis) is unaffected by satellite spin.

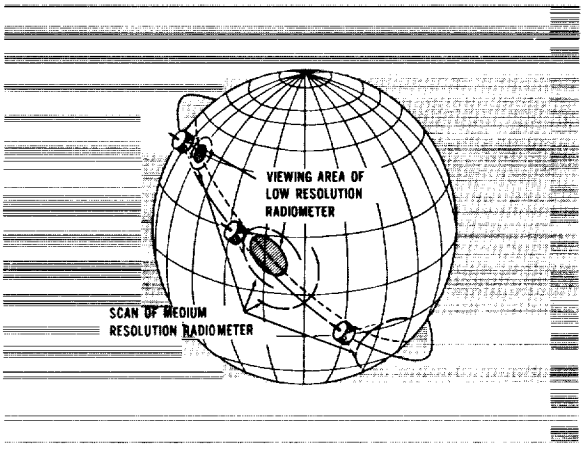

FIGURE 25–14.—Geometry of the scanning motion of the medium resolution and of the viewing area of the low resolution Tiros radiometers. The scan pattern of the medium resolution radiometer varies from a circle on earth when the spin axis is parallel to the local vertical to a pair of alternating, hyperbola-like branches when the spin axis is perpendicular to the local vertical.

Data Flow From the Medium and Low Resolution Radiometer Sensors to the CDA Station

The data flow from the medium and low resolution radiometers within the satellite (refs. 6 and 10) is shown in figure 25–15. The output of the five medium resolution channels is fed to five subcarrier oscillators. A sixth channel is provided for telemetry of the low resolution cone

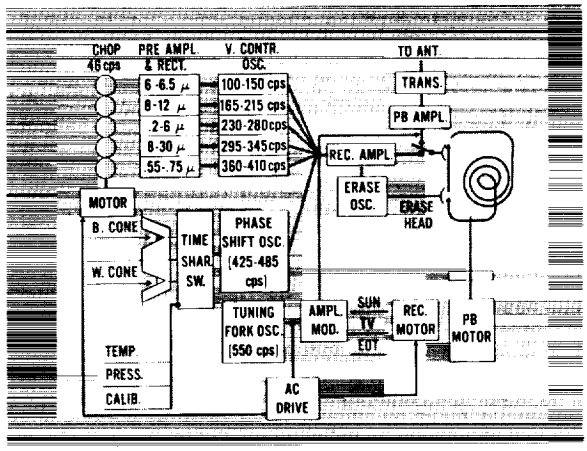

FIGURE 25–15.—Block diagram of information flow in the radiation experiment in the Tiros satellite.

data, environmental temperatures, instrumentation canister pressure, and calibration levels. Other low data density experiments, when flown on Tiros, also use channel 6. Examples of these are the University of Wisconsin's isolated hemisphere experiments flown on Tiros III and IV and an electron temperature probe experiment scheduled for a future Tiros mission. A mechanical commutator switches resistive sensors in one branch of a phase-shift oscillator. The seventh channel, a tuning-fork oscillator, serves as a reference frequency and timing signal. The outputs from these seven different channels are summed, and the resultant composite signal is recorded by a miniature tape recorder. An oscillator provides an alternating-current bias to the record head and the signal required for the erase head. Erase of the magnetic tape occurs immediately before recording. The record spectrum extends from 100 to 550 cps. The tape recorder is an endless-loop, two speed design, running at a speed of 0.4 ips during the record mode and 12 ips during playback. The endless loop records continuously, day and night, except during a playback sequence. The record motor also drives a camshaft that activates a bank of microswitches connected to the five commutated subchannels of the time-sharing sixth channel. Each subchannel is sampled for 6 seconds, and one is further subcommutated to accept up to eight separate inputs.

To permit ready identification of the coincidence of television with radiation data, each TV shutter action generates a 1.5 second pulse that

amplitude-modulates channel 7. To facilitate the determination of spin rate and of relative sun position, one of the nine sun sensors on the satellite generates a 0.5 second pulse that amplitude-modulates channel 7. Reconstruction of the radiation data vitally depends on its correlation with absolute time. The channel 7 tuning-fork oscillator provides an accurate but relative timing signal. Upon interrogation to playback the radiation data, an "end-of-tape" (EOT) pulse whose absolute time of occurrence is known within milliseconds is transmitted to the satellite, causing a 1-second dropout of channel 7 and thereby correlating all data in absolute time. The composite signal is played back over an FM telemetry transmitter and recorded on magnetic tape at the CDA station. These tapes are mailed daily to the Aeronomy and Meteorology Division at GSFC.

Data Flow in the Analog-to-Digital Converter

At the Aeronomy and Meteorology Division the master tapes are demultiplexed, demodulated, and fed to an analog-to-digital converter (refs. 6 and 10), figure 25–16. The pressure is read separately. The analog-to-digital converter produces a magnetic "Radiation Data Tape" made up of 36 bit words suitable for an IBM 7090 computer. In addition, an analog record may be produced on an oscillograph for special hand analyses. (Examples of such hand analyses are shown in figs. 25–27 and 25–29.)

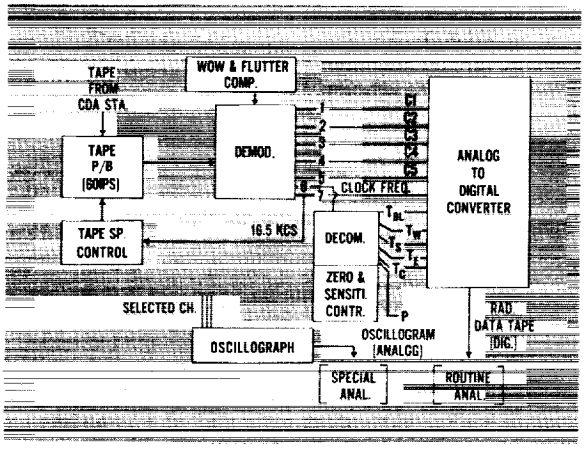

FIGURE 25–16.—Block diagram of information flow at the Aeronomy and Meteorology Division in producing a digital magnetic tape from the Tiros radiation experiment for computer input. The output of the decommutator consists of temperatures of the black and white cones and three environmental temperatures and canister pressure.

Data Flow in the Large Computers

Final automatic reduction of the medium resolution radiation data is carried out on an IBM 7090 computer at GSFC (figs. 25–17).

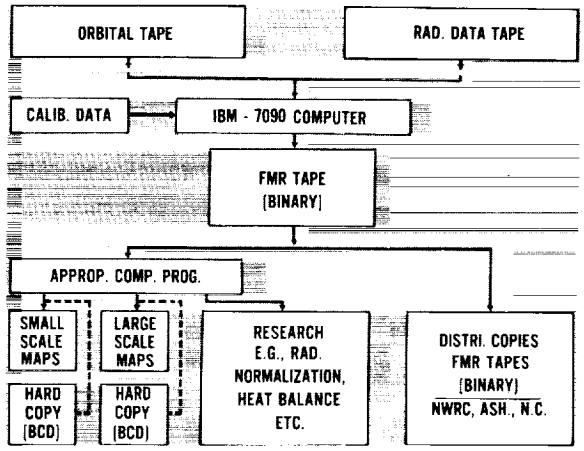

FIGURE 25–17.—Block diagram of information flow through the IBM–7090 computer in producing the Final Meteorological Radiation Tapes containing reduced data from the Tiros medium resolution radiometer.

The computer requires inputs from three sources to produce the Final Meteorological Radiation (FMR) Tapes. One source is the Radiation Data Tape containing radiation and satellite environmental parameters in digital form. A second source is the Orbital Tape from GSFC containing satellite position and attitude data. A third source is the Calibration for converting the digital information to meaningful physical units. The Final Meteorological Radiation Tape, then, is the basic repository of data from the medium resolution scanning radiometer. To study and utilize the scanning radiometer data, appropriate computer programs must be written to "talk" to the FMR tapes and provide for printing out data, punching cards, or producing maps.

The outputs of both the two-cone low resolution and University of Wisconsin isolated hemisphere experiments are vastly smaller than the output from the medium resolution radiometer.

Because of instrumental difficulties, only selected orbits of Tiros II low resolution data have been reduced by hand. Since both of these experiments are recorded on the commutated channel 6 in Tiros III and Tiros IV, it has been found convenient to program their reduction simultaneously on a large CDC–1604 computer at the University of Wisconsin. This program is now in the final stages of checkout.

Machine-Processed Radiation Data

Several forms of machine-processed radiation data are shown in figures 25–18 to 25–26. The computed programs for these forms of processing were written by personnel of the Meteorological Satellite Laboratory. In the high-speed printer output shown in figure 25–18, the computer distributed channel 2 data from orbit 132 of Tiros III, during the time period 1545 to 1557 GMT over a grid field having a mesh interval between points of 2.5 degrees of longitude (about 278 km square at the equator). The average value of the measurements in terms of equivalent blackbody temperatures was obtained at each grid point, after which the average of all of these values was placed at all remaining grid points in order to minimize abrupt gradients and discontinuities at the edges of the data. Contour printing was accomplished in the form of filler numbers for alternate 10° K contour intervals. Analogous to the television pictures, geographic location of the radiation data is necessary to enhance their usefulness. This is accomplished by a latitude-

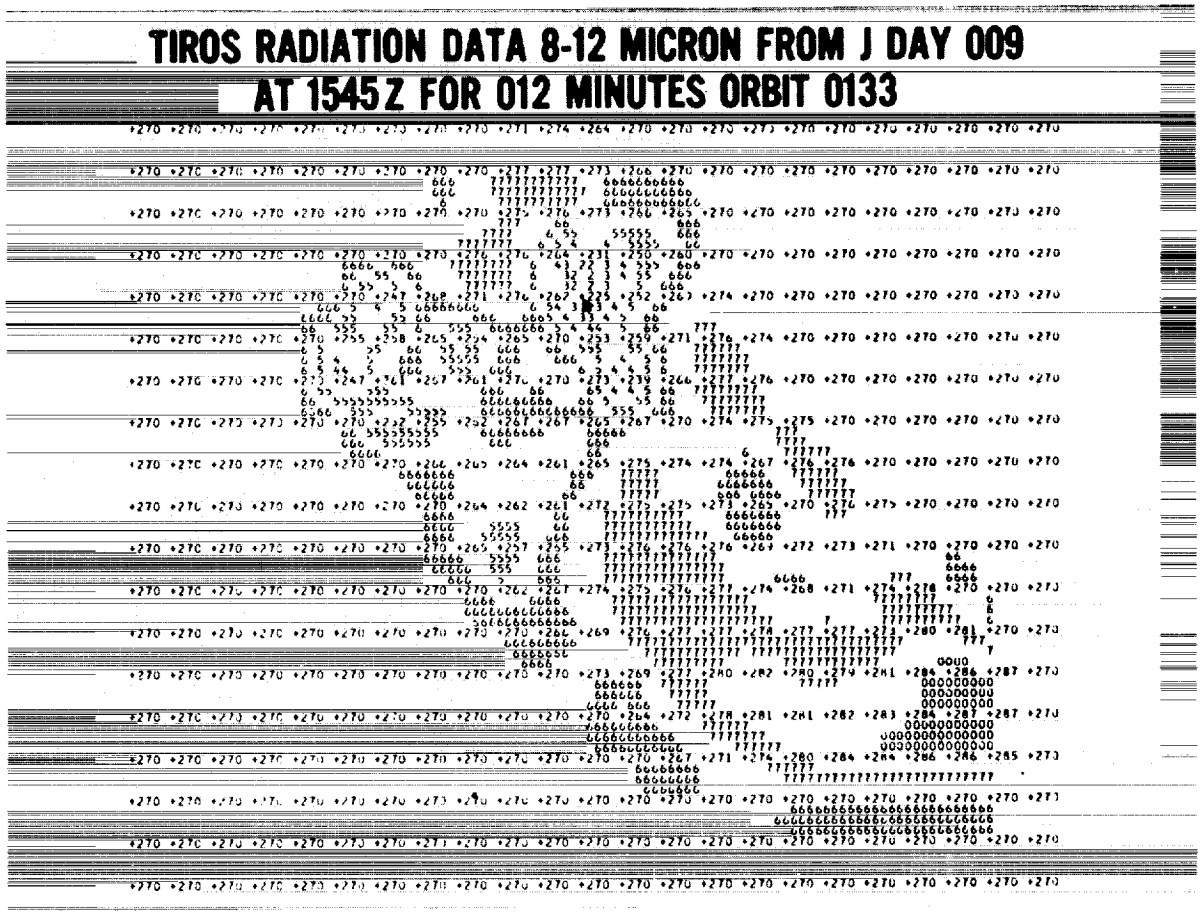

FIGURE 25–18.—Grid print map of data from the window channel of the Tiros III medium resolution radiometer, acquired during orbit 132 between 1545–1557 GMT on 21 July 1962 and read out on the following orbit. The Mercator Projection mesh interval is 2½ degrees of longitude between grid points. Grid point averages are in terms of equivalent blackbody temperatures (°K), and contouring by filler numbers is accomplished for every 10° K. An arrow points to 225° K, the lowest grid point average on the map.

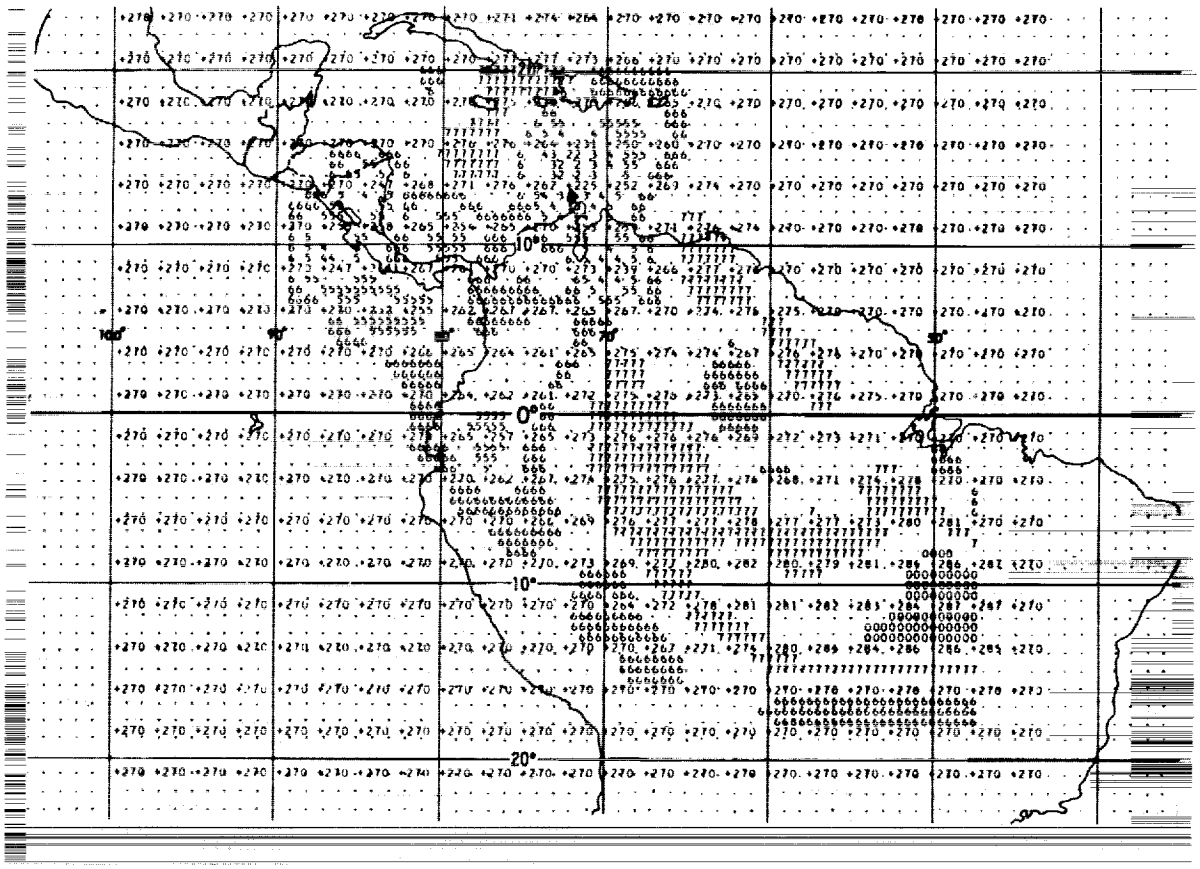

FIGURE 25–19.—The data of figure 25–18 geographically located by a latitude-longitude overlay. The minimum of 225° K coincides with the position of Hurricane Anna.

longitude overlay illustrated in figure 25–19. The population of measurements within a mesh interval varied from 1 along the southwestern edge to more than 60 along the northeastern edge of the data. This large variance results from the complicated nature of the scan.

A more vivid presentation can be effected by replacing the filler numbers by manually shading between contour intervals. The channel 2 data of figure 25–19 plus the corresponding data from the other four medium resolution channels were processed in this way and are shown in figures 25–20 to 25–24. An outstanding feature on all five maps is seen at about 13.8° N, 72.3° W, where the three thermal channels show minimum temperatures and the two solar channels show maximum reflectances. Such a combination over tropical waters could

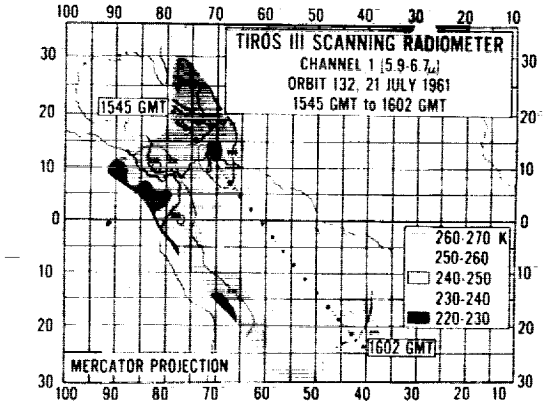

FIGURE 25–20.—Radiation map from the Tiros III medium resolution radiometer; channel 1, orbit 132, 21 July 1961, 1545–1602 GMT. Hurricane Anna is centered at about 13.8° N, 72.3° W. Original grid scale: 2.5 degrees of longitude per mesh interval.

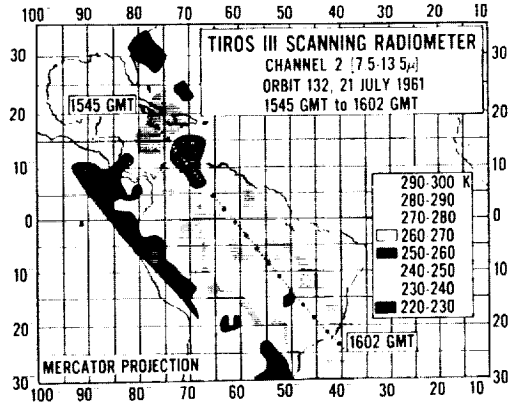

FIGURE 25–21.—Radiation map from the Tiros III medium resolution radiometer; channel 2. Original grid scale: 2.5 degrees of longitude per mesh interval.

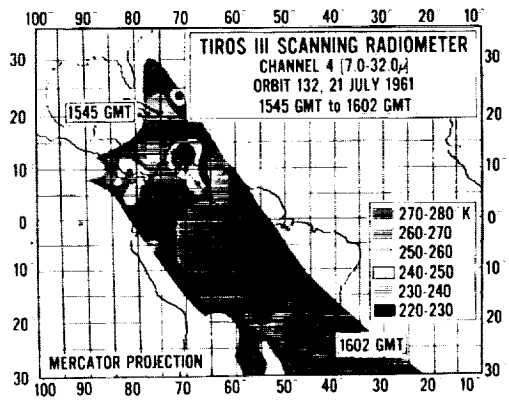

FIGURE 25–23.—Radiation map from the Tiros III medium resolution radiometer; channel 4. Original grid scale: 2.5 degrees of longitude per mesh interval.

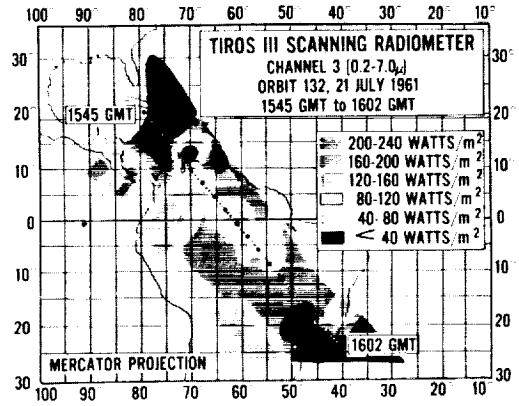

FIGURE 25–22.—Radiation map from the Tiros III medium resolution radiometer; channel 3. Original grid scale: 2.5 degrees of longitude per mesh interval.

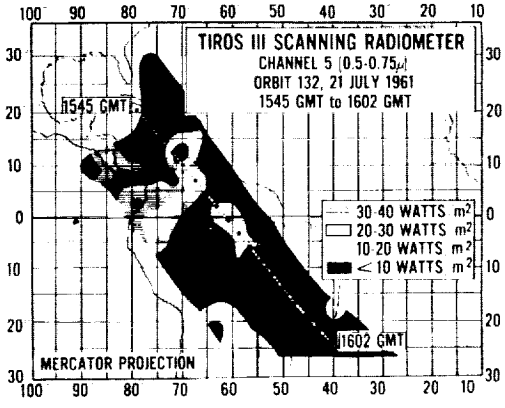

FIGURE 25–24.—Radiation map from the Tiros III medium resolution radiometer; channel 5. Original grid scale: 2.5 degrees of longitude per mesh interval.

only mean high thick clouds of wide expanse which in these examples were present in the form of the first North Atlantic tropical cyclone of 1961, Hurricane Anna. Further implications of these data have been published elsewhere (ref. 11).

To increase resolution, grid print maps of the data can be produced at larger scales, although for fewer than 2.5 degrees per mesh interval the data density is generally not sufficient to insure measurements at every grid point. For higher resolutions, therefore, the grid prints are generally produced without machine contouring, and contouring is accomplished by hand only for those points where data exist. A map produced in this way is shown in figure 25–25, where a portion of the data of figure 25–18 was processed at a scale four times as large, i.e., a mesh interval of 0.625 degrees of longitude between points. Much of the fine structure inherent in the data is evident at this scale.

Two limitations of the forms of display shown in figures 25–18 to 25–25 are emphasized, viz., (1) the direction from which a measurement is made (i.e., nadir and azimuth angles), and (2) the number of individual measurements making up each grid point average (or the amount of the data smoothing) are not readily apparent. To circumvent these limita-

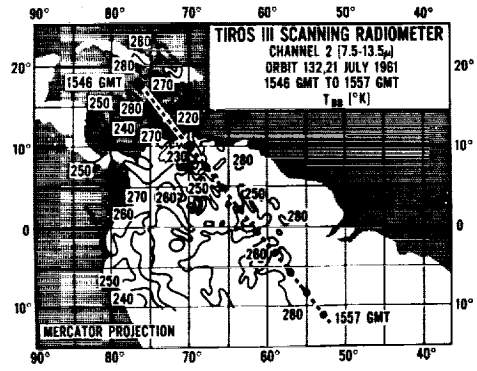

FIGURE 25-25.—Radiation map from the Tiros III medium resolution radiometer; channel 2, orbit 132, 21 July 1961 1546–1557 GMT. Hurricane Anna is centered at about 13.8° N., 72.3° W. Original grid scale: 0.625 degree of longitude per mesh interval.

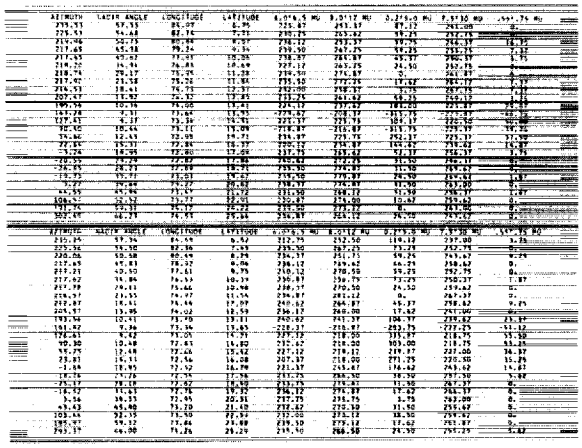

FIGURE 25-26.—Computer listing from a Final Meteorological Radiation Tape of two swaths viewed by the medium resolution radiometer of Tiros III during orbit 132 at about 1548 GMT on 21 July 1961 over Hurricane Anna. Azimuth and nadir angles and geographic locations are listed for each "spot" viewed, together with the calibrated measurements from each of the five channels. The calibration of the infrared channels is in terms of equivalent blackbody temperatures (°K) and of the solar channels, in terms of radiant emittances (w m $^{-2}$). The minus signs before several radiation measurements are for diagnostic purposes and do not mean "negative."

tions for limited hand analysis, a data listing program is available. Calibrated information is presented for all five sensors for each earth-viewed spot in a spin cycle, along with its latitude and longitude and nadir and azimuth angle information. The nadir angle is measured at the satellite between the subpoint radius vector and the ray to the viewed spot. Azimuth is measured in the plane tangent to the earth at the subsatellite point, clockwise from north to the great circle arc connecting the subpoint and the viewed spot. The data list is grouped by earth-viewed swaths—viewed either through the "floor" (baseplate) or the "wall" (side) of the satellite. Figure 25–26 illustrates a listing of two swaths viewed through the floor of Tiros III at about 1548 GMT, 21 July 1961, over Hurricane Anna. The reader may compare the data in the listing with figures 25–18 to 25–25 and 25–29. The small differences that exist can be attributed to the different processing methods and amounts of smoothing.

Hand-Processed Radiation Data

In spite of their speed and sophistication, our computers have not yet been made immune to every logical flaw in attempting to cope with all possible time, space, and noise aberrations in the data. Hence, hand processing involving simultaneous work with photographs taken at nearly the same time and including an indi-

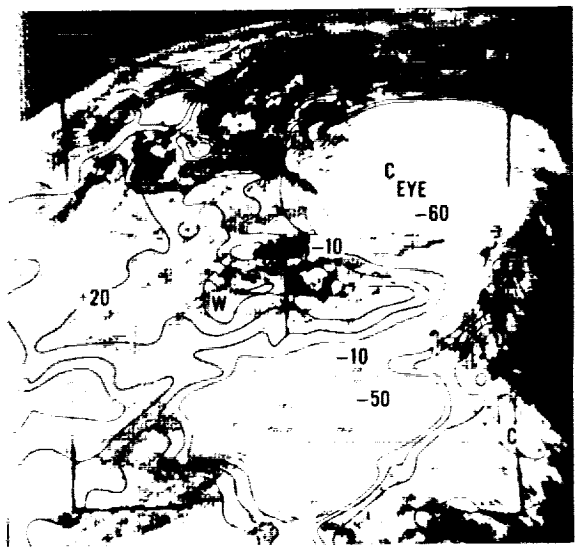

FIGURE 25-27.—Photograph of Hurricane Anna taken by Tiros III during orbit 132 at 1550 GMT on 21 July 1961 on which are superimposed hand-reduced isoradiance lines of the window channel data from the medium resolution radiometer. The numbers pertaining to the isolines are relative and have no absolute meaning.

vidual attitude determination from these photographs yields the most precise presentation of the data. Very precise work of this type has been done by Dr. Fujita of the University of Chicago (ref. 4). Figure 25–27 shows a Tiros photograph of Hurricane Anna taken at about 1550 GMT, 21 July 1961, with hand-reduced isoradiance lines of channel 2 data superimposed upon it. The numbers pertaining to the isolines are relative and have no absolute meaning, but the extremely fine structure and striking correlation with the clouds is remarkable. A section of the analog record from which the analyses of figures 25–27 and 25–29 were made is shown in figure 25–28. The swaths illustrated pass directly over the hurricane. The extremely cold temperatures of the cloud tops are clearly evident in the thermal channels, whereas their high reflectance of sunlight stands out in the solar channels.

Figure 25–29 illustrates a detailed radiation map of Hurricane Anna produced by Dr. Fujita using channel 2 data. Again, the extremely fine structure of the presentation is outstanding (cf. fig. 25–25). The isolines are in terms of

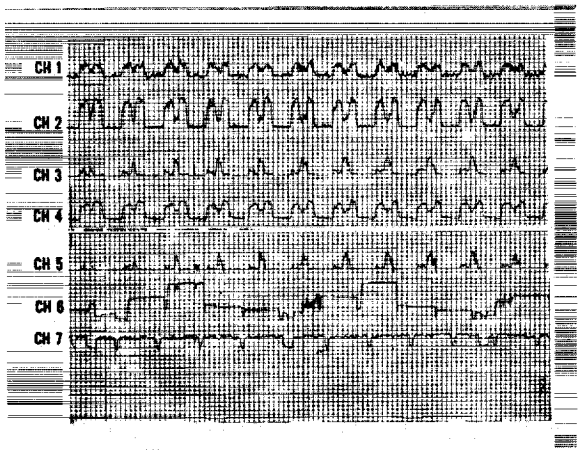

FIGURE 25–28.—Analog record showing eleven swaths of the Tiros III medium resolution radiometer acquired about 1548 GMT on 21 July 1961 during orbit 132 over Hurricane Anna. Time increases to the right and the amplitude of channels 1–5 is approximately proportional to the radiant energy received. The marked dip at the center of each thermal channel swath and the corresponding peaks in the solar channels occur over the hurricane. Channel 6 contains housekeeping information. The envelope of channel 7 is modulated by narrow sun pulses once every spin cycle (6.44 seconds) and by three wide pulses where television pictures were taken 30 seconds apart.

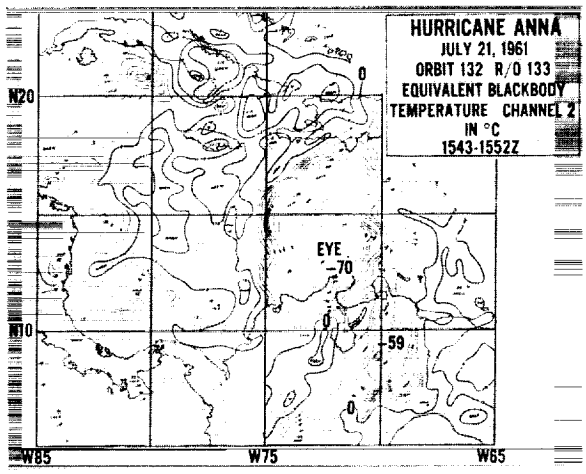

FIGURE 25–29.—Hand-reduced radiation map of Tiros III medium resolution radiometer window channel data over Hurricane Anna. The minimum equivalent blackbody temperature of −70° C indicates that the highest clouds were near the tropopause.

equivalent blackbody temperatures, and the extremely low values near −70° C indicate that the cloud tops must have been near the tropopause. The existing system for reduction of the Tiros medium resolution radiation data is not suited for real-time applications. However, the synoptic potential of the data seems clear, and plans are underway to process such data for operational as well as research use in the second generation Nimbus satellite system. In addition to the radiation mapping illustrated here, the radiation data lend themselves to many theoretical studies in such areas as the planetary heat balance, vertical structure of the atmosphere, and the global distribution of water vapor (refs. 12 and 13).

Documentation of the Medium Resolution, Scanning Radiometer Data

The "Tiros Radiation Data Catalog" and a companion volume, the "Tiros Radiation Data Users' Manual," are published for each satellite carrying a medium resolution radiometer and are available without charge to prospective users of the data from the Aeronomy and Meteorology Division, GSFC, Greenbelt, Maryland. Supplementary material is published as needed and is similarly available without charge. Copies of the Final Meteorological Radiation Tapes are available at cost from the National

Weather Records Center, Asheville, North Carolina.

Engineering Data

In addition to attitude calculations, there are several other types of data that must be processed for engineering or data documentation purposes. These include (1) satellite telemetry of housekeeping parameters; (2) horizon and sun senor data from which spin rates are calculated; and (3) various summaries of station operations, satellite interrogations, and data events, quality, and documentation. In Tiros these data are generally processed by hand except that spin rate calculations are carried out on a small digital computer.

THE NIMBUS METEOROLOGICAL SATELLITE

A Comparison of Tiros and Nimbus

Although the Tiros satellite has been very successful, it has certain limitations. Perhaps the two most important of these are:

1. Tiros is spin stabilized; hence much of the time its sensors are looking into space, blind to developments on the earth beneath.
2. The inclination of the Tiros orbit is 48° or 58°; hence the earth's polar regions are inaccessible to its sensors.

To correct these and other limitations, NASA has developed the Nimbus satellite. Nimbus is built on a modular concept, facilitating the addition or deletion of various sensory subsystems as they may be developed or superseded by new and better designs or concepts. The first Nimbus launch is scheduled for the third quarter of 1963. Until that time NASA's policy is to launch a Tiros satellite every four months, thus keeping an active weather satellite in orbit at all times.

The first Nimbus will carry an advanced vidicon camera subsystem consisting of three cameras, one facing straight down and the others inclined by 35° on either side of the vertical in the plane normal to the velocity vector. The cameras will provide cloud cover data over the daytime side of the earth. The first Nimbus will also carry a high resolution infrared radiometer (HRIR) whose purpose is to map nighttime cloud cover in the 4 micron window. A medium resolution infrared radiometer (MRIR) sensitive in five spectral regions similar to those in the Tiros radiometer is also planned for future Nimbus satellites, but will not be included in the first. Figure 25–30 shows a comparison of the significant features of Nimbus and Tiros. In all respects it can be seen that Nimbus represents a more sophisticated and complex spacecraft.

TIROS VS NIMBUS

	TIROS	NIMBUS
GEOMETRY	PILLBOX	DUMBELL
WEIGHT (LBS)	300	650
ORBITAL ALTITUDE (NAUTICAL MILES)	380	600
ORBITAL INCLINATION	48° - 58° DIRECT	80° POLAR, RETROGRADE
STABILIZATION	SPIN-STABILIZED	3-AXES EARTH ORIENTED
EARTH COVERAGE	10 TO 25	100
CAMERA RASTER	500 LINES/FRAME	800 LINES/FRAME
TV RESOLUTION (MILES)	1	½
MAXIMUM POWER AVAILABLE (WATTS)	20	400
IR SENSORS (RESOLUTION, MILES)	MRIR (30)	MRIR (30) HRIR (5)

FIGURE 25–30.—Comparison of the Tiros and Nimbus meteorological satellites.

The Spacecraft

The basic configuration of the Nimbus spacecraft is shown in figure 25–31. The height of the spacecraft is 9½ feet; the diameter of the toroidal ring is 4¾ feet; and the dimensions of each solar paddle are about 8 feet by 3 feet. Horizon sensors and a rate gyro, together with

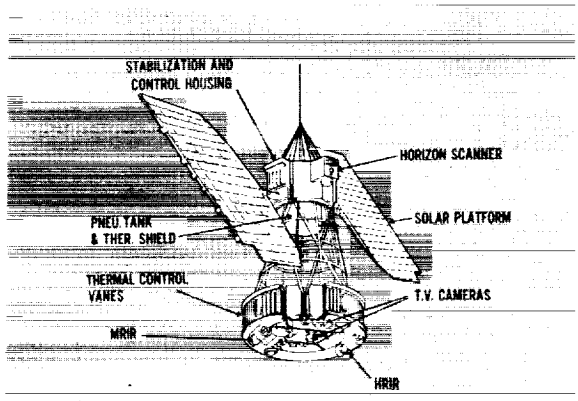

FIGURE 25–31.—Basic configuration of the Nimbus spacecraft.

reaction wheels and gas jets, are utilized to keep the spacecraft oriented along three axes with respect to the local vertical and the orbital plane.

Orbital Characteristics

Figure 25–32 illustrates the nature of the Nimbus orbit and the coverage by the camera subsystem. The nodal motion of the retrograde Nimbus orbit is eastward at exactly the same rate as that of the mean sun. This means that, if at launch the orbital ascending node occurs at local noon, the ascending node of every subsequent orbit throughout the lifetime of the satellite will also occur at local noon. About 32 sets of three pictures (a total of 96) will cover the entire daytime portion of the orbit with about 10 percent overlap between successive frames. During the approximately 107 minute period between successive equator crossings, the earth rotates 26.7° beneath the orbit. Each new orbital sequence of pictures, therefore, borders on the previous sequence at the equator with increasing overlap toward the pole.

The problem of ground data acquisition is considerably simplified by a near-polar orbit. One CDA station presently being installed at Fairbanks, Alaska, will be capable of interrogating 10 out of the 13.5 orbits per day. A second CDA station along the northeastern coast of North America will make the interrogation of all orbits possible.

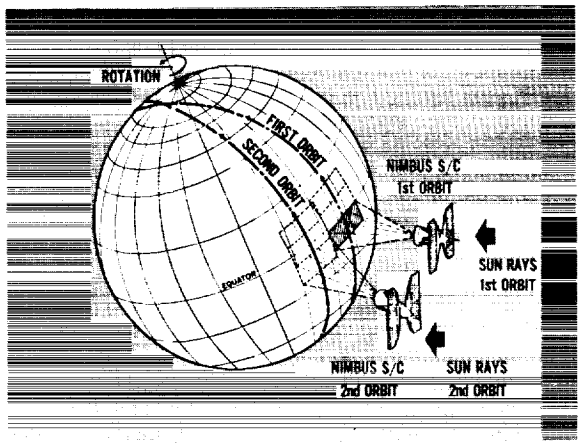

FIGURE 25–32.—The Nimbus orbit and coverage by the three-camera television subsystem. The nodal motion of the retrograde Nimbus orbit is eastward at the same rate as the relative motion of the sun.

On-Board Calibration

In contrast to the Tiros instrumentation, the Nimbus pictures will include a grey-scale calibration strip, and the radiometers will include an on-board calibration in the form of viewing a black target of known temperature by the thermal channels and viewing a diffuser illuminated by the sun once per orbit by the solar channels.

Data Utilization

The daily output of data from Nimbus will be an order of magnitude larger than the present output from Tiros. With virtually every spot on the globe observed twice daily (once in daylight and once in darkness) by improved sensory systems with on-board calibration, it is anticipated that utilization of the data for both operational and research purposes will also vastly increase. Therefore, it is imperative that the Tiros data handling system be revolutionized to incorporate the broadest possible use of automatic data processing methods.

These problems are presently under study by GSFC and NWSC. Although the data handling plan is not yet completed, it is being built around a framework including two CDC–924 digital computers at each CDA station, two IBM–7094 computers in the Washington area—one at GSFC and one at NWSC, and a 96 kcs wideband communication circuit linking these activities together.

In part, the overall concept envisions the following points:

1. The real-time computer processing of telemetry at the CDA stations for trouble shooting of satellite performance and for rapidly extracting the time, attitude, and satellite environmental parameters necessary for meteorological data reduction;
2. The real-time transmission of television and radiation data from the CDA stations to the Nimbus Technical Control Center (NTCC) in Washington, D.C., with the capability of electronically mixing latitude-longitude grids at either end of the wide-band communications link;
3. The automatic rectification and production of nephanalyses of television and radiation data, in addition to the high speed repro-

duction of photographs, assembly of mosaics, and incorporation of data into various prediction models and forecasting methods;

4. The delayed playback of master tapes at NWSC to produce archival photographs and at GSFC to produce archival radiation data tapes;
5. The delayed playback of telemetry tapes for a complete engineering performance evaluation at GSFC.

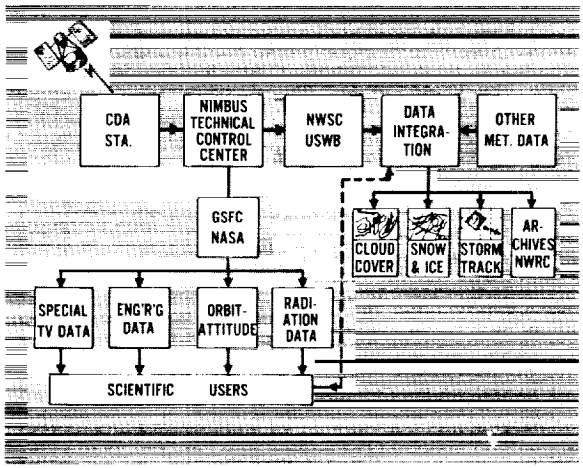

FIGURE 25–33.—Schematic representation of the Nimbus Data Distribution and Utilization System. A 96 kcs wide-band data link connects the Nimbus Technical Control Center (NTCC) with the Command and Data Acquisition (CDA) stations. The National Weather Satellite Center (NWSC) and the National Meteorological Center (NMC) combine satellite and conventional data into operational analyses and forecasts.

A schematic representation of the Nimbus Data Distribution and Utilization System is shown in figure 25–33. Among the most important elements of the system are scientific research of a basic and applied nature and the development of new and better instrumentation.

Possible future instrumentation for meteorological satellites includes spectrometers, lasers, microwave detectors, and sensors to measure the solar irradiance of the earth. Of particular interest in the latter experiment would be precise measurements of the solar "constant" and of those portions of the solar spectrum that are important in the photochemistry of ozone.

CONCLUDING REMARKS

We have discussed the Tiros satellite instrumentation, the flow of data from the orbiting sensors to the final output for utilization on the ground, and some of the problems associated with the reduction of the data. We have also briefly reviewed plans for the forthcoming second generation Nimbus meteorological satellite system. Meteorological satellites have already contributed significantly to the benefit and knowledge of mankind. We hope that many of the unsolved problems of the earth and atmosphere will soon be better understood because of meteorological satellite data, and we especially invite the Nation's universities to help in their solutions.

REFERENCES

1. STERNBERG, S., and W. G. STROUD: *TIROS I—Meteorological Satellite.* Astronautics, Vol. 5, June 1960, pp. 32–34 and 84–86.
2. BANDEEN, W. R., and W. P. MANGER: *Angular Motion of the TIROS I Meteorological Satellite Due to Magnetic and Gravitational Torques.* J. Geophys. Res., Vol. 65, Sept. 1960, pp. 2992–2995.
3. BRISTOR, C. L., E. G. ALBERT, and J. B. JONES: *Problems in Mapping Data from Meteorological Satellites.* Proceedings of the Second International Space Science Symposium, Florence, April 10–14, 1961, North-Holland Publishing Company, Amsterdam.
4. FUJITA, T.: *Outline of a Technique for Precise Rectification of Satellite Cloud Photographs.* Research Paper No. 3, Dept. of the Geophys. Sci., University of Chicago, Nov. 1961 (Technical Report to the U.S. Weather Bureau, Contract No. 10047).
5. HUBERT, L., and A. KRUEGER: *Satellite Pictures of Mesoscale Eddies.* Monthly Weather Review, Vol. 90, (to be published in November 1962).
6. BANDEEN, W. R., R. A. HANEL, JOHN LICHT, R. A. STAMPFL, and W. G. STROUD: *Infrared and Reflected Solar Radiation Measurements from the TIROS II Meteorological Satellite.* J. Geophys. Res., Vol. 65, Oct. 1961, pp. 3169–3185.

7. HANEL, R. A.: *Low Resolution Radiometer.* ARS Journal, Vol. 31, Feb. 1961, pp. 246–250.

8. HANEL, R. A. and W. G. STROUD: *Infrared Imaging from Satellites.* J. of the SMPTE, Vol. 69, Jan. 1960, pp. 25–26.

9. HANEL, R. A. and D. Q. WARK: *TIROS II Radiation Experimcnt and Its Physical Significance.* J. Opt. Soc. Amer., Vol. 51, Dec. 1961, pp. 1394–1399.

10. DAVIS, J. F., R. A. HANEL, R. A. STAMPFL, M. G. STRANGE, and M. R. TOWNSEND: *Telemetering Infrared Data from the TIROS Meteorological Satellites.* NASA Technical Note D–1293, Goddard Space Flight Center, Greenbelt, Maryland.

11. BANDEEN, W. R., B. J. CONRATH, W. NORDBERG, and H. P. THOMPSON: *A Radiation View of Hurricane Anna from the TIROS III Meteorological Satellite.* To be published in Proceedings of the International Symposium on Rocket and Satellite Meteorology, Washington, D.C., April 23–25, 1962, North-Holland Publishing Company, Amsterdam.

12. NORDBERG, W., W. R. BANDEEN, B. J. CONRATH, V. KUNDE, and I. PERSANO: *Preliminary Results of Radiation Measurements from the TIROS III Meteorological Satellite.* J. Atmos. Sci., Vol. 19. Jan. 1962, pp. 20–30.

13. WARK, D. Q., G. YAMAMOTO, and J. H. LIENISCH: *Methods of Estimating Infrared Flux and Surface Temperature from Meteorological Satellites.* J. Atmos. Sci., Vol. 19, Sept. 1962, pp. 369–384.

26. Data Acquisition at Planetary Ranges

By Charles C. Kirsten

CHARLES C. KIRSTEN, *Group Supervisor in the Communications System Development Section of Jet Propulsion Laboratory, was born in Asheville, North Carolina. He was graduated from the University of California at Los Angeles with a B.S. degree in Electrical Engineering in 1952. Mr. Kirsten is a member of IRE and Tau Beta Pi.*

To date, space communications at interplanetary distances have been largely limited to "bounce" experiments such as the Venus bounce experiments carried on by Jodrell Banks (Ref. 1), Stanford University (Ref. 2), Jet Propulsion Laboratory (JPL) at California Institute of Technology (Ref. 3), and others, or direct reception during radiotelescope, neutral-hydrogen, and noise-source plots (Refs. 4, 5).

In the bounce experiments, the transmitter power has been limited only by practical transmitter and feed powers (often going to megawatt pulses) and both transmitting and receiving antennas may be of very high gain.

In radioastronomy noise plots, the receiving antennas may also have very high gains. In both cases, the bandwidth of reception has been made as narrow as possible, with the antenna structures often being designed expressly for a very narrow frequency range.

Spacecraft communications at interplanetary distances borrow heavily from these techniques of radioastronomy in the matters of signal-source resolution, Earth rate tracking, and the general problems of interference-noise rejection.

However, because of the wide bandwidth requirements of some information signals for interplanetary telemetry (such as television or high-rate data), the technique of information transmission and reception at planetary distances assumes a somewhat different nature. This difference is characterized by the methods of information coding and filtering to assist in making the signals unique and distinguishable from the unavoidable noise in the system.

In short, it may be said that the requirements of long distance space telemetry are such that it must combine techniques from the fields of both radio astronomy and conventional telemetry systems.

Let us review the factors affecting space communications to put them in the proper perspective.

The problem, basically, is one of transferring intelligence energy from the transmitter location to the receiver location at a sufficiently high signal-to-noise ratio for the intelligence energy to be correctly interpreted by the receiver during a specified percentage of the time.

Ignoring the noise problem for the moment, let us examine the present means of transferring the intelligence power.

As may be seen in Figure 26–1, if energy is propagated from an isotropic source, the energy per unit area at a radius of X from the source will be $P_0/4\pi X^2$. The receivable energy will then be equal to the power per unit area times the area of the receiving antenna. Another way of stating this is that the received energy is proportional to the ratio of the receiving antenna area at some distance, X, to the total area over which the transmitted power has spread at that distance.

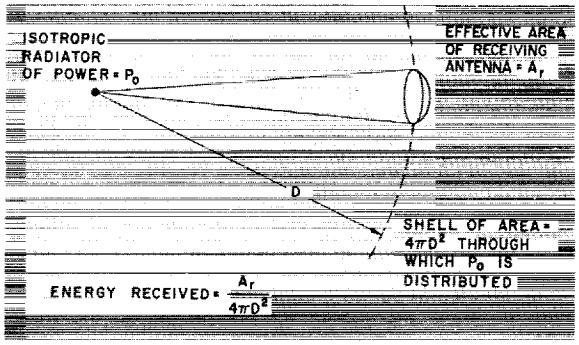

FIGURE 26–1.—Energy from isotropic source.

From Figure 26–2 we may deduce the manner of determining the transmitting-antenna power gain in the following manner.

$$G_t=\frac{A_{\text{space}}}{A_{\text{illuminated}}}=\frac{4\pi(X+L)^2}{\frac{\pi D_t^2}{4}\left(\frac{X+L}{L}\right)^2} \tag{1}$$

but $L<<X$, so

$$G_t=\frac{4\pi X^2}{\frac{\pi D_t^2}{4}\frac{X^2}{L}}=\frac{16L^2}{D_t^2} \tag{2}$$

From Figure 26–2:

$$\beta=\sin\beta=\frac{D_t}{L}=\frac{1.22\lambda}{D_t} \text{ (Ref. 6)}$$

or

$$L=\frac{D^2}{1.22\lambda}$$

Substituting in Eq. (2):

$$G_t=\frac{16D^2}{1.22^2\lambda^2}=10.7\,\frac{D^2}{\lambda^2}=\frac{\pi^2D^2}{\lambda^2} \tag{3}$$

Thus we see that G_t equals approximately ten times the aperture diameter in wave lengths squared.

Again looking at Figure 26–2, it is apparent that only that portion of the transmitted energy which is intercepted by the area, A_r, of the receiving antenna will be received. Thus:

$$\text{Power received}=P_o\frac{A_r}{A_i}=P_t\frac{A_r}{A_s}$$

$$P_r=P_oG_t\frac{A_r}{4\pi X^2}\approx P_o\frac{\pi^2D_t^2}{\lambda^2}\cdot\frac{A_r}{4\pi X^2} \tag{4}$$

$$P_r=P_oA_r\frac{\pi D_t^2}{4\lambda^2X^2}$$

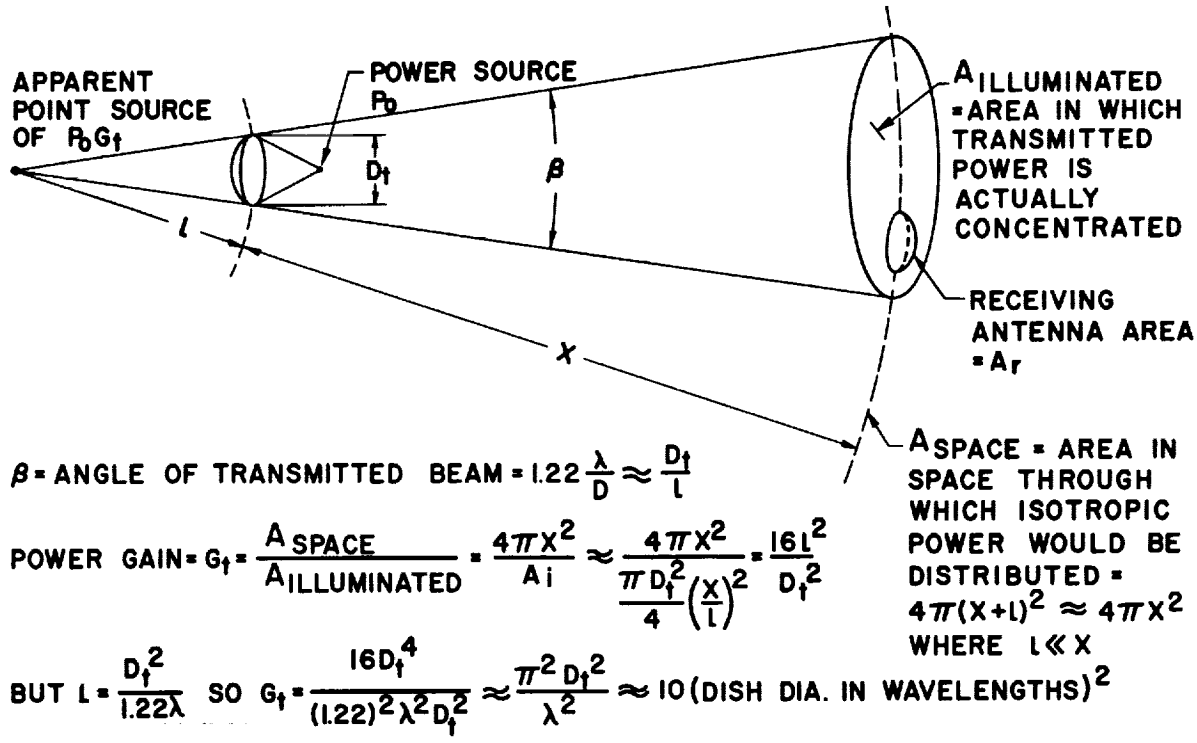

FIGURE 26–2.—Directivity G_t of circular aperture radiator.

If the area of the receiving antenna is taken as $A_r=\pi D_r^2/4$

$$P_r=P_o\frac{\pi D_t^2}{4\lambda^2}\cdot\frac{\pi D_r^2}{4}\cdot\frac{1}{X^2}=P_o\frac{\pi^2 D_t^2 D_r^2}{16\lambda^2 X^2} \qquad (5)$$

where

P_r=power received

P_o=power transmitted

A_r=area of receiving antenna

D_t=diameter of transmitting parabola

X=distance from spacecraft to receiver

D_r=diameter of receiving parabola

Let us now see how noise affects the transmission.

Noise in the communication sense is composed of randomly varying signals which are introduced into a system by the statistical nature of the universe.

Noise signals in an information-transmission system have two effects on the information, both of which produce the same end result: inability to distinguish the information.

First, noise perturbs the information by adding and subtracting from its components until the information is no longer recognizable, and second, it "suppresses" the information. This latter effect is caused by the fact that practical communication systems must be built with limited dynamic signal range. When power-plus-noise exceeds the system dynamic capability, both noise and the information power will be limited or suppressed. This effect is exceedingly common because many mechanizations of receivers deliberately use limiters to suppress noise in situations of high signal-to-noise energy. (In these cases, the noise is largely suppressed leaving signal).

Since noise is never absent from any communication system, particularly in interplanetary communication systems where the receivable signal power is small, its effects define the limits of communication distance and information bandwidth.

The sources of noise in an interplanetary communication system are numerous, but the largest contributors may be arbitrarily classified as follows (Ref. 7):

1. Man-made interference
2. Extra galactic background
3. Discrete galactic sources
4. Atmospheric noise (and absorption)
5. Earth noise
6. Antenna Johnson noise
7. Receiver noise

The first five sources of noise are external to the antenna, and impart noise into the system as receivable energy in both the bandwidth and the "look angle" of the antenna.

Referring to Figure 26–3, and recognizing that the receiving antenna has an included angle of reception which is wider than the angle subtended by the transmitting antenna, it is apparent that the receiving antenna must pick up extraneous noise energy from galactic sources as well as energy from the transmitted signal. If the receiving cone angle were small enough so that the transmitting antenna filled the receiving field of view, these extraneous noise sources would be excluded, and the receiving antenna would assume the noise temperature of the transmitted signal.

However, for practical antenna beam widths and antenna sizes, the transmitter must always be considered to be a point source at the distances we are considering.

Thus the noise sources associated with the sky, atmosphere, and Earth are the only considerations in determining the effective antenna noise temperature.

The total antenna noise temperature due to radiative sources can be determined by integrating over the entire 4π steradians surrounding the antenna, with the temperature, (T_e), and the antenna directivity (G_r) expressed as functions of the solid pointing angle $d\Omega$ (θ, ϕ),

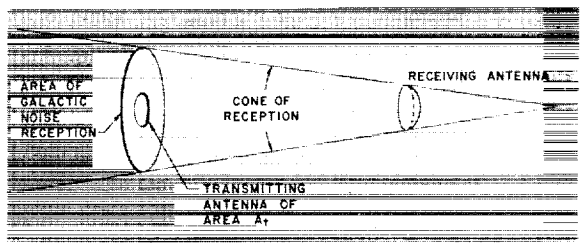

FIGURE 26–3.—Galactic noise cone.

and dividing by 4π steradians to obtain an average (Ref. 8). Thus:

$$T_a = \frac{1}{4\pi}\int\int_0^{4\pi} T_e(\theta, \phi), D_i(\theta, \phi) d\Omega$$

Fortunately, any one specific communication system operates on a comparatively narrow frequency spectrum, so the antenna look angle and resultant noise energies may be defined at a single frequency with fair accuracy.

Assuming a reasonable isolation from man-made interferences, which is the primary reason why deep-space tracking stations are located at isolated and inaccessible (Ref. 7) sites, the natural radiative noise sources may be examined separately.

Galactic noise was first observed by Karl G. Jansky in 1932 (Ref. 5), and is a steady noise emission from all parts of the sky. Its intensity varies with the galactic population, being greatest across the Milky Way, and reducing to a low value at the galactic poles, giving an irreducible "galactic background" noise which is attributed to extra-galactic sources.

The amount of received "galactic background" noise is dependent upon the antenna area, but is almost completely independent of the antenna directivity, or pointing, since the noise arrives from all directions (Ref. 9).

There are, however, many discrete and narrowly distributed noise sources in the sky which are received only when they are included in the antenna "look angle" or happen to be at one of the side-lobe, spurious response points in the antenna reception pattern (Ref. 8).

The total galactic noise is the sum of the background plus any discrete noise sources which may be included in the antenna field of view, and is therefore dependent upon the antenna beam width, becoming more "granular" as the receiving antenna beam is made smaller (antenna gain is increased).

The population of the discrete noise sources along the galactic equator becomes most numerous in the direction of the center of our galaxy which causes the variation in total galactic noise. Fortunately, the plane of the solar ecliptic is tilted relative to the plane of the Galaxy; but unfortunately, as shown in Figure 26–4, the axis of tilt passes very close to the galactic cen-

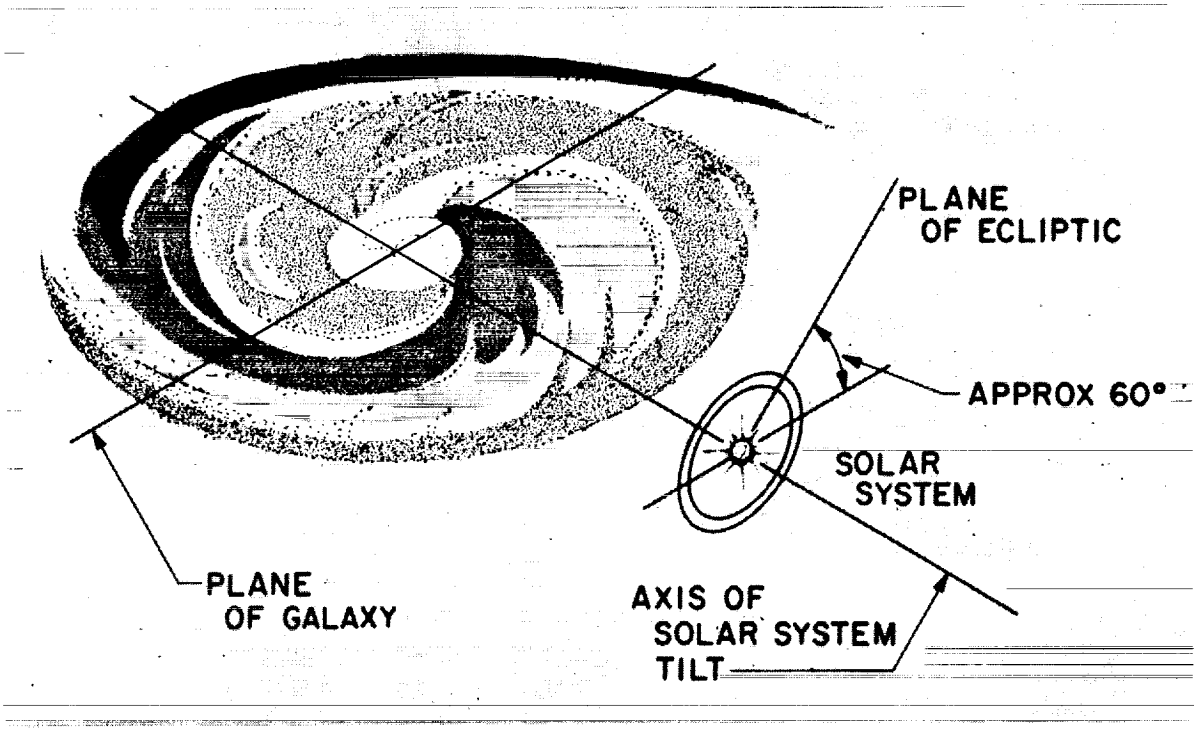

FIGURE 26–4.—Galaxy-ecliptic plane perspective.

ter (Ref. 5). Since most interplanetary communications will be in the plane of the ecliptic, it is inevitable that some tracking will be across the noisiest part of the sky. Some control over this pointing may be effected by choice of trajectory, and the time of year in which the tracking is done.

It should be mentioned here that in the case of planetary or spacecraft radio reception from the Earth, that the Earth becomes one of the primary noise sources. Also, in receiving Earth-based signals at outer planets, the Sun becomes a very serious source of communication noise, especially during periods of sun spots and solar excitement. The following table shows the maximum angle which may be expected between the Sun and the necessary antenna pointing for communication between planets.

Transmitting from	Receiver	Maximum antenna-angle from Sun, deg
Mercury	Earth	22
Venus	Earth	36
Earth	Mars	33
Earth	Jupiter	11
Earth	Saturn	6
Earth	Uranus and beyond	<3

The galactic noise is augmented by earth and atmosphere noise captured by the antenna. The warmth of the earth causes noise to be injected directly into the back lobes of the receiving antenna, and also, by refraction from the ionosphere, directly into the side lobes, and even into the main beam of the antenna when it is depressed below critical angles (Ref. 8, 10).

Noise energy generated in the atmosphere is collected by the main antenna beam and, as can be seen in Figure 26–5, is a function of the depth of atmosphere which the received beam must traverse (Ref. 10, 11).

All of these radiated noise energies are measured in watts per square meter per steradian per cycle per second. This has the dimensions of Boltzmann's constant per square meter per steradian, and has been arbitrarily defined as a Jansky unit (Ref. 5).

A more convenient terminology is often used,

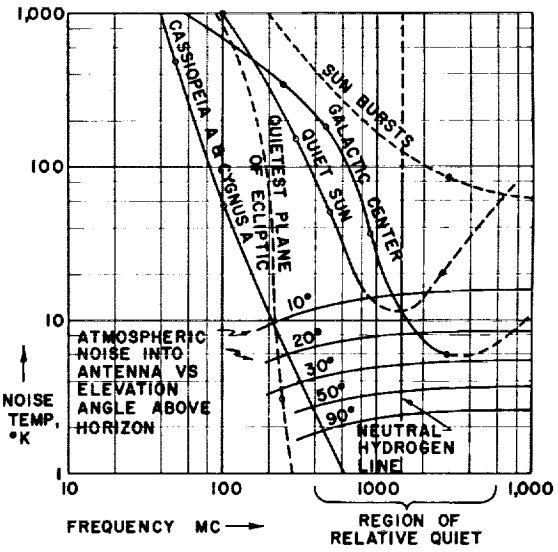

FIGURE 26–5.—Space noise sources.

however, by converting these normalized power-density measurements into equivalent temperatures (Ref. 9). This conversion is made by equating the power density at a given frequency received at earth to the radiation which would be received from a black-body enclosure of a corresponding temperature. Thus, for the galactic background noise temperature, an average measurement of received energy per square meter is made of the clear sky at the frequency of interest, and this value is used in the Rayleigh-Jeans approximation of Planck's radiation law to determine the equivalent black-body radiating temperature (Ref. 12).

$$B=\frac{2kf^2T}{c^2}\Delta f$$

where

B=brightness in w/m²/cps (assuming unit solid angle)

c=velocity of light=3×10^8 m/sec

K=Boltzmann's constant=1.3803×10^{-23} Joules/°K

f=frequency, cps

T=temperature of source, °K

f=bandwidth in cps

The same technique is used in determining

the "radio temperatures" of radio stars or noise sources. For example, the quiet sun energy averages approximately 4×10^{-21} w/m²/cps Janskys at 300 Mc.
Thus:

$$4\times10^{-21}=\frac{(2)(1.38\times10^{-23})(3\times10^{8})(T)}{(3\times10^{8})^{2}}$$

$$T=145°\text{K (at 300 Mc)}$$

It should be noted that this "radio temperature" is a fiction for most sources, since none of the discrete radio sources are "black body" radiators, and only a few of the distributed sources could be said to approximate this condition (Ref. 9).

More frequently given now, is a "total absolute brightness" temperature which may be determined by integrating the entire spectral emission from a source by deducing its radiant energy per steradian of solid angle, around the source itself (Refs. 4, 7).

Unfortunately, most of the radiating sources do not follow Planck's radiation law at the radio frequencies, so it is not always possible to deduce the amount of radiant energy in any one narrow band of frequencies just by knowing a "temperature" of the source.

Thus, "radio temperatures" defined at specific frequencies are still a useful, though most usually fictitious, concept.

The remaining sources of received noise are the Johnson or thermal noise in the internal resistance of the antenna, and the equivalent thermal noise at the input of the receiver.

The antenna noise is caused by thermal disturbance of electrons in the resistive components in the antenna impedance, and is determined by the familiar Nyquist equation (Ref. 6):

$$e^{2}=2KTR\triangle f$$

where

e=noise voltage RMS
K=Boltzmann's constant (1.38×10^{-23}
R=antenna resistance
$\triangle f$=frequency band considered

Again, the antenna Johnson noise may be defined in terms of equivalent temperature, and is defined to be the temperature of a resistor equal in value to the internal antenna impedance which would produce a thermal noise energy across the resistor equivalent to the Johnson noise contribution being seen at the output of the antenna in the frequency bandwidth in question.

Occasionally it is convenient to treat the entire noise being received by the antenna in a similar fashion, in order to derive an equivalent "antenna temperature" (Refs. 5, 6, 7).

This, of course, is only valid for one pointing direction and one frequency. Occasionally, the clear sky pointing at zenith is used as a reference temperature for an antenna, since it usually represents an irreducible minimum noise figure for that configuration of the antenna.

The last noise source to consider is the active receiver noise caused by shot noise and Johnson noise in the input elements of the receiver. This noise is dependent upon the thermal temperature of these elements, the impedance, and, of course, the mechanization (vacuum tubes, solid state elements, etc.).

In years past, the input noise of receivers has been so high that it was the primary limitation in the "low noise" frequency region shown in Figure 26–6. Recent developments (Refs. 13, 14) in parametric amplifiers and masers have essentially pulled this mask away from the galactic noise problems previously hidden beneath the receiver noise. This is shown in Figure 26–6 (Refs. 5, 7, 9, 10, 11).

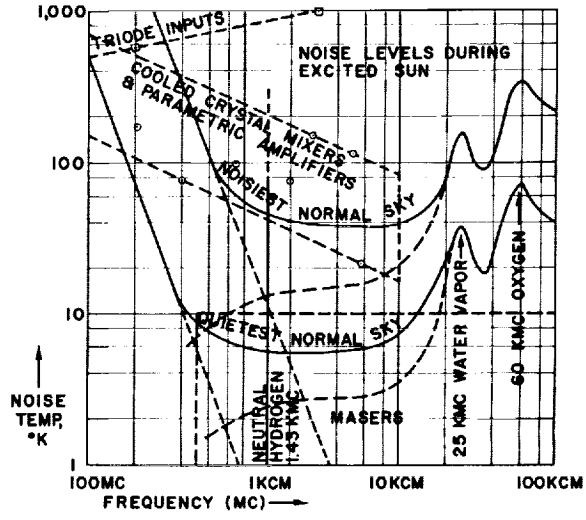

FIGURE 26–6.—Noise environment of reception.

Notice that the noise above approximately 250 Mc is primarily a function of the Earth's atmosphere. This strongly suggests that future communications with distant planets might better be served by satellite-or-moon-based deep space tracking stations. The tremendous advantage to the designer of a large-surface, precision dish for use under the low-gravity, no-wind conditions of the moon is interesting to imagine.

The noise energy received by an antenna from an extended galactic source is equal to the bandwidth times the flux density per square meter per steradian multiplied by the effective area of the antenna times the solid angle of reception of the source.

Using the Rayleigh-Jeans approximation (Ref. 9), we have

$$N=\frac{2KT_e}{\lambda^2}A_{eff}\Omega\Delta f$$

where

N=noise from diffuse source
T=effective temperature of source
K=Boltzmann's constant=1.38×10^{-23} Joule/°K
λ=wavelength, m
A_{eff}=effective area, m^2
f=bandwidth, cps
Ω=antenna solid beam angle, steradians (the source is assumed to fill the antenna look angle)

However, the expression for antenna beam width is:

$$\Omega=\frac{4\pi}{G_r}\approx\frac{4\pi\lambda^2}{10.7D^2}$$

and

$$A_{eff}\approx\frac{\pi D^2}{4}$$

so

$$N\approx\frac{2KT_e}{\lambda^2}\frac{\pi D^2}{4}\frac{4\pi\lambda^2}{10.7D^2}\Delta f$$

$$\approx 2KT_e\Delta f$$

Thus, the noise appears to be independent of frequency. However, examination of the general slope of the noise temperature vs. frequency dependence as shown by the averaged galactic noise data in Figure 26-6 shows that the slope of the exponent of f is closer to -2.5 than it is to -2 as given by the Rayleigh-Jeans approximation.

Since the temperatures given are defined in terms of the Rayleigh-Jeans approximation, we cannot use the -2.5 power directly. However, if we examine the differential noise relationship from one frequency (f_1) to another (f_2) we can express the differential resultant noise:

$$\Delta N=\frac{2K(T_2-T_1)\Delta f}{\lambda^{2.5}}\frac{\pi D^2}{4}\frac{4\pi\lambda^2}{10.7D^2}$$

which reduces to approximately:

$$\Delta N=\frac{2K(T_2-T_1)\Delta f}{\lambda^{0.5}}$$

The total received noise would then be:

$$N+\Delta N=2KT_e\Delta f+\frac{2K(T_2-T_1)\Delta f}{\lambda^{0.5}}$$

$$=2K\left(T_e+\frac{\Delta T}{\lambda^{0.5}}\right)\Delta f$$

Thus the energy received from diffuse galactic sources may be considered to vary directly as the square root of the frequency.

For reasonably wide antenna beam widths, a scattered field of point sources should appear similar to an extended source, so in most situations it is reasonable to treat the galactic noise as an extended source (Refs. 5, 7).

This is particularly true in planet-to-Earth communications, since much of the noise arises in the very extended atmospheric noise source in the Earth's atmosphere.

However, in those cases where there are high-energy point sources in the field of view of the receiving antenna, a different set of criteria exists. This will quite naturally be realized should we at some future time depend upon a satellite relay station outside the Earth's atmosphere.

The ultimate distance over which we can satisfactorily communicate rests largely on the degree of degradation we are willing to accept in the received intelligence. The definition of

satisfactory "threshold" may be very arbitrarily made, but the intelligence-signal degradation is a direct function of the ratio of the signal to noise powers.

Let us combine the results of the communication power transmission and the probable received noise power to ascertain their relationship.

We have seen from Figure 26–6 that masers make noise input contributions to the overall communication system which can be, and usually are, lower than the galactic and atmospheric noise contributions (Ref. 14). It is also true that by use of the maser preamplifier right at the input feed to the antenna, the contribution of the antenna itself can be made extremely low.

Assuming this, and that we are treating all sky noise as an extended source, the signal-to-noise ratio of a signal received at Earth may be stated thus:

$$\frac{P_r}{N+\Delta N}=\frac{P_o\frac{\pi^2D_t^2D_r^2}{16\lambda^2x^2}}{2K\left(T_e+\frac{\Delta T}{\lambda^{0.5}}\right)\Delta f}$$

However, since we have postulated fully coherent polarization of our transmitted signal, and the noise is completely random in its polarization, we will receive only one-half of the noise energy (Ref. 12). Thus, the noise energy would be:

$$(N+\Delta N)_{\text{receivable}}=K\left(T_e+\frac{\Delta T}{\lambda^{0.5}}\right)\Delta f$$

The simplified expression for the signal-to-noise power is:

$$\frac{P_r}{N+\Delta N}=\frac{P_o\pi^2D_t^2D_r^2}{16\lambda^2x^2K\left(T_e+\frac{\Delta T}{\lambda^{0.5}}\right)\Delta f}$$

This may also be written in terms of the antenna gains:

$$\frac{P_r}{N+\Delta N}=P_o\frac{\pi^2D_t^2}{\lambda^2}\frac{\pi^2D_r^2}{\lambda^2}\frac{\lambda^2}{16\pi^2X^2K\left(T_e+\frac{\Delta T}{\lambda^{0.5}}\right)\Delta f}$$

$$=\frac{P_oG_tG_r\lambda^2}{16\pi^2X^2K\left(T_e+\frac{\Delta T}{\lambda^{0.5}}\right)\Delta f}$$

Defining $P_r/(N+\Delta N)=Q$ as the minimum acceptable signal-to-noise input to the receiver, and solving for the distance:

$$X=\left(\frac{P_oG_tG_r\lambda^2}{16\pi^2K\left(T_e+\frac{\Delta T}{\lambda^{0.5}}\right)Q\Delta f}\right)^{1/2}$$

$$=\left(\frac{P_o\pi^2D_t^2D_r^2}{16\lambda^2K\left(T_e+\frac{\Delta T}{\lambda^{0.5}}\right)Q\Delta f}\right)^{1/2}$$

$$=\frac{\pi D_tD_r}{4\lambda}\left(\frac{P_o}{K\left(T_e+\frac{\Delta T}{\lambda^{0.5}}\right)Q\Delta f}\right)^{1/2}$$

$$\approx 222D_tD_rf\left(\frac{P_o}{Q\left(T_e+\frac{\Delta T}{\lambda^{0.5}}\right)\Delta f}\right)^{1/2}$$

From this it can be seen that the distance of transmission is directly proportional to the antenna-dish diameters, to the frequency, and to the one-half power of the transmitted power.

Distance is inversely proportional to the one-half powers of the acceptable receiver signal-to-noise ratio, the sky temperature, and the noise bandwidth. Notice that where T_e is small, the differential distance approaches being proportional to the three-fourths power of the frequency.

This frequency-to-noise relationship is very approximate, and holds only over the frequency range from 200 Mc to about 1000 Mc for communications through the Earth's atmosphere. Outside the atmosphere, the relationship would continue on up in frequency to some (at this time) unknown limit—probably at least beyond 50–100 k Mc.

However, starting at about 1000 Mc, the Earth's atmospheric noise contribution grossly changes the received noise-to-frequency relationship, so that noise power rises sharply with frequency.

The region of relative noise power minimum is in the range of frequencies from 1 k Mc to 10 k Mc, having its lowest point at approximately 1.5 k Mc to 2.5 k Mc at zenith pointing, and depending upon the galactic sources included in the beam. Assuming that distance has been minimized by selecting a time of opera-

tions during planetary perigee, the most effective controlling parameters are dish diameters and the frequency.

To those who follow radio astronomy it is apparent that receiving-dish diameters are rapidly approaching their technical and economic limits. The present JPL Deep Space Instrumentation Facility parabolic antennas are 85 feet in diameter with a gain above an isotropic source of approximately 45 db. A single new dish under consideration for construction at the Goldstone, California, facility is 210 feet in diameter, with a theoretical gain of 56 db at 960 Mc, but the technical problems of keeping the dish surface sufficiently accurate under varying attitudes, sun-heat, and wind-loading conditions is indeed formidable. The reflecting surface must be controlled within approximately ±10 electrical degrees to assure no appreciable degradation of gain characteristics.

Figure 26-7 (Ref. 10) illustrates the degradation of gain which is experienced with increasing frequency where the antenna surface irregularities limit the coherence of the collected energy. This "gain limiting" effect makes it fruitless to raise the frequency of operation beyond the capabilities of the antenna and, in fact, when the wave length is reduced to the point where the irregularities are of the order of $\lambda/_4$, causes complete loss of gain.

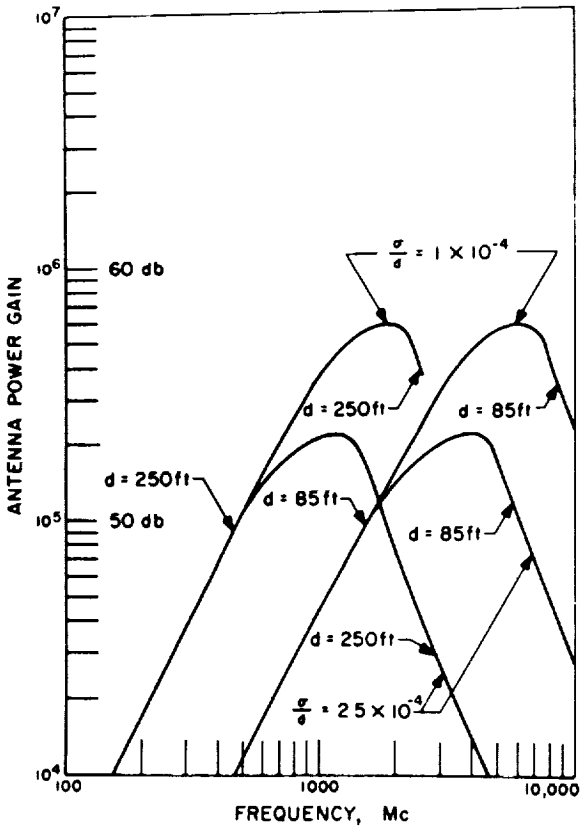

FIGURE 26-7.—Antenna gain vs frequency.

The inference from practical measurements on typical antennas is that there is a maximum gain factor ratio, D/λ, which is very difficult to exceed, and this appears, for fully-steerable parabolic antennas, to be somewhere around 300–400. For example, the tolerances imposed by this figure on our 85-ft dish at Goldstone is approximately $\pm 1/16$ in. over the entire surface for no appreciable degradation at 3000 Mc.

This constraint is also a function of the overall size of the antenna since, in general construction practice, the deflections tend to assume magnitudes proportional to the overall size. This can be mitigated by very careful design and construction practices on the larger antennas, but the cost becomes prohibitive when related to the relative increase in performance (Ref. 10).

This forces us to build antennas to no greater accuracy than is foreseeably required, and to use them in a "gain limited" manner—that is, the operating frequency is generally as high as the antenna accuracy permits. As can be seen from Figure 26-7 (where $\sigma/D \approx \lambda/12D$) we still have a little way to go in raising our operating frequency above the present 890–960 Mc Mariner 2 operating frequencies before the performance is seriously impaired.

The transmitting antenna on the Mariner spacecraft is a modest 48 inches in diameter with a gain of 18 db. It might be felt that this size and gain could very easily be increased by clever mechanical design. This is probably true, but the pointing problem of the resulting thin radio beam from a stabilized spacecraft can be a far more severe constraint than other aspects of the system. The present spacecraft antenna has a transmitting beam width included angle of approximately 18 deg. This allows a reasonable off-set pointing error in spacecraft attitude control, with additional latitude for some angular cycling.

These factors have already set a limit on the improvement which may reasonably be obtained through an increase in antenna size for future planetary space probes. The other factor which will definitely be changed is the operating frequency. The present JPL Mariner operating frequency of 890–960 Mc will be increased to 2300 Mc in the near future. According to the above dependencies, we should realize approximately twice the distance for the same transmitter power and antenna diameters. Since range determination and other factors in the communication system are frequently varied, it is much more convenient to have a less cumbersome notation. This is easily accomplished by using a logarithmic form for the equation:

$$X^2=\frac{P_oG_tG_r\lambda^2}{16\pi^2KT\Delta f\left(\frac{P_r}{N}\right)}$$

This becomes:

$$\text{Log } P_oG_tG_r=\text{Log }\frac{16\pi^2X^2}{\lambda^2}+\text{Log }\frac{P_r}{N}+\text{Log }\Delta f+\text{Log }KT$$

but

$\frac{16\pi^2X^2}{\lambda^2}$ = space loss ratio

$\frac{P_r}{N}$ = required signal-to-noise ratio in Δf

Δf = noise bandwidth, cycles

KT = noise power per cycle

Martin (Ref. 16) has refined this notation to an easily usable form by separating the KT power into two parts: that from 0° K to 290° K, and the additional power in decibels above the 290° K level. All units are now expressed in decibels, and the logarithmic notation is dropped so that in db:

P_t = total transmitted power (dbm)

G_t = transmitting antenna power gain over isotropic (db)

G_r = receiving antenna power gain over isotropic (db)

$2B_{L0}$ = ten times the log of the noise bandwidth (db) (this may be either the predetection noise bandwidth in cycles or subsequent filtering bandwidth, whichever determines the uncorrupted noise bandwidth of the system)

$\left(\frac{S}{N}\right)_{2B_{L0}}$ = ten times the log of the required signal-to-noise ratio in $2B_{L0}$ for defined threshold (db).

Φ_{KT} = noise power per cycle at 290°K = 10 log (290) (Boltzmann's Constant) = −174 dbm/cps

Φ_{NF} = ten times the log of the excess noise power per cycle above 290°K (db); this is the stated overall noise figure in decibels where ambient temperature is used as a reference.

L_s = ten times the space loss ratio expressed by

$$\frac{16\pi^2\chi^2}{\lambda^2}, \text{ db}$$

L_p = any uncertainty factor required to assure operation under worst case conditions (db)

L_m = any miscellaneous losses in cables, etc. (db)

As we have just seen, most of the parameters entering into the range equation are well defined or definable. These include P_t, G_t, G_r, $2B_{L0}$, Φ_{KT}, L_s and L_p.

The two parameters which are not easily defined, unless all conditions are known, are: (a) Φ_{NF}, the input noise power and (b) $\left(\frac{S}{N}\right)_{2B_{L0}}$, the acceptable threshold signal-to-noise ratio in the noise bandwidth. For this reason, and small uncertainties which add up in measuring the other parameters, it is common practice to insert a "fudge factor" of approximately four to eight decibels in a practical communication system to take care of the uncertainties of antenna pointing, atmospherics, etc., which may be expected but are not definitely known, in order to assure successful communications.

We have already reviewed, to a certain extent, the vagaries of cosmic and atmospheric noise, so let us now turn our attention to the other rather vague term, $\left(\frac{S}{N}\right)_{2B_{L0}}$, the "required signal-to-noise in the noise bandwidth."

In the past, the ultimate distance to which we could satisfactorily communicate rested largely upon our definition of how much degradation we were willing to accept in the received intelligence before calling it "threshold". It has always been a problem to the telemetering engineer that there was no discrete threshold on some of the simpler analog mechanizations of AM and FM telemetry. The data simply became more and more noisy until it became a matter of conjecture whether you were receiving noise-like data, or data-like noise.

Much of this uncertainty was removed by the advent of phase tracking filters (Ref. 17), and similar correlation devices.

Although these devices work much closer to the Shannon limit of information transfer for specified bandwidths, they do this by a method of averaging-out the interfering noise either in the time domain, or the frequency domain, or both. This averaging, in the usual case, requires a certain integration time before the detector is able to decide that it is truly receiving distinctive data, and once it loses track of the signal in time (loss of phase coherence) it must again perform its integration function to "reacquire". The result, of course, is that at some much lower "break point", phase coherence will be lost momentarily, with attendant loss of time in resynchronization, resulting in a very quick degradation of the output signal-to-noise as the input signal-to-noise is lowered.

Any reasonable discussion of coding theory is beyond the scope of this paper, but JPL has been particularly active in this field, and there are many excellent JPL references which are the basis of the present Mariner 2 telemetry system and of JPL communication systems which are now in development (Refs. 18, 19, 20, 21).

A description of some of the practical constraints of design for the Mariner system are probably worth mentioning, since they are seldom mentioned in rigorous treatments.

Figure 26–8 gives the theoretical probability of bit error versus the ratio of the information energy per information bit to the noise energy per cycle of bandwidth for several common coding methods. The threshold S/N at which degradation begins, becomes lower as the coding

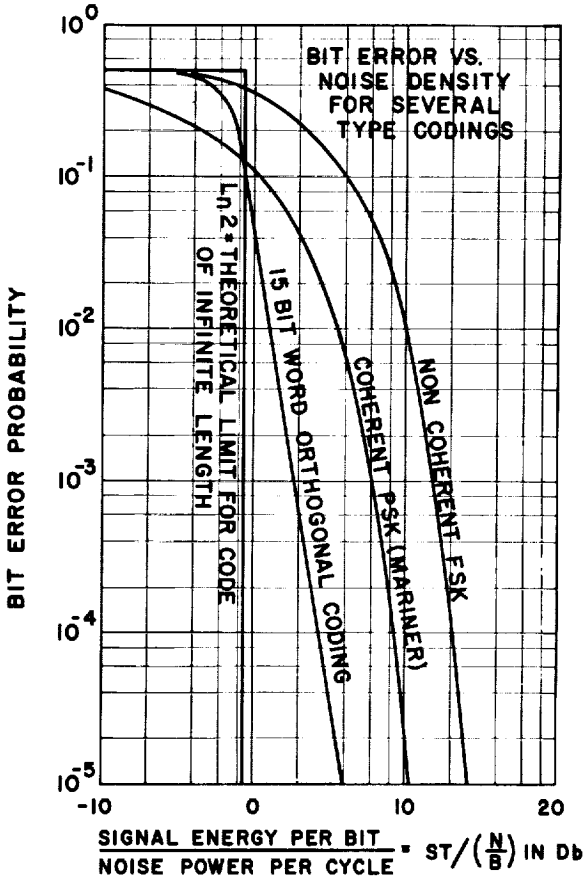

FIGURE 26–8.—Bit error vs noise density for several type codings.

of information becomes increasingly redundant, with a theoretical limit (Ref. 19) of:

$$BT\Big/\frac{S}{N}=\text{Ln } 2$$

The middle curve is the theoretical performance limit for a phase-shift keyed binary coded communication system. The Mariner system is a coherent PSK coded system using separate subcarrier channels for synchronization and information. Tests on the subcarrier demodulation system reveal performance within 0.5 to 1.0 db of the theoretical.

This performance has been accomplished by the use of pseudo-noise coding in the synchronization channel to give both matched filter detection of the data bits, and data word synchronization.

Both subcarrier channels in the Mariner are modulated ± 90 deg in phase, allowing simple

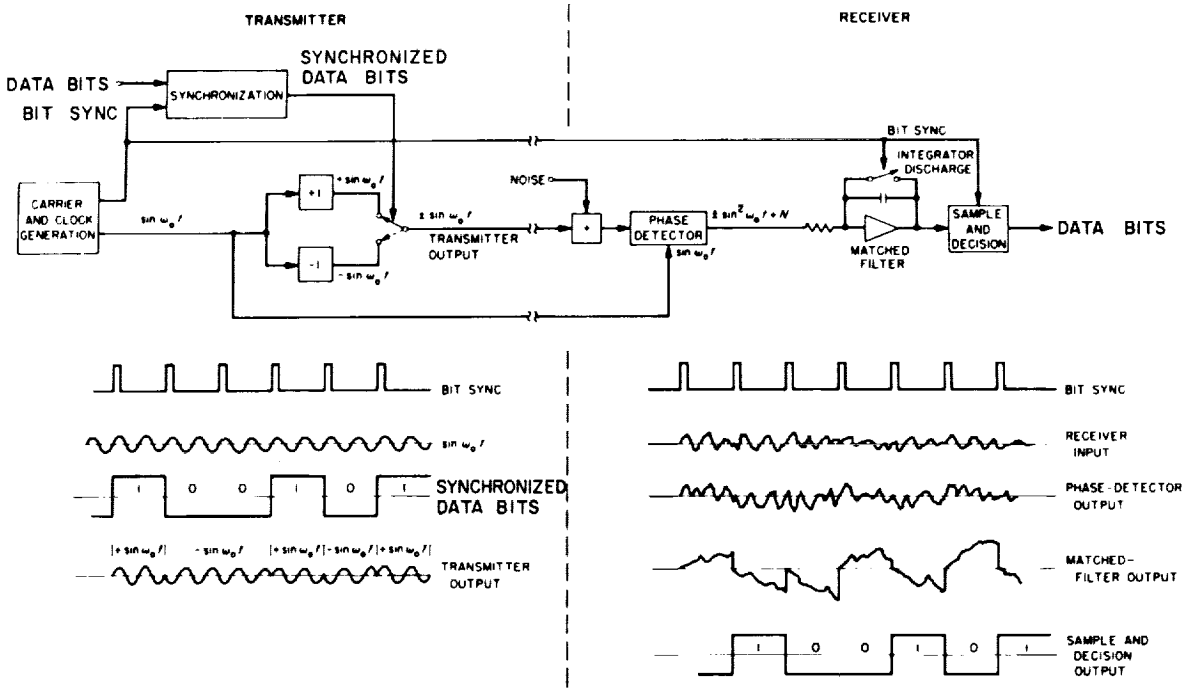

FIGURE 26–9.—Matched bit filter by "integrate and dump."

logical circuitry to be used in the modulation and demodulation equipment. Figure 26–9 shows the method of performing optimum detection of a transmitted signal being phase modulated ±90 deg, where

$$\text{Sin}\ (\omega t + 90\ \text{deg}) = \pm \text{Sin}\ \omega t$$

The transmitted signal is disturbed in both amplitude and phase during its transmission, giving $\pm\sin \omega t + \overline{N}$.

This is phase detected against a locally generated reference of sin (ωt + 90 deg). The resultant output of $N \pm 1/2$ is applied to a high quality integrator.

The integrator is "dumped" or reset at the very beginning of each possible incoming data bit, and the integrated level is sampled just at the end of each period of integration to detect whether a "one" or a "zero" was being transmitted during that bit period. The final decision device is a precision level detector which samples the integrator.

Typical waveforms are given to illustrate the action of the integrator in separating the information bit from the noise.

No hint is given in Figure 26–9 of the method of transmitting the bit synchronization pulses which are necessary to time the integration and dump times. As previously stated, this is done by a separate synchronization channel which is shown in simplified form in Figure 26–10.

As may be seen, a pseudo-noise code generator is the local coding device in both the transmitter and the receiver, being stepped in synchronism by the $2f_s$ source in the transmitters and by a phase locked, voltage controlled local oscillator in the receiver. The two PN generators cyclically produce the same code of a predetermined length, which is random in the statistical distribution of ones and zeros that its spectrum is pseudo-noise. For this purpose, a particular code is chosen, which has only one point of autocorrelation along its entire length, even when compared to a series of the same code taken in sequence. As a result, the codes may be used in a phase locked loop as shown, by performing a modulo 2 addition between the incoming and the local PN codes, and integrating the serial result. When the two codes are out of phase, the sum will be essentially zero, but when the codes are aligned, the integrated value will be the sum of all the bit agreements along the entire code length. The PN code

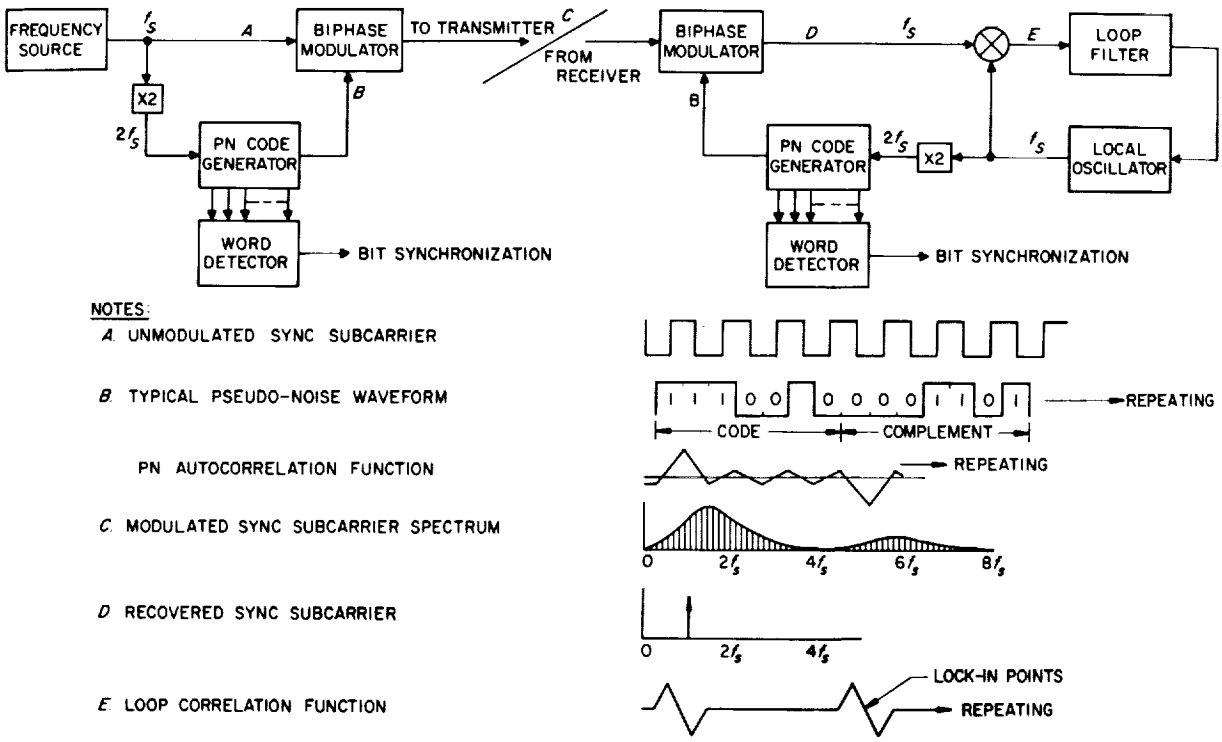

FIGURE 26–10.—Pseudo-noise sync channel.

length used in the Mariner 2 is 63 bits long for these reasons:

1. The code must be sufficiently long so that occasional bit errors will not appreciably degrade its correlation properties.
2. The code should not be so long that it requires any more generation equipment than necessary.
3. It must meet the criteria of bit length= 4n –1 to meet the transorthogonal criteria of having only one comma-free autocorrelation point.
4. It should meet the criteria of bit length= 2n –1 to allow the longest code to be derived from the least number of flip-flops.
5. It must have 7 as a factor.

The last criterion was imposed, because it was decided early in the Mariner design to acquire word syncronization as well as bit sync from the PN mechanization. The desired quantization level for measurements was 2 (Ref. 7), so a seven bit information word, transmitted simultaneously with a 63 bit PN code would allow the assignment of an even nine bits of PN code to each information bit.

The spectrum of a PN modulated synchronization subcarrier channel is graphically shown in line C of Figure 26–10. Notice that there is a null in the spectrum around the region of four times the subcarrier which is being PN modulated. Advantage has been taken of this in the Mariner to place the information subcarrier at a frequency which would have the least common spectrum occupancy with the sync channel. This results in a fully coherent system of frequencies which hold the same relative ratios, no matter what information rate may be transmitted. These ratios are: 1 word =7 information bits=63 PN bits=126 cycles of PN clock=252 cycles of information subcarrier.

The sync channel provides its own local phase-locked frequency drive for the PN code generator in the ground equipment using the usual narrow band servo feedback techniques. The information channel also derives its own sin ωt reference frequency in a similar manner. In the present ground demodulator, either one of these loops may be used as reference for the other by multiplying up in frequency or divid-

ing down, whichever is necessary. Minimum phase jitter is experienced when the system is being phase clocked by the highest available frequency, which also happens to have the strongest spectral energy. This is the information subcarrier.

There is of course, a slight technical detail which so far has been omitted for the sake of simplicity. This detail concerns the fact that when the composite correlation function of a PN code modulated on a coherent subcarrier is taken on itself, the correlation function reverses sign at each successive match point for the PN code. The necessary logic to correct this problem has the unfortunate characteristic that it destroys the sync channel subcarrier frequency by bi-phase modulating it. Consequently, phase lock information can only be derived from the sync subcarrier by autocorrelation (squaring the sync subcarrier). This causes some complication to the system, but has not appeared to degrade its ultimate performance, since final sync is taken from the data subcarrier which has more inherent power, and being four times higher in frequency is a better phase reference.

At this point, it should be pointed out that the incoming RF signal is essentially divided into two components—that part of the carrier power which is converted into sideband information energy, and the remaining unmodulated RF carrier power.

Since the RF receivers are used for tracking as well as for information, the tracking noise bandwidth is made extremely narrow (20 cps) and the wideband information channel (3000 cps) is taken from the error function of the RF tracking servo loop in the receiver.

The narrow band unmodulated RF carrier energy defines the energy available to the RF receiver for its acquisition and tracking, and the sideband energy defines the available energy in the coded information channel.

It has been common practice at JPL to adjust the relative RF and sideband information energies so that the subcarrier demodulator threshold is 3–6 db higher than the RF receiver threshold. This ensures proper RF tracking beyond actual data capability, and also simplifies operational lock-acquisition procedures, particularly on marginal signals.

The JPL Deep Space Instrumentation receivers have an RF signal threshold of -160 dbm to -162 dbm using parametric RF preamplifiers (Ref. 13).

By using a helium cooled maser at the Goldstone Pioneer Site, this threshold is dropped an additional 5 db to -167 dbm.

The telemetry subcarrier demodulator has a theoretical defined threshold of 6.5 db signal-to-noise at its input for a resultant word error probability of one word in one hundred at its output. This is equivalent to a bit error probability of one bit in 1.4×10^3 bits for the 7 bit words being used.

What does all this mean in terms of a practical interplanetary system such as the Mariner 2? Since no-one has ever really transmitted over these distances one way, it means that very close attention to all noise and threshold criteria is mandatory throughout the communication system design to assure predicted performance.

For this purpose, design control tables are carefully tabulated for each spacecraft communication system design, and these are constantly reviewed and revised as changes or modifications are made in the DSIF equipment or spacecraft communications. Table 26–I shows a typical control table as compiled by R. P. Mathison for Mariner 2.

During flight, a constant check through telemetered data is made on the spacecraft transmitter power output, its receiver A.G.C. and phase lock loop error voltages. The ground system transmitter power and receiver parameters are also monitored, and the results are compared to the design tables. These are used to check spacecraft performance, and to look for inadequacies or inaccuracies in the design table figures.

As may be seen from the tables, we have a design which looks very reasonable for our lower data rates at Venus encounter, and thus far, the performance of the communication link to the spacecraft is remarkably close to theoretical prediction.

Returning to the range equation, let us see what our potentialities are for immediate communications with other planets than Venus.

TABLE 26-I.—*Mariner 2 Communications Design Control Table*

TELECOMMUNICATION DESIGN CONTROL TABLE DATE 3-13-62

PROJECT: MARINER 2 PAGE 1 of 2

CHANNEL: S/C TO EARTH

MODE: L BAND HI GAIN 2G (MODE 2B WITH PREPLATE) W/O DIPLEX

NO	PARAMETER	VALUE	TOLERANCE	SOURCE
1	Total Transmitter Power	+ 34.1 dbm	+0.0 −1.0 db	
2	Transmitting Circuit Loss	− 0.7 db	± 0.2 db	
3	Transmitting Antenna Gain	+ 20.0 db	± 0.3 db	
4	Transmitting Antenna Pointing Loss	− 0.33 db	+0.33 −0.1 db	
5	Space Loss	− 247.66 db	−	
	•960.050 MC. R = 6X10⁷ KM			
6	Polarization Loss	− 0.0 db	−	
7	Receiving Antenna Gain	+ 45.7 db	± 0.8 db	
8	Receiving Antenna Pointing Loss	− 0.0 db	−	
9	Receiving Circuit Loss	− 0.2 db	± 0.1 db	
10	Net Circuit Loss	− 183.19 db	+1.73 −1.5 db	
11	Total Received Power	− 149.09 db	+1.73 −2.5 db	
12	Receiver Noise Spectral Density (N/B)	− 177.24 dbm/cps	+0.87 −1.13 db	
	T System = 137°			
13	Carrier Modulation Loss	− 2.48 db	+0.42 −0.34 db	
14	Received Carrier Power	− 151.57 dbm	+2.15 −2.84 db	
15	Carrier APC Noise BW ($2B_{LO}$ = 20 CPS)	+ 13.01 db	+0.79 −0.97 db	
	CARRIER PERFORMANCE - TRACKING (one-way)			
16	Threshold SNR in $2B_{LO}$	+ 0.0 db	−	
17	Threshold Carrier Power	− 164.23 dbm	+1.66 −2.10 db	
18	Performance Margin	+ 12.66 db	+4.25 −4.50 db	
	CARRIER PERFORMANCE - TRACKING (two-way)			
19	Threshold SNR in $2B_{LO}$	+ 2.0 db	−	
20	Threshold Carrier Power	− 162.23 dbm	+1.66 db −2.10	
21	Performance Margin	10.66 db	+4.25 db −4.50	

JPL 0456 SEPT 61

TELECOMMUNICATION DESIGN CONTROL TABLE DATE 3-13-62

PROJECT: MARINER 2 PAGE 2 of 2

CHANNEL: S/C TO EARTH

MODE: L BAND HI GAIN 2G (MODE 2B WITH PREPLATE) W/O DIPLEX.

NO.	PARAMETER	VALUE	TOLERANCE	SOURCE
	CARRIER PERFORMANCE -			
22	Threshold SNR in $2B_{LO}$	+ 4.0 db		
23	Threshold Carrier Power	− 160.23 dbm	+1.66 db −2.10	
24	Performance Margin	8.66 db	+4.25 db −4.50	
	DATA CHANNEL			
25	Modulation Loss	− 4.3 db	+0.47 db −0.4	
26	Received Data Subcarrier Power	− 153.39 dbm	+2.20 −2.9 db	
27	Bit Rate (1/T) 8.33 BPS	+ 9.21 db	± 0.4 db	
28	Required ST/N/B	+ 8.0 db	+1.0 −1.0 db	
29	Threshold Subcarrier Power	−160.03 dbm	+2.27 −3.90 db	
30	Performance Margin	+ 6.64 db	+6.10 −5.17 db	
	SYNC CHANNEL			
31	Modulation Loss	− 16.34 db	+0.25 −0.38 db	
32	Receiver SYNC Subcarrier Power	−165.43 dbm	+1.95 −2.88 db	
33	SYNC APC Noise BW($2B_{LO}$ = .5 CPS)	− 3.01 db	± 0.4 db	
34	Threshold SNR in $2B_{LO}$	+ 7.5 db	± 0.5 db	
35	Threshold Subcarrier Power	−172.75 dbm	+1.77 db −2.03	
36	Performance Margin	+ 7.32 db	+4.01 −4.65 db	

COMMENTS:

JPL 0456 SEPT 61

Separating the space loss, $L_s=16\pi^2X^2/\lambda^2$ into two components, $L_s=(4\pi/\lambda)^2+X^2$, grouping all coupling, uncertainty, modulation, polarization and miscellaneous losses together, and letting Δf=noise bandwidth ($2B_{Lo}$), we get, in decibels:

$$P_t+G_t+G_r=L_{total}+\left(\frac{4\pi}{\lambda}\right)^2$$

$$+X^2+\Phi_k+T+\Delta f+\left(\frac{S}{N}\right)_{\Delta f}$$

Substituting approximate but realistic figures (Ref. 15) for the present Mariner 2 implementations [i.e., 1 cps noise bandwidth, 15° K antenna temperature, 9db=$(S/N_{\Delta f}$] introducing 2300 Mc as the operating frequency, and solving for transmitter power as a function of distance:

$$P_t+52+25=10+40+X^2-198.6+15+\Delta f+9$$

or

$$P_t=X^2-202+\Delta f$$

At Moon distance:

$$P_t=172-202+\Delta f$$

$$=-30\text{dbm}+\Delta f$$

This implies a 1000 cps communication bandwidth for one milliwatt to Moon distance.

Table II shows the power requirements for a normalized, 1-cps communication bandwidth for the other planetary distances. Note that the distance in db is *not* the space loss. The space loss may be determined by adding 40 db to the figures given, where the 40 db represents the $(4\pi/\lambda)^2$ portion of the space loss.

Admittedly these are pessimistic figures, for they are based on items currently in use, or near imminent use. The inference however is clear; communications to all of these planets is not only feasible but reasonable within the limitations of currently available designs.

TABLE 26-II.—*Representative Normalized Capability of Mariner System at 2300 Mc*

Planet	Relative distance (1 meter reference), db	Power for 1 cps, dbm	Transmitted power for 1 cps, w	Bandwidth for 3 watts (35 dbm), cps
Moon	172	−30	Below capability	Above capability
Venus (near)	215	13	0. 02	160
Venus (far)	228	26	0. 4	8
Mars (near)	221	16	0. 04	80
Mars (far)	234	32	0. 16	2
Mercury (near)	219	17	0. 05	65
Mercury (far)	226	24	0. 25	12
Jupiter (near)	236	34	2. 5	1. 2
Jupiter (far)	240	38	6. 3	0. 5
Saturn (near)	242	40	10. 0	0. 3
Saturn (far)	244	42	16. 0	0. 2
Uranus (near)	249	47	50	0. 06
Uranus (far)	250	48	63	0. 05
Neptune (near)	252	50	100	0. 03
Neptune (far)	253	51	125	0. 02
Pluto (near)	252	50	100	0. 03
Pluto (far)	257	55	316	0. 01

REFERENCES

1. Evans and Taylor, "Radio Echo Observations of Venus," *Nature*, October 31, 1959.
2. Eshleman, Barthle, and Gallagher, "Radar Echos from the Sun," *Science*, February 5, 1960.
3. Victor and Stevens, "Exploration of Venus by Radar," *Science*, July 1961.
4. Heeschen, D. S., "Observation of Radio Source at Four Frequencies," *The Astrophysical Journal*, January 1961.
5. Proceedings of IRE "Radio Astronomy Issue," January 1958: entire issue with particular reference to articles by P. D. Strum, J. D. Kraus, H. C. Ko, C. H. Mayer, T. P. McCullough and R. M. Sloanaker, Aarons, Barron, and Castelli.
6. Kraus, John D., *Antennas*, McGraw-Hill Book Co., New York, 1950.
7. Proceedings of IRE "Space Electronics Issue" April, 1960: entire issue with particular reference to articles by G. E. Mueller, R. W. Sanders, R. H. Dimond, M. H. Brockman, H. R. Buchanan, R. L. Choate and L. R. Malling, F. E. Bond, C. R. Cahn and H. F. Meyer, A. G Smith
8. Rawer, Karl, "Propagation Problems with Space Radio Communications," *Journal of Research of National Bureau of Standards*, Vol. 66D, July–Aug., 1962.
9. Ko, H. C., "Temperature Concepts in Modern Radio," *The Microwave Journal*, June, 1961.
10. Rechtin, E., "Communication Techniques for Space Exploration," IRE Transactions on Space Electronics and Telemetry, September, 1959.
11. Shapiro, K. L., "Interference from the Ionosphere," *Electronic Industries*, March 1959.
12. Condon and Odishaw, *Handbook of Physics*, McGraw-Hill Book Co., New York, 1958.
13. Stelzried, Charles T., "A Cooled, Negative Conductance Degenerate Parametric Amplifier," Microwave Journal, July 1961.
14. Ewen, H. I., "A Thermodynamic Analysis of Master Systems," Microwave Journal, March 1959.
15. Riddle, F. M., Mathison, R. P., Martin, B. D., Springett, J. C., and Bourke, D. G., "JPL Contributions to the 1962 National Telemetry Conference," JPL Technical Memorandum No. 33–88, May 21, 1962.
16. Schwarz, M., *Information Transmission, Modulation, and Noise*, McGraw-Hill Book Co., New York, 1959.
17. Gilchriest, C. E., "The Application of Phase-Locked-Loop Discriminators for Threshold Improvement and Error Reduction in F.M.–F.M. Telemetry," JPL External Publication No. 364, January 7, 1957.
18. Viterbi, A., "Classification and Evaluation of Coherent Synchronous Sampled-Data Telemetry Systems," *IRE Transactions on Space Electronics Telemetry*, March 1962.
19. Viterbi, A., "On Coded Phase-Coherent Communications," JPL Technical Report 32–25, August 15, 1960.
20. Gilchriest, C. E., "Correlation Functions of Filtered PN Sequences," JPL Space Program Summary No. 37–16, August 31, 1962.
21. Springett, J. C., "Command Techniques for the Remote Control of Interplanetary Spacecraft," JPL Technical Report No. 32–314, August 1, 1962.